Distributed Sensing and Control of a Simply Supported Plate

by

Fariborz Fariborzi

A thesis
presented to the University of Waterloo
in fulfilment of the
thesis requirement for the degree of
Doctor of Philosophy
in
Mechanical Engineering

Waterloo, Ontario, Canada, 1998

I hereby declare that I am the sole author of this thesis.

I authorize the University of Waterloo to lend this thesis to other institutions or individuals for the purpose of scholarly research.

I further authorize the University of Waterloo to reproduce this thesis by photocopying or by other means, in total or in part, at the request of other institutions or individuals for the purpose of scholarly research.

The University of Waterloo requires the signatures of all persons using or photocopying this thesis. Please sign below, and give address and date.

Abstract

A mathematical model of the transverse vibration of a plate, with collocated piezoelectric actuators/sensors, to be used for free and forced vibration control purposes is presented. For the analysis of plate flexural vibration, the "Finite Element", and "Galerkin" procedures are described. Hamilton's Principle is used to derive the equations of the motion of a Mindlin plate model, which takes into account the transverse shear effects. The coupled differential equations of the motion are solved using the finite element method. Test results show that the application of this theory along with an appropriate choice of basis functions allows the analysis of a wide range of thicknesses. The formulated approach avoids shear locking and provides excellent accuracy and convergence characteristics. The performance of the plate with/without attached layers of piezoelectric material is compared using a finite element model. The comparison between the Galerkin formulation and the finite element method shows the accuracy of each method within the desired plate thickness range. The eigenfunctions of a Poisson-Kirchoff plate model have been used as basis functions in the Galerkin formulation. The state transition matrix of a Poisson-Kirchoff plate model is computed.

To ensure the highest energy efficiency, controllability, and observability of the system a process of optimization is described. Separation of variables, a double Fourier expansion, coupled with Navier's method are used in the Poisson-Kirchoff plate model to find the optimal location of the sensors/actuators.

A quadratic control objective is defined as a measure of system performance. The control objective is composed of those error variables that are important to the design and they are used to approximate the high order plant system by a lower order model. To guarantee that the error in the reduced model is smaller than the

desired error, a minimum required number of modes in the plate model is specified. The application of the formulated techniques is illustrated via numerical example.

The energy based control strategy "Linear Coupling Control (LCC)" is used for controlling free and forced vibrations in a simply supported plate. The control strategy is implemented by coupling a virtual second order linear system (controller) to an oscillatory plant and creating an energy exchange between the two systems. The energy transfer phenomenon between two oscillators is maximized by coupling the appropriate states of the plant and the controller. Once energy is transfered from the plant to the controller it is dissipated via linear damping. To provide a basis for comparing the results of the proposed control algorithm and the conventional control methods, linear quadratic optimal control was implemented as a control algorithm for the plate. The experimental verification of these approaches to vibration suppression is presented for the cases where it is undesirable to add actuators with significant mass and stiffness to the structure. The virtual controller is implemented on a personal computer. The experimental results have shown the controller's potential to eliminate free and forced vibration. In free vibration the controller reduces the oscillation time to one fourth. For forced vibration, the energy coupling control law provides an over 80% reduction of the steady state amplitude.

Acknowledgements

I thank GOD for His grace, love and faithfulness.

I would like to thank my supervisors Dr. Farid Golnaraghi and Dr. Glenn R. Heppler for their encouragement and support, and being source of inspiration throughout my Ph.D. program.

I am grateful to the members of my examining committee Dr. F. Ismail, Dr. J. P. Huissoon, Dr. S. T. Ariaratnam, and Dr. S. C. Sinha for their time and effort to read this document.

I must admit that in completing this venture, I am eternally indebted to numerous people. In particular, I would like to thank Dr. D. Wang, Dr. A. Khajehpour, Dr. D. Boulahbal, and Dr. D. Lin for their clarifying my doubts during numerous impromtu, but highly informative, discussions.

I have been very fortune to be surrounded by some very giving friend, Ali, Ashraf, Corey, Hamid, Jalal, Mehran, Sultan, Shahyar and all my friends in the Automation and Control group, who have made the graduate life one the most memorable experience of my life.

I would also like to extended my thanks to Mr. Hitchman, K. Kraul, and Mr. M. Vanreenen for helping me sort out various software and hardware difficulties. I appreciate all the administrative assistance from Ms. K. Roenspiess.

The love and support provided by my parents and family has been a source of strength and comfort throughout my life. Their faith and encouragement in me for all endeavour have been a major influence in my achievement to this day and help me to accomplish my full potential. word cannot express the love I have for them.

I am thankful for the financial support provided by the Natural Sciences and Engineering Research Council (NSERC) and the Ontario Graduate Scholarship (OGS).

I pray, may God give me the strength to live out the set of principles and disciplines, inculcated in me, to its legitimate end.

Contents

1 Introduction 1

1.1 Research objectives 2

1.2 Layout of the Thesis 4

2 Finite Element Model 6

2.1 Introduction 6

2.2 Theory 10

2.2.1 Piezoelectric Phenomena 10

2.2.2 Mindlin Plate-Bending theory 11

2.2.3 Main Assumptions 12

2.2.4 Strain Energy 12

2.2.5 Kinetic Energy 15

2.3 Finite Element Model 16

2.4 Tests and Results 19

2.5 Conclusion and Summary 25

3 Mathematical Model 29

3.1 Introduction 30

3.2 Theoretical Formulation 33

3.2.1 Classical Plate-Bending Theory 33

3.2.2 Solution of the State Equations 38

3.3 Optimization of Actuator/Sensor Locations 41

3.3.1 Formulation of the Problem 41

3.4 Modal Cost Analysis 45

3.5 Conclusion and Summary 58

4 Optimal Controller 60

4.1 Introduction 60

4.2 Optimal Control 63

4.2.1 LQ "Linear Quadratic" Optimal Control 63

4.2.2 Stability Margin of the LQ Optimal Control 66

4.3 Controller Design 67

4.4 Conclusion and Summary 78

5 Experimental Implementation 88

5.1 Introduction 89

5.2 Experimental Apparatus 91

5.2.1 Aluminum Plate 91

5.2.2 Control System 92
5.2.3 Data Acquisition 92
5.3 System Identification 93
5.4 Free Vibration Control results 94
5.5 Forced Vibration Control results 97

6 Conclusion and Summary of the Research **109**

A Computer program **113**

A.1 Subroutine DATAF.m 113
A.2 Subroutine STIFF.m and MKQ.m 114
A.3 Subroutine EIGV.m and PERDIS.m 114
A.4 Subroutine EIGV1.m, FRF.m, and ZDRAW.m 114
A.5 Subroutine RESP.m 115
A.6 DATAF.m 117
A.7 STIFF.m 118
A.8 MKQ.m 121
A.9 EIGV.m 127
A.10 EIGV1.m 130
A.11 PERDIS.m 131
A.12 ZDRAW.m 133
A.13 FRF.m 134

B SYSTEM DYNAMIC RESPONSE MATRICES 138

References 140

List of Tables

2.1 Maximum deflection of a plate under a static centre point load (FEM method) 20

2.2 Comparison of the FEM plate modes of vibration under different boundary conditions 21

2.3 Maximum deflection of a plate under static loading (analytical method [32]) 21

2.4 Natural frequencies of a plate (analytical method [33]) 25

2.5 Comparison of plate modes of vibration under different boundary conditions 26

3.1 Number of Modes Required in Plate Model to Satisfy the Error requirements 52

3.2 Material characteristics and dimensions of the Plate 53

3.3 Material characteristics and dimensions of the Piezoelectric 54

List of Figures

2.1 Mindlin Plate element after loading. 13

2.2 Basic sixteen-node element; 48 degrees of freedom; (w, θ_x, θ_y) at each node. 17

2.3 Square plate test model, $\frac{1}{4}$ plate symmetry used; edges may be simply supported or clamped. 22

2.4 Uniform load on a square plate. 23

2.5 Point load on a square plate. 24

2.6 Mode shape predicted by finite element for cantilever plate (a) Mode 1. (b) Mode 2. (c) Mode 3. (d) Mode 4. 27

2.7 (a) Predicted Frequency Response Function by Finite Element Analysis for Simply Supported Plate. (b)Predicted Frequency Response Function by Finite Element Analysis for Clamped Plate. 28

3.1 Kirchoff plate element after loading. 34

3.2 Simply Supported Plate with a Concentrated Moment 42

3.3 a) Beat phenomenon in plate and actuator ($\omega_{mn} \approx \omega_f$), b) Resultant response of the plate and actuator in a, c) Beat phenomenon in plate and actuator ($\omega_{mn} = \omega_f$), d) Resultant response of the plate and actuator in c 46

3.4 Contribution of inputs to the cost function at observation point $(\frac{5L_x}{12}, \frac{5L_y}{12})$ (a)Effect of piezo located at $(\frac{L_x}{2}, \frac{L_y}{4})$ (b)Effect of piezo located at $(\frac{L_x}{2}, \frac{L_y}{2})$. (c)Effect of all piezos (d)Effect of external point load 59

4.1 Damping Effects on the Forced Coupled System 79

4.2 Oscillatory response of a simply supported plate to a pulse input a)Uncontrolled plant response at $(\frac{5L_x}{12}, \frac{7L_y}{12})$ b)FFT of the uncontrolled plant c) Controlled plant response at $(\frac{5L_x}{12}, \frac{7L_y}{12})$ using LQ d)Controller Input using LQ 80

4.3 Oscillatory response of a simply supported plate to four harmonic inputs a)Disturbance b)FFT of the disturbance c)Plant response at $(\frac{L_x}{2}, \frac{7L_y}{12})$ using LQ d)Controller Input using LQ 81

4.4 Oscillatory response of a simply supported plate to a pulse input a)Uncontrolled plant response at $(\frac{5L_x}{12}, \frac{7L_y}{12})$ b) Controlled plant response at $(\frac{5L_x}{12}, \frac{7L_y}{12})$ for $\alpha_p = -1500, \alpha_c = 750$ and $\xi_c = 0.05$ c)Controlled plant response at $(\frac{5L_x}{12}, \frac{7L_y}{12})$ for $\alpha_p = -1000, \alpha_c = 500$ and $\xi_c = 0.05$ d)Controlled plant response at $(\frac{5L_x}{12}, \frac{7L_y}{12})$ for $\alpha_p = -1500, \alpha_c = 750$ and $\xi_c = 0.1$ 82

4.5 Oscillatory response of a simply supported plate to a pulse input a)Uncontrolled plant response at $(\frac{5L_x}{12}, \frac{7L_y}{12})$ b)FFT of the uncontrolled plant c) Controlled plant response at $(\frac{5L_x}{12}, \frac{7L_y}{12})$ for $\alpha_p = -2000, \alpha_c = 1000$ and optimal ξ_c c)Controlled plant response at $(\frac{5L_x}{12}, \frac{7L_y}{12})$ for $\alpha_p = -1000, \alpha_c = 500$ and $\xi_p = \xi_c = 0.05$ d)Controller input 83

4.6 Oscillatory response of a simply supported plate to four harmonic inputs a)Disturbance b)FFT of the disturbance c)Plant response at $(\frac{5L_x}{12}, \frac{7L_y}{12})$ for $\alpha_p = -2000, \alpha_c = 1000$ and $\xi_c = .15$ d)Controller Input 84

4.7 Oscillatory response of a simply supported plate to four harmonic inputs a)Disturbance b)FFT of the disturbance c)Plant response at $(\frac{L_x}{2}, \frac{7L_y}{12})$ for $\alpha_p = -1500, \alpha_c = 500$ and optimal ξ_c d)Controller Input 85

4.8 Oscillatory response of a simply supported plate to four harmonic inputs a)Disturbance b)FFT of the disturbance c)Plant response at $(\frac{5L_x}{12}, \frac{7L_y}{12})$ for $\alpha_p = -2000, \alpha_c = 500$ and optimal ξ_c d)Controller Input 86

4.9 Oscillatory response of a simply supported plate to four harmonic inputs a)Disturbance b)FFT of the disturbance c)Plant response at $(\frac{5L_x}{12}, \frac{7L_y}{12})$ for $\alpha_p = -1000, \alpha_c = 500$ and optimal ξ_c d)Controller Input 87

5.1 Plate in the experimental set-up 100

5.2 Boundary condition in the experimental set-up 101

5.3 Piezoelectric elements in the experimental set-up 102

5.4 Strain gauge in the experimental set-up 103

5.5 Signal conditioner and amplifier in the experimental set-up 104

5.6 Control system in the experimental set-up 105

5.7 Frequency Response Function of Point $(\frac{5L_x}{12}, \frac{5L_x}{12})$ a)Magnitude b)Real, Frequency Response Function of Point $(\frac{7L_x}{12}, \frac{5L_x}{12})$ c)Magnitude d)Real. 106

5.8 Oscillatory response of to a simply supported plate to the pulse inputs a) Uncontrolled plant response at $(\frac{L_x}{2}, \frac{L_y}{2})$ b)Controlled plant response at $(\frac{L_x}{2}, \frac{L_y}{2})$ using LQ c)Controlled plant response at $(\frac{L_x}{2}, \frac{L_y}{2})$ using LCC 107

5.9 Oscillatory response of a simply supported plate to a harmonic input a) Plant response at $(\frac{L_x}{2}, \frac{L_y}{2})$ using LQ b) Plant response at $(\frac{L_x}{2}, \frac{L_y}{2})$ using nonoptimal LCC c)Plant response at $(\frac{5L_x}{12}, \frac{7L_y}{12})$ using optimal LCC 108

A.1 Flow chart for plate vibration analysis 116

Table of Nomenclature

σ	stress
$\mathcal{E}$	electric field
ϵ	strain
D	electric displacement
ϵ^{σ}	permittivity
$\mathcal{D}$	piezoelectric coefficient
s^{E}	compliance
u	displacement field in x direction
v	displacement field in y direction
w	displacement field in z direction
$\dot{u}$	velocity in x direction
$\dot{v}$	velocity in y direction
$\dot{w}$	velocity in z direction
$\ddot{w}$	acceleration in z direction
θ_i	rotation of the normal to the mid-surface with respect to i axis
$\dot{\theta}_i$	angular velocity of θ_i
$\theta_{i,j}$	curvature
ϵ_{ij}	infinitesimal strain
γ_{ij}	shear strain
n, m, p, q	mode number
L	Lagrangian
T	kinetic energy
U	total potential energy
σ	stress

ε	total strain
Λ	actuation strain
t_s	plate thickness
t_a	piezoelectric thichness
κ	curvature
E_s	plate constitutive matrix
E_a	actuator constitutive matrix
ν_s	plate Poisson's ratio
ν_a	actuator Poisson's ratio
$\mathcal{M}$	moment applied to the plate
ϕ_i	basis functions
D	bending rigidity
L_x	plate length in x direction
L_y	plate length in y direction
ϕ_x	shape function on x
ϕ_y	shape function on y
ϕ_{ij}	i shape function on j
Z_{nm}	time function for mode nm in separation of variables
F	external forcing term
T	external moment
$\gamma_{f_{pq}}$	parametric gain
$\gamma_{xu_{pq}}$	parametric gain
C	Rayleigh damping
ζ_{ij}	damping factor for the ij mode
ω_{ij}	natural frequency of the ij mode
ξ	location of the PZT in x direction
η	location of the PZT in y direction

$\varphi(t_0, t)$ state transition matrix

Chapter 1

Introduction

Sandwich laminates are used in the primary structure of aircraft because of their high specific strength and high specific stiffness. These properties, along with their excellent fatigue strength, ease of formability, wide range of operating temperatures, low coefficient of thermal expansion, high damping, and their general tailorability result in materials with almost unlimited potential. Piezoelectric materials are excellent candidates as sensors and actuators for laminated materials.

The piezoelectric effect was discovered experimentally by the Curie brothers. Piezo is derived from a Greek word meaning to press, and piezoelectricity is an electro mechanical phenomenon which couples mechanical deformation with an electrical field [1]. Since the discovery of piezoelectric materials, significant progress has been made in understanding their material properties, formulation, mechanical properties and their usage as actuators and sensors. Recently piezoelectric and other ceramic actuators have been used for vibration suppression, mode shape control and pointing accuracy. These applications mainly use an active control method to increase the damping or alter the static and dynamic shape of the structure.

Piezoelectric materials generate a charge in response to a mechanical deformation or, conversely, provide mechanical strain when an electric field is applied across them. As a result, piezoelectric elements are very effective sensors and actuators in the vibration control applications. Because of their small size, a large number of piezoelectric elements may be distributed along a structure without significantly increasing the mass or modifying its passive dynamic properties. Once charged however, piezoelectric actuators allow direct control of the local deformation of a structure without applying rigid body torques and forces, and can be electrically tuned to maximize the damping in the structure.

1.1 Research objectives

In proceeding towards the goal of establishing an active vibration absorber for a simply supported plate all the important issues associated with the analysis and the experiments will be addressed. Based on the deficiencies identified during the literature review the following research objectives are proposed to bring together all aspects associated with plate vibration control.

a) *Mathematical formulations of a plate, with a thin piezoelectric element bonded to the surface, based on Mindlin plate theory and Kirchoff plate theory.* The philosophy of this work revolves around the development of a mathematical model of the transverse vibration of a plate to be used for free and forced vibration control purposes. For the analysis of plate flexural vibration, the "Finite Element" and "Galerkin" procedures are described. In numerical simulation the Mindlin plate theory, which takes into account the effects ignored in the classical plate, has been used to study the plate vibration. The eigenfunctions of a Poisson-Kirchoff plate have been used as basis functions in a Galerkin formulation. The advantages and

disadvantages of each method of modelling, "analytical" and "numerical", have been high lighted.

b) *Optimization of the placement of the piezoelectric sensors and actuators.* The ultimate goal of this research is to determine the optimal location of piezoelectric sensors and actuators to minimize the number of employed piezoelectrics.

c) *Introduction of a vector of error variables in the measure of performance.* The control objective is composed of those error variables that are important to the design and they are used to approximate the high order plant system by a lower order model. The number of modes required in the plate model to guarantee that the error in the objective function is smaller than a specified error is derived.

d) *Establishment of a control strategy based on the use of piezoelectric actuators.* A modular control law based on linear coupling control theory is established, including developing relations to quantify the characteristics of the controlled system, ascertaining the conditions for which the controlled systems are optimal, stable, and establishing the energy removal mechanisms to achieve a desired suppression goal. A linear quadratic optimal control is implemented to provide a basis for comparing the results of the proposed control algorithm and the conventional control methods. To investigate the performance of the control method, a laminated simply supported plate and the controller are numerically simulated.

e) *Conduct of an Experimental Investigation.* Experimental observations have been produced for determining the nature of the actual system, illustration of the effectiveness and performance of the proposed techniques. The experimental verification

of these approaches to vibration suppression is presented for a simply supported plate with attached piezoelectric actuators, where the effects of mass and stiffness of the actuators are not significant in compare to the structure itself.

f) *A comparison between theoretical and experimental results.* A comparison between theoretical and experimental has been performed to evaluate the accuracy of the mathematical model. As well, an evaluation of a conventional controller and the proposed controller has been investigated.

1.2 Layout of the Thesis

This thesis presents the development of the theoretical and experimental application of a linear coupled controller for a simply supported plate. After introducing the scope of the thesis in chapter 1, chapter 2 through 4 deal with specific theoretical aspects of the problem such as modelling, analysis, control system, and numerical simulation of the system. The subsequent chapter illustrates the laboratory work involved in realizing a functional controller. It should be noted that the general review of related literature, categorized into four groups, is given at the beginning of each chapter.

Chapter 2 describes the development of a mathematical model which is used for the numerical simulation of the Mindlin plate. Lagrangian dynamics is used to derive the equation of motion. In the last section of this chapter, a comparison between classical theory and this first-order theory shows the significance of the formulation in the range of interest. It is also shown that a lower order system formulation will be sufficient in the vicinity of our research requirements.

Chapter 3 presents an analytical method of modelling the system. In the for-

mulation, the Galerkin method is used to analyze the structure with attached distributed actuators. Optimal locations of the actuators/sensors are determined, followed by describing the beat phenomena that will be used for control purposes in the next chapter. This chapter will close by defining a measure of the system performance to approximate the plant system by a lower order system. It also shows the percent error in the reduced model.

Chapter 4 discusses two control strategies, namely quadratic optimal control and linear coupling control. In addition, the associated tasks of quantifying closed loop response characteristics and ascertaining closed loop stability are also detailed. The chapter ends with a numerical example and a comparision between two control methods.

Chapter 5 deals with the experimental verification of the theoretical and numerical results. Experimental observations have been rendered for system identification, model verification and ultimately controller performance analysis. The components of the experimental plant are described and illustrated. Two control strategies have been tested under free and forced vibrations. Experimental results are then presented and discussed.

Chapter 6 is a summary of the work. It presents the highlights of the work, with conclusions drawn from this research endeavor, and recommendations for further work on the subject.

Chapter 2

Finite Element Model

A finite element model of a plate with collocated piezoelectric actuators/sensors to be used for free and forced vibration control purposes is presented. The performance of the plate with attached layers of piezoelectric material is evaluated by a finite element model based on the Mindlin plate theory. Hamilton's Principle is used to derive the equations of motion.

2.1 Introduction

The present chapter focuses on the mathematical model of plate vibration with multiple layers of piezoelectric actuators. It addresses: (a) an analytical method of modelling the system, and (b) a numerical method of the modelling the system. A valuable reference for the analysis and design of composite structures is the broad literature review of recent developments by Kapania and Raciti [2]. This work presents a large variety of research and developments in studying shear effects, buckling, post buckling of geometrically imperfect plates, local buckling and post

buckling analysis of thin walled stiffeners and delamination buckling and growth in laminated plates. These are added to recently developed analytical (closed form, Galerkin, Rayleigh-Ritz) and numerical methods for various geometric shapes and edge conditions.

The review of the literature on the finite element modelling of the plate shows that the previous analyses of laminated composite plates are based on either three dimensional elasticity theory or lamination theory. Three dimensional elasticity theory treats each layer as an elastic continum with distict material properties. This approach become intractable as the number of layers becomes large. In lamination theories it is assumed that the laminate is in a state of plane stress, the individual laminae are elastic, and there is perfect bonding between layers. Thus lamination theories are equivalent to the single layer theories. The classical lamination theory, which is an extension of the classical plate theory, ignores the transverse stress components. This theory is adequate for many engineering problems [3].

The origin of displacement based theories is attributed to Basset [4]. He began his analysis with the assumption that the displacement components in a shell can be expanded in a power series of the thickness coordinate. The first stress based shear deformation plate theory was developed by Mindlin [5]. The differential equations and the boundary conditions of the theory were obtained using Castigiliano's theorm of least work. The shear deformation theory based on the displacement field is often referred to as Mindlin's plate theory or the first-order shear deformation theory. Mindlin [5] presented a complete theory based on the displacement field taken from Hencky [6]. The literature review points out that the basic idea came from Basset [4], Hildebrand [7], and Reissner [8]. Hildebrand [7] and Hencky [6] presented a displacement based shear deformation theory for shells that can be specialized to plates.

The development of a mathematical formulation for laminated plates has been investigated by many researchers. The list includes the works of Reddy and Chao [9], Lajczok [10], and Phan [11]. Additional work on laminated plates using a high-order theory was done by Bhimaraddi and Stephens [12], Reissner [8] who developed a twelfth order theory for transversely isotropic plates, and by Krishna Murty and Vellaichamy [13] who examined the suitability of higher order deformation theory based on cubic in-plane displacements and parabolic normal displacements.

Reddy [14] reviewed the literature on finite element modelling of laminated composite plates, and presented a historical background of the development of shear deformation plate theories. The classical Kirchhoff plate theory, which neglects transverse shear deformations, were extensively used in the analysis of thin isotropic plates. This theory can lead to considerable errors when analyzing laminated plates, since it underpredicts deflections and overpredicts natural frequencies. In the literature, two categories for shear deformation displacement based plate theories can be identified; that is, the first-order and higher-order theories. The first order theory is the well known Reissner-Mindlin theory where the general differential equations are derived by using the principle of minimum potential energy. This theory provides good results for the global response of the plate; that is, for deflection, natural frequencies, and buckling loads. However, a more sophisticated theory would be required for studying the through the thickness stress response in the regions of discontinuities such as boundaries. To account for this three dimensional distribution of stresses, which are neglected in the classical lamination theory, three dimensional theories in which each layer is treated as a homogeneous anisotropic material have been developed [15] [16]. Although these theories lead to more accurate results, their storage requirement due to the large number of variables and computer cost make them impractical. Later, Liaw and Little [17] solved

bending problems of multilayered sandwich plates based on the theory developed Reissner. Azar [18] extended Liaw and Little's results to the same problems, but with orthotropic facing.

The general finite element formulations for piezoelectric sensors and actuators are proposed by Chen [19], Tzou [20], Lammering [21], Lee [22], and others. Chen *et al* [23] employed the virtual work principle to form the general sensing and actuating finite element formulations. The formulations are derived from first-order shear plate theory which can be employed for very thin to moderately thick structures. Tzou [20] developed the theory based on a generic continuum shell element coupled with a distributed piezoelectric layer serving as a distributed sensor and the other piezoelectric layer serving as a distributed actuators. Based on the derived theory, it is concluded that a distributed sensor is capable of sensing all shell vibration modes and the distributed actuator is capable of controlling all the shell modes. Lammering [21] focuses on the finite element analysis of shell structures with thin piezoelectric layers bonded to the surfaces. The finite element formulation is based on the shear elastic shell theory of the Reissner Mindlin type. To establish stability in vibration control, the second or direct method of Lyapunov is used. The time integration is computed by means of the Newmark algorithm.

Lee [24] developed a finite element analysis of composite sandwich plates. The purpose of this work was to include the transverse normal deformation, in addition to the transverse shear stresses. In this study the face plates of composite sandwich structure are modelled based on Mindlin's plate theory. The vibrational analysis shows that all the natural frequencies calculated in this method are lower than those methods which consider the core transmission only for the transverse shear forces. Thus the obtained frequencies are more conservative than those found by other methods.

In the following, after a brief description of the piezoelectric phenomena, the mathematical model of the flexible structure based on the Mindlin theory is developed. As a method of investigation the finite element method is employed to evaluate the performance of the Mindlin plate equation.

2.2 Theory

2.2.1 Piezoelectric Phenomena

Piezoelectricity is a phenomenon whereby mechanical strain produces an electrical response in the material. This is also known as the direct effect and it can be used for sensing purposes. The converse piezoelectric effect is the mechanical response to an electrical excitation which is used for piezoelectric actuation. In the linear theory of piezoelectricity both electrical and mechanical forcing functions affect the electromechanical behavior of the materials. The forcing terms arise from the applied excitation, boundary constraints, or the combination of both. The piezoelectric characteristics can be approximately modelled by assuming a linear relationship among different physical variables [1]. This set of linearly coupled electro-elastic constitutive relations can be written as [25],

$$\begin{aligned} \{\epsilon\} &= [s^E]\{\sigma\} + [\mathcal{D}]^T\{\mathcal{E}\} \\ \{D\} &= [\mathcal{D}]\{\sigma\} + [\epsilon^\sigma]^T\{\mathcal{E}\} \end{aligned} \tag{2.1}$$

The stress vector $\{\sigma\}$ and the electric field vector $\{\mathcal{E}\}$ are the independent variables while the strain vector $\{\epsilon\}$ and the electric displacement vector $\{D\}$ are the dependent variables. According to linear theory of piezoelectricity, the dependent variables are expressed as a linear combination of independent variables where the permittivity $[\epsilon^\sigma]$, the piezoelectric coefficient $[\mathcal{D}]$, and the compliance $[s^E]$ matrices

are assumed as constant coefficients. The superscript of a coefficient corresponds to an independent variable, and indicates that the value of the coefficient is determined at the operating point where that independent variable is set to zero. The superscript T indicates transpose operation.

2.2.2 Mindlin Plate-Bending theory

The classical Poisson-Kirchoff theory of plates requires C^1 continuity in a finite element formulation, as does the classical Euler-Bernoulli beam theory. Following the development of the Kirchoff plate equations one finds that the order of governing equations derived by neglecting transverse shearing deformations permits only two of the three obvious force conditions to be enforced at a free edge [26]. For thin plates, this shortcoming appears to be largely academic and the elementary plate theory is adequate. However, as a plate becomes relatively thick, the transverse shearing effects become more important and cannot be ignored. The Reissner-Mindlin plate theory [27] includes these effects and requires C^0 finite element interpolation functions which are easily constructed. For these reasons we turn away from Poisson-Kirchoff type of elements to elements based upon upon theories which accommodate transverse shear strains (Reissner and Mindlin theories [27]) and which require only C^0 continuity in the finite element formulations. Although the inclusion of transverse shearing deformations complicates the problem considerably for a direct formulation, incorporation of these effects is relatively easy in an energy-based approach.

2.2.3 Main Assumptions

In Mindlin plate theory it is assumed that a plane which is straight and normal to the mid-surface before loading remains plane but not necessarily normal to the mid-surface after loading. Thus, transverse shear deformation is allowed. The motion of a point on the mid-surface is dependent on rotations of the normal to the mid surface of the undeformed plate (θ_x and θ_y). Thus, the displacement field can be assumed to be,

$$\begin{aligned} u(x,y,z) &= -z\theta_x(x,y,z) \\ v(x,y,z) &= -z\theta_y(x,y,z) \\ w(x,y,z) &= w(x,y) \end{aligned} \tag{2.2}$$

and the strain components $\{\epsilon\} = \{\epsilon_{xx}\ \epsilon_{yy}\ \gamma_{xy}\ \gamma_{yz}\ \gamma_{xz}\}^T$ are given by

$$\begin{aligned} \epsilon_{xx} &= -z\theta_{x,x} & \gamma_{xy} &= -z(\theta_{x,y} + \theta_{y,x}) \\ \epsilon_{yy} &= -z\theta_{y,y} & \gamma_{yz} &= w_{,y} - \theta_y \\ & & \gamma_{xz} &= w_{,x} - \theta_x \end{aligned} \tag{2.3}$$

where, for example, $(\cdot)_{,x}$ is the partial derivative with respect to x.

We will use Hamilton's Principle to derive the equations of motion for the plate which requires us to form the Lagrangian

$$L = T - U \tag{2.4}$$

where T is the kinetic energy, and U is the total potential energy.

2.2.4 Strain Energy

The general stress-strain relationship for the material for an entire cross section can be written as:

$$\{\sigma\} = [E](\{\varepsilon\} - \{\Lambda\}) \tag{2.5}$$

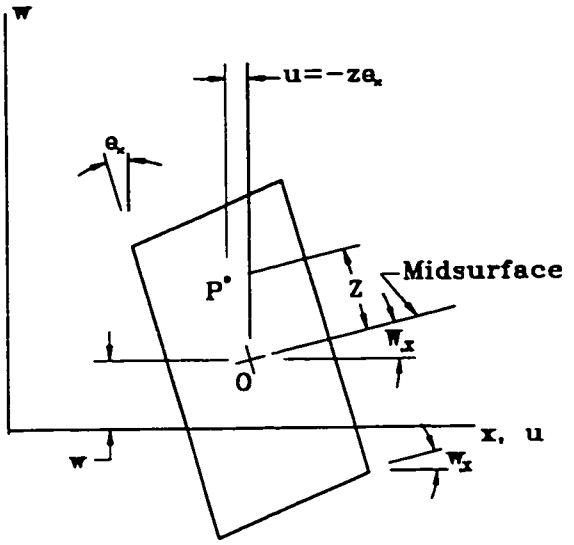

Figure 2.1: Mindlin Plate element after loading.

Where σ, ε, Λ and E are stress, total strain, actuation strain and the constitutive matrix, respectively. The actuation strain is nonzero only for that part of the cross section which contains a piezoelectric material actuator. Consider a homogeneous, linearly elastic plate; then the total strain energy in such an element is given by

$$U = \frac{1}{2}\int_V (\{\varepsilon\} - \{\Lambda\})^T [E](\{\varepsilon\} - \{\Lambda\}) dV \tag{2.6}$$

or

$$U = U_1 + U_2 + U_3 \tag{2.7}$$

Integration of the first term with respect to z will give:

$$U_1 = \frac{1}{2}\int_A \int_{-(\frac{t_s}{2}+t_a)}^{+(\frac{t_s}{2}+t_a)} \{\varepsilon\}^T [E]\{\varepsilon\} dz dA = \frac{1}{2}\int_A \{\kappa\}^T [\mathcal{D}]\{\kappa\} dA \tag{2.8}$$

where t_s and t_a present plate thickness and piezoelectric thickness respectively. The vector

$$\{\kappa\} = \{\theta_{x,x}\ \theta_{y,y}\ \theta_{x,y} + \theta_{y,x}\ w_{,y} - \theta_y\ w_{,x} - \theta_x\}^T$$

is the curvature, a superscript T denotes transpose and $\mathcal{D}$ is a constant coefficient matrix, and is defined according to

$$[\mathcal{D}] = \begin{bmatrix} \mathcal{D}_{11} & \mathcal{D}_{12} & 0 & 0 & 0 \\ \mathcal{D}_{21} & \mathcal{D}_{22} & 0 & 0 & 0 \\ 0 & 0 & \mathcal{D}_{33} & 0 & 0 \\ 0 & 0 & 0 & \mathcal{D}_{44} & 0 \\ 0 & 0 & 0 & 0 & \mathcal{D}_{55} \end{bmatrix} \tag{2.9}$$

where

$$\begin{aligned} \mathcal{D}_{11} = \mathcal{D}_{22} &= \frac{t_s^3}{12}\left[\frac{E_s}{1-\nu_s^2} - \frac{E_a}{1-\nu_a^2}\right] + \frac{2E_a}{3(1-\nu_a^2)}\left(\frac{t_s}{2}+t_a\right)^3 \\ \mathcal{D}_{12} = \mathcal{D}_{21} &= \frac{t_s^3}{12}\left[\frac{E_s\nu_s}{1-\nu_s^2} - \frac{E_a\nu_a}{1-\nu_a^2}\right] + \frac{2E_a\nu_a}{3(1-\nu_a^2)}\left(\frac{t_s}{2}+t_a\right)^3 \\ \mathcal{D}_{33} &= \frac{t_s^3}{24}\left[\frac{E_s}{1+\nu_s} - \frac{E_a}{1+\nu_a}\right] + \frac{2E_a}{3(1+\nu_a)}\left(\frac{t_s}{2}+t_a\right)^3 \\ \mathcal{D}_{44} = \mathcal{D}_{55} &= \frac{E_s t_s}{2(1+\nu_s)} + \frac{E_a t_a}{1+\nu_a} \end{aligned} \tag{2.10}$$

By integrating the second term in (2.7) we obtain

$$U_2 = \int_A \int_{-(\frac{t_s}{2}+t_a)}^{+(\frac{t_s}{2}+t_a)} \{\varepsilon\}^T [E]\{\Lambda\} dz dA = \int_A \{\kappa\}^T \{\mathcal{M}\} dA \tag{2.11}$$

where $\{\mathcal{M}\}$ is the moment applied to the plate by the actuators. The piezoelectric devices suitable for use as flexural elements are poled in the zx (commonly termed as 31) mode [1]. If we assume the piezoelectric layers are polarized in the zx mode and that the piezoelectric layers are long then

$$\mathcal{M} = \begin{Bmatrix} \mathcal{M}_{xx} \\ \mathcal{M}_{yy} \\ 0 \\ 0 \\ 0 \end{Bmatrix} = \begin{Bmatrix} \frac{E_a t_a t_s}{(1+\nu_a)}[1+\frac{t_a}{t_s}]\Lambda \\ \frac{E_a t_a t_s}{(1+\nu_a)}[1+\frac{t_a}{t_s}]\Lambda \\ 0 \\ 0 \\ 0 \end{Bmatrix} \tag{2.12}$$

If there is no piezoelectric sensor or actuator on the element then $E_a = t_a = 0$. The last term in (2.7) is independent of extension strain and curvature and is denoted as

$$U_3 = \frac{1}{2}\int_A \int_{-(\frac{t_s}{2}+t_a)}^{+(\frac{t_s}{2}+t_a)} \{\Lambda\}^T[E]\{\Lambda\} dz dA = \int_A U^*(\Lambda) dA$$

The total strain energy can now be expressed as

$$U = \int_A \left[\frac{1}{2}\{\kappa\}^T[\mathcal{D}]\{\kappa\} + \{\kappa\}^T\{\mathcal{M}\} + U^*(\Lambda)\right] dA \tag{2.13}$$

2.2.5 Kinetic Energy

The kinetic energy can be written as:

$$T = \frac{1}{2}\int_A \int_{-(\frac{t_s}{2}+t_a)}^{+(\frac{t_s}{2}+t_a)} \rho(\dot{w}^2 + z^2\dot{\theta}_x^2 + z^2\dot{\theta}_y^2) dz dA = \frac{1}{2}\int_A \{\dot{d}\}^T[m]\{\dot{d}\} dA \tag{2.14}$$

where

$$\{\dot{d}\} = \{\dot{w}\ \dot{\theta}_x\ \dot{\theta}_y\}^T$$

is the velocity vector, and the inertia density matrix $[m]$ is given by

$$[m] = \begin{bmatrix} \rho_s t_s + 2\rho_a t_a \\ \frac{2}{3}\left\{\rho_s(\frac{t_s}{2})^3 + \rho_a[(\frac{t_s}{2}+t_a)^3 - (\frac{t_s}{2})^3]\right\} \\ \frac{2}{3}\left\{\rho_s(\frac{t_s}{2})^3 + \rho_a[(\frac{t_s}{2}+t_a)^3 - (\frac{t_s}{2})^3]\right\} \end{bmatrix} \tag{2.15}$$

where ρ is the volume mass density of the structure.

Combining the kinetic energy (2.14) with the potential strain energy (2.13), the Lagrangian can be written as:

$$L = \int_A (\frac{1}{2}\{\dot{d}\}^T[m]\{\dot{d}\} - \frac{1}{2}\{\kappa\}^T([\mathcal{D}]\{\kappa\} + 2\{\mathcal{M}\}) - U^*(\Lambda)) dA \tag{2.16}$$

By direct application of Hamilton's Principle to (2.16) the equations of motion can be derived. The result will be a system of coupled partial differential equations. To solve this complex continuum problem, the finite element method will be used.

2.3 Finite Element Model

As a preliminary mode of investigation, the finite element method will be employed to evaluate the performance of the proposed model.

Nodal degrees of freedom consist of lateral deflections w_i and rotations θ_{xi} and θ_{yi} of the mid-surface normals. The corresponding deflections and rotations within an element are now approximated in the usual manner by employing a suitable set of basis functions ϕ_i, such that [27]

$$\begin{Bmatrix} w \\ \theta_x \\ \theta_y \end{Bmatrix} = \sum_{i=1}^{N} \begin{bmatrix} \phi_i & 0 & 0 \\ 0 & \phi_i & 0 \\ 0 & 0 & \phi_i \end{bmatrix} \begin{Bmatrix} w_i \\ \theta_{xi} \\ \theta_{yi} \end{Bmatrix} \tag{2.17}$$

or

$$\underset{3 \times 3N}{\{U\} = \quad [\phi] \quad \{d\}_e} \tag{2.18}$$

where N = Number of nodes per element and the element displacement vector is

$$\{d\}_e = \lfloor w_1 \ \theta_{x1} \ \theta_{y1} \ \ldots \ w_N \ \theta_{xN} \ \theta_{yN} \ \rfloor^T \tag{2.19}$$

The choice of basis functions will determine the element performance, and generally the ϕ may be different for each degree of freedom. For plate elements it has been shown that very good results are obtainable by choosing basis functions of different type [28] [29] and different orders for the normal displacements and rotations respectively. Results from other studies show that the Lagrangian element formulation is much less susceptible to shear locking than the serendipity formulation. It is well known that the cubic Lagrange element exhibits no locking, no spurious eigenvalues and rapid convergence to the thin plate solution. For a general plate element it has been recommended that the displacement trial functions should be

at least bi-cubics [30]. Therefore the chosen basis functions are bi-cubics formed from cubic Lagrange polynomials given as [27].

$$\phi_{mn} = \prod_{\substack{i=0 \\ i \neq m}}^{m=3} \prod_{\substack{j=0 \\ j \neq n}}^{n=3} \frac{(\zeta - \zeta_i)(\eta - \eta_j)}{(\zeta_m - \zeta_i)(\eta_n - \eta_j)} \tag{2.20}$$

where m,n=0,...,3 and ζ_i, η_j are assumed to be distinct. The basic element is shown in Figure 2.2 with the ordinal numbering of the nodes as indicated. The

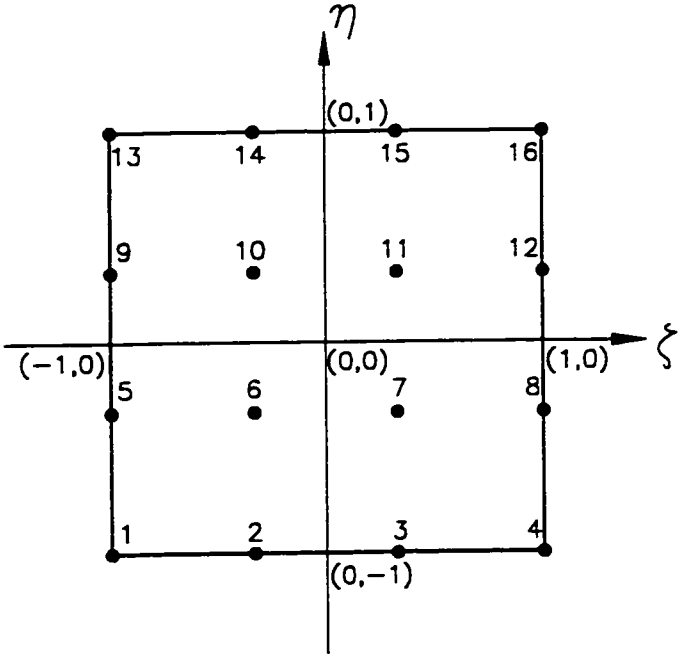

Figure 2.2: Basic sixteen-node element; 48 degrees of freedom; (w, θ_x, θ_y) at each node.

interpolated displacement vector $\{w\ \theta_x\ \theta_y\}^T$ can be used to state the curvatures κ

in terms of nodal displacements as

$$\{\kappa\} = \left\{ \begin{array}{c} \theta_{x,x} \\ \theta_{y,y} \\ \theta_{x,y} + \theta_{y,x} \\ w_{,y} - \theta_y \\ w_{,x} - \theta_x \end{array} \right\} = [\partial]\{U\} \tag{2.21}$$

where $\{U\}$, the nodal degrees of freedom vector consists of the lateral deflection w and the mid-surface normal rotations θ_x and θ_y. The $[\partial]$ matrix relates the displacement field and the curvature and is given by

$$[\partial] = \begin{bmatrix} 0 & \frac{\partial}{\partial x} & 0 \\ 0 & 0 & \frac{\partial}{\partial y} \\ 0 & \frac{\partial}{\partial y} & \frac{\partial}{\partial x} \\ -\frac{\partial}{\partial y} & 0 & 1 \\ -\frac{\partial}{\partial x} & 1 & 0 \end{bmatrix} \tag{2.22}$$

Substituting (2.17) into (2.21) gives

$$\{\kappa\} = [\partial][\phi]\{d\} \quad or \quad [\kappa] = [B]\{d\} \tag{2.23}$$

where

$$[B] = [\partial][\phi] = \begin{bmatrix} 0 & \phi_{1,x} & 0 & \cdots \\ 0 & 0 & \phi_{1,y} & \cdots \\ 0 & \phi_{1,y} & \phi_{1,x} & \cdots \\ -\phi_{1,y} & 0 & \phi_1 & \cdots \\ -\phi_{1,x} & \phi_1 & 0 & \cdots \end{bmatrix} \tag{2.24}$$

$$5 \times 3N$$

By using Hamilton's Principle the inertia matrix $[M]$, and the stiffness matrix $[K]$ can be obtained. These matrices are given by

$$[K] = \int_{A'} [B]^T [\mathcal{D}][B]|J|dA' \tag{2.25}$$

$$[M] = \int_{A'} [\phi]^T [m][\phi]|J|dA' \tag{2.26}$$

where $|J|$ is the determinant of the Jacobian of the transformation. The inertia density matrix $[m]$, with the presence of piezoelectric elements, is defined according to 2.16. The integrations in (2.25), and (2.26) are performed numerically by way of Gauss-Legendre quadrature.

2.4 Tests and Results

Initially, the plate finite element model was tested to determine the accuracy of the model in which the mass and stiffness of the piezoelectric layers have been ignored. The maximum deflection of a simply supported and clamped plate under normal load or centre point load is given in [31]. For the test, the force acting on the plate is assumed to be a concentrated load acting at the centre of the plate. The boundary conditions are considered to be simply supported and clamped.

To determine the sensitivity of the plate model to the mass of piezoelectric layers, the natural frequencies of a simply supported plate are examined. Table 2.2 shows the results of numerical simulation of a simply supported plate. From these results it is apparent that disregarding the mass and stiffness of the piezoelectric layers in the plate model does not alter the results by more than 0.2%. Overall, these two tests suggest that by ignoring the piezoelectric layers in a simply supported plate model, the results deviate less than 0.3% (from Table 2.2 there

Table 2.1: Maximum deflection of a plate under a static centre point load (FEM method)

Boundary conditions	Simply Supported	Clamped
FEM with PZT	16.6342mm	7.8762mm
FEM without PZT	16.6731mm	7.8952mm
Discrepancy%	0.2339	0.2412
$Plate = 0.5m \times 0.5m \times 0.815mm$		
$Piezoelectric = 5cm \times 2cm \times 0.3mm$		
$\rho_s = 2710\frac{Kg}{m^3}$ $\nu_s = 0.3$ $E_s = 70 \times 10^9 Pa$ $P = 20Pa$		
$\rho_a = 6800\frac{Kg}{m^3}$ $\nu_s = 0.3$ $E_a = 50 \times 10^9 Pa$		
$Piezoelectric\ locations = (0.25m, 0.25m), (0.25m, 0.125m), (0.125m, 0.25m)$ (0.25m,0.375m),(0.125m,0.375m)		

is 0.2339% discrepancy in the maximum deflection and from Table 2.4 there is 0.1970% discrepancy for the 3rd mode.)

In order to show that the present formulation can analyze different ranges of plate thicknesses and is free of shear locking, a series of tests on square plates under a variety of loading and boundary conditions were performed. For the test a $\frac{L}{t}$ ratio range from thick ($\frac{L}{t} = 1 \times 10^1$) to very thin ($\frac{L}{t} = 1 \times 10^7$) was considered, where L and t are the length and thickness of the plate respectively.

For the test a uniform normal load or a centre point load was applied to the simply supported or clamped plates for the length to thickness ratio range of $\frac{L}{t} \in [10^1, 10^7]$. The model is illustrated in Figure 2.3 where it should be noted that due to symmetry only one quarter of the plate is considered.

Table 2.2: Comparison of the FEM plate modes of vibration under different boundary conditions

Mode (Hz)	1st	2nd	3rd
FEM with PZT	14.4151	28.3831	43.6587
FEM without PZT	14.4015	28.3482	43.5727
Discrepancy%	0.0943	0.1230	0.1970
$Plate = 0.45m \times 0.65m \times 0.815mm$			
$Piezoelectric = 5cm \times 2cm \times 0.3mm$			
$\rho_s^{'} = 2710\frac{Kg}{m^3}$ $\nu_s = 0.3$ $E_s = 70 \times 10^9 Pa$			
$\rho_a = 6800\frac{Kg}{m^3}$ $\nu_s = 0.3$ $E_a = 50 \times 10^9 Pa$			

Table 2.3: Maximum deflection of a plate under static loading (analytical method [32])

Boundary conditions	Centre point load	Uniform normal load
Simply Supported	$0.0116\frac{PL^2}{D}$	$0.00416\frac{Q_0 L^4}{D}$
Clamped	$0.0056\frac{PL^2}{D}$	$0.00126\frac{Q_0 L^4}{D}$

For the test, two types of loading along with two different types of boundary conditions are considered. Initially the force acting on the plate is assumed to be a concentrated load acting at the centre of the plate, and later the load was considered to be a uniformly distributed load. In each trial simply supported boundary conditions or clamped boundary conditions are considered. In order to solve the

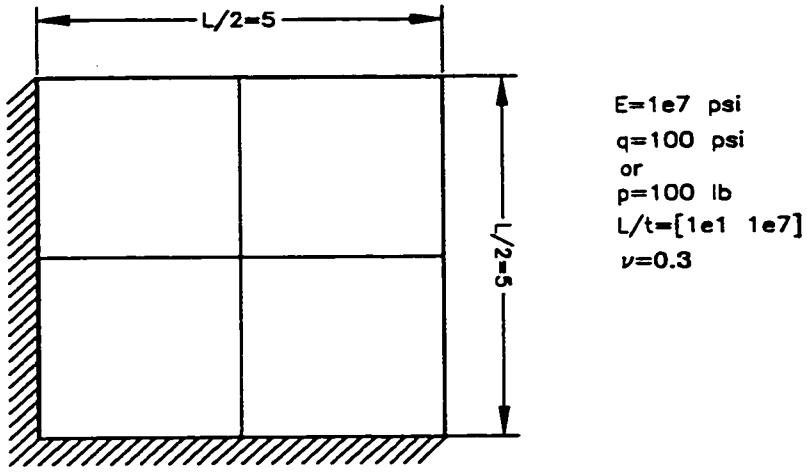

Figure 2.3: Square plate test model, $\frac{1}{4}$ plate symmetry used; edges may be simply supported or clamped.

problem, the plate is subdivided to one element per quarter plate and four elements per quarter plate.

The test results are shown in Figures 2.4, 2.5 where the discrepancy of maximum deflection for the computed solution and the exact thin plate solution [32] is plotted against the logarithm of the side length to thickness ratio. The large disagreement for $\frac{L}{t} = 10$ is due to thin plate theory being inapplicable in this range of aspect ratios while the large errors for $\frac{L}{t} = 10^7$ arise from numerical errors due to the finite computer word length and the extreme thinness of the model. From this result it is obvious that the plate element is not susceptible to shear locking and in addition possesses good convergence characteristics.

To validate the mass matrix, an analytical solution, as outlined in [33], for modes of vibration was used. The frequencies of vibration of a simply supported and cantilever plate are given in table 2.4, where n and m are the mode number for vibration in the a and b directions respectively. D, ρ, and t are the bending rigidity,

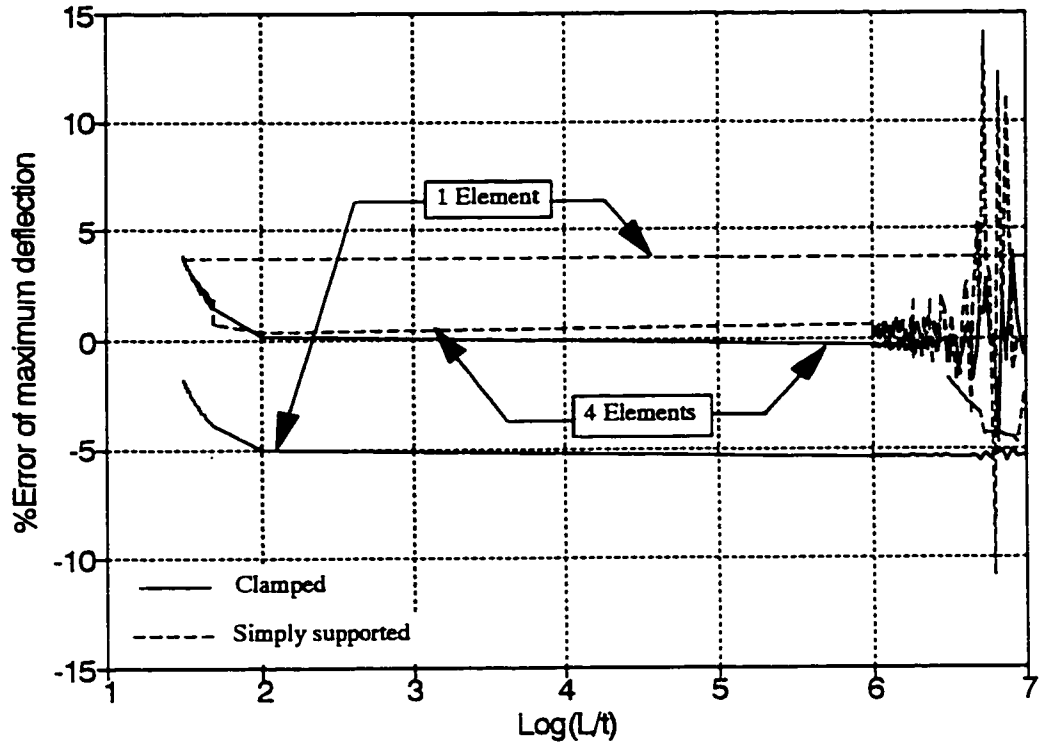

Figure 2.4: Uniform load on a square plate.

material density, and the plate thickness respectively. i is the mode of vibration and λ_i is a constant value and for $\frac{b}{a} = 2$, $\lambda_1 = 3.41$, $\lambda_2 = 21.3$, and $\lambda_3 = 59.7$.

A comparison between the analytical results and the finite element approximation for the first three modes of vibration is shown in Table 2.5. As can be seen for these two cases the percentage error for the first three modes is less than 0.5 percent.

Figure 2.6 displays the first four modes of a cantilever plate. As can be seen the first two modes are pure bending modes. In the third mode, a wave travels across

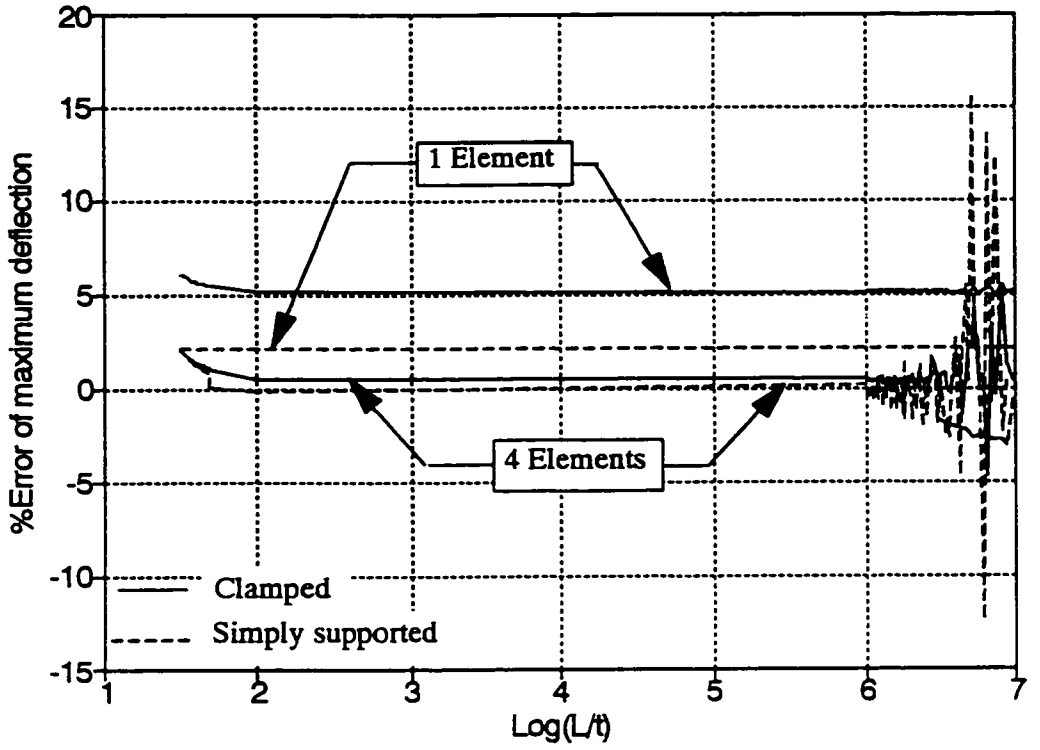

Figure 2.5: Point load on a square plate.

the width of the plate and it is a torsional mode. The forth mode is again a pure bending mode.

The frequency response functions of the finite element model has also been plotted (Figure 2.7) as outlined in [34].

Table 2.4: Natural frequencies of a plate (analytical method [33])

Boundary conditions	Natural Frequencies	Constants
Simply Supported	$\omega_{mn} = \pi^2((\frac{m}{a})^2 + (\frac{n}{b})^2)\sqrt{\frac{D}{\rho t}}$	$m, n = 1, 2, 3, ...$
Cantilever	$\omega_i = \frac{\lambda_i}{a^2}\sqrt{\frac{D}{\rho t}}$	$i = 1, 2, 3, ...$

2.5 Conclusion and Summary

The mathematical modelling of a plate with collocated piezoelectric actuators/sensors is presented. The basic theory of piezoelectricity and Mindlin plate theory is described. Then a mathematical model of the flexible structure is developed by considering the interaction between a typical piezoelectric actuator and the plate. A finite element formulation of plate elements with thin piezoelectric layers bonded to the surface as actuators/sensors is formulated in the form of the well known equations of structural dynamics. In this formulation, the Mindlin plate theory is utilized. By applying the Mindlin theory along with an appropriate choice of basis functions, the formulation can be used over a wide range of plate thicknesses, while avoiding shear locking, but still giving excellent accuracy and convergence characteristics. In order to show that the formulation can analyze different ranges of plate thicknesses, a series of tests on square plates under a variety of static loading and boundary conditions were performed. The comparison of the computed solution with the exact thin plate solution shows good agreement. To validate the mass matrix, the finite element modes of vibration are compared with analytical solutions. In this comparison, the vibration of a simply supported and a cantilever plate is considered. The two compared cases confirmed the accuracy of the model. The frequency response functions obtained using the finite element model for a simply

Table 2.5: Comparison of plate modes of vibration under different boundary conditions

Mode (Hz)	1st	2nd	3rd
Simply Supported			
Analytical	14.0542	32.1393	38.1320
FEM	14.0558	32.2125	38.2396
%difference	0.0114	0.2277	0.2822
$a = 0.4953m \quad b = 0.5715m \quad t = 0.000815m$ $\rho = 2710\frac{Kg}{m^3} \quad \nu = 0.3 \quad E = 70 \times 10^9 Pa$			
Cantilever			
Analytical	0.6803	4.2492	11.9098
FEM	0.6809	4.2575	11.9683
%Error	0.0882	0.1953	0.4912
$a = 2m \quad b = 1m \quad t = 0.000815m$ $\rho = 2710\frac{Kg}{m^3} \quad \nu = 0.3 \quad E = 70 \times 10^9 Pa$			

supported and a clamped plate is plotted.

The numerical examinations of a plate with/without piezoelectric layers indicate a maximum discrepancy of 0.3% between the two models. Based on this result, we will ignore the mass and the stiffness of the piezoelectric elements patched to the plate, allowing a model of a rectangular plate to be developed based on classical laminated plate theory.

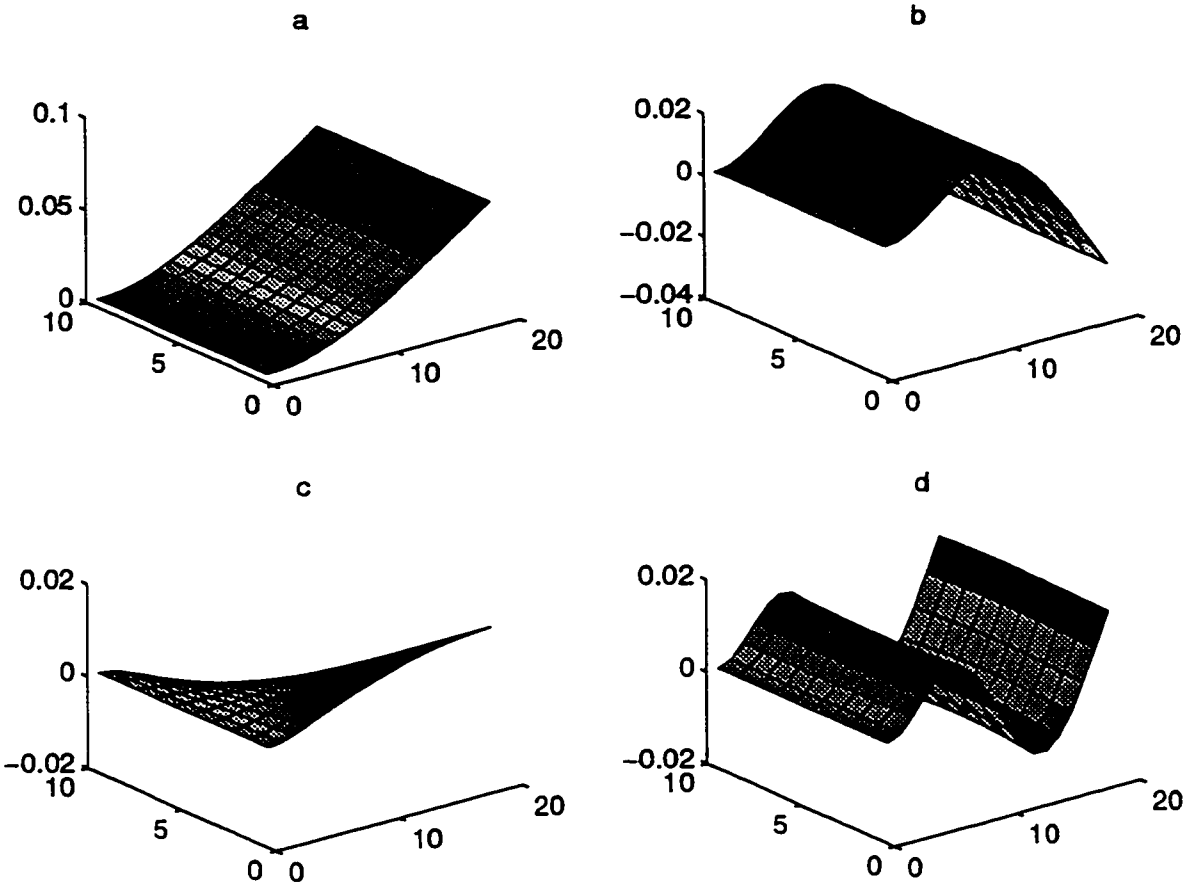

Figure 2.6: Mode shape predicted by finite element for cantilever plate (a) Mode 1. (b) Mode 2. (c) Mode 3. (d) Mode 4.

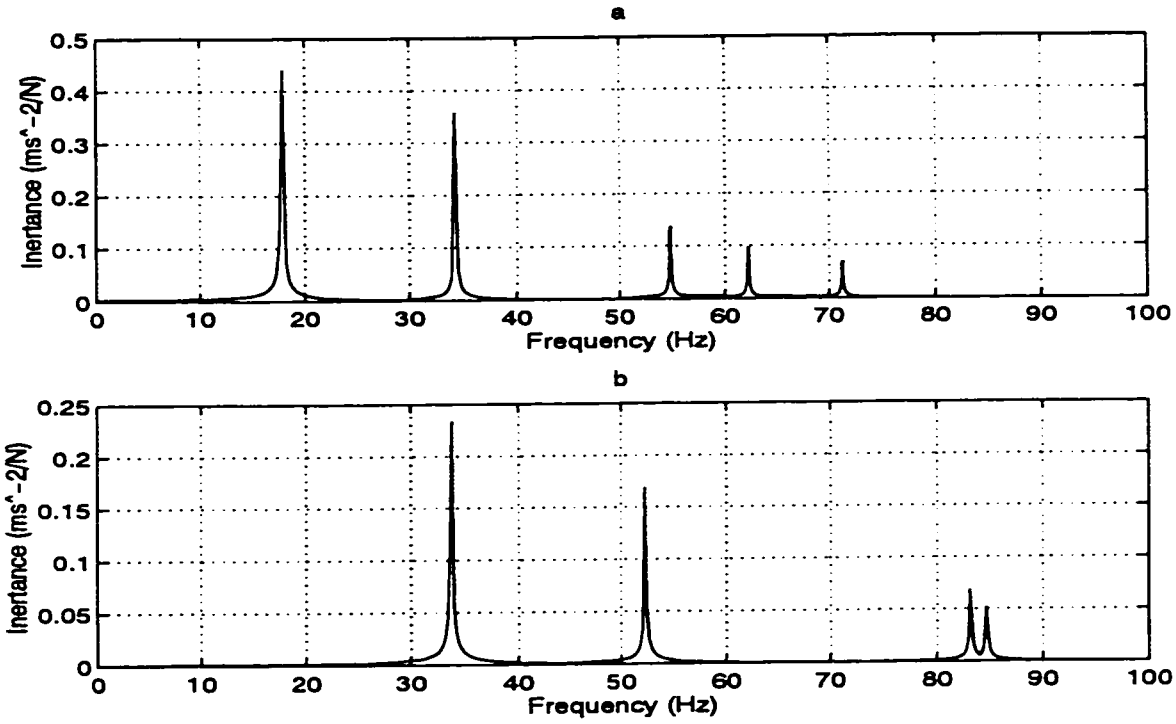

Figure 2.7: (a) Predicted Frequency Response Function by Finite Element Analysis for Simply Supported Plate. (b)Predicted Frequency Response Function by Finite Element Analysis for Clamped Plate.

Chapter 3

Mathematical Model

From earlier research, it can be seen that there are two major approaches to the analysis of laminated plates, the classical Poisson-Kirchhoff plate theory and the Reissner-Mindlin plate theory. Following the development of the Kirchoff plate equations, one finds that the order of the governing equations derived by neglecting transverse shearing deformations permits only two of the three obvious force conditions to be enforced at a free edge. Since the problem of the plate vibrations deals mainly with thin plates, this shortcoming appears to be largely academic and the elementary plate theory is adequate. However in the finite element formulation, the classical theory requires C^1 finite element interpolation functions which in comparison with C^0 finite element interpolation requirement for Mindlin theory is much more sophisticated. For this reason in the previous chapter we turned away from Poisson-Kirchoff type of elements to elements based upon theories which require only C^0 continuity. However in an analytical method, due to the simplicity of the classical theory, this theory is used to analyze the plate vibrations.

In this chapter a mathematical model of the transverse vibration of a plate to

be used for free and forced vibration control purposes is presented. For the analysis of plate flexural vibration, the eigenfunctions of a Poisson-Kirchoff plate have been used as basis functions in a Galerkin formulation. Separation of variables and a double Fourier expansion coupled with Navier's method are used to find the optimal location of the sensors/actuators. A quadratic control objective is defined as a measure of system performance. The control objective is composed of those error variables that are important to the design, and they are used to approximate the high order plant system by a lower order model. To guarantee that the error in the reduced model is smaller than the desired error, a minimum required number of modes in the plate model is specified. The application of the formulated techniques is illustrated via numerical example.

3.1 Introduction

This chapter focuses on the mathematical modelling of a plate with multiple layers of piezoelectric actuators. It addresses: (a) an analytical method of modeling the system, (b) optimization of the location of the sensors and actuators, and (c) approximation of a high-order plant and controller by low order models as part of the control system design process. A valuable reference for the analysis and design of composite structures is the broad literature review by Kapania and Raciti [2].

The development of a mathematical formulation for laminated plates has been investigated by many researchers [24] [35]. One major stream in this development is the analytical formulation. A significant number of investigations have been conducted on the analytical treatment of linear vibrations of laminated plates. Young [36] used Ritz's method to obtain approximate solutions for the frequencies and modes of vibration of thin elastic plates. Solutions were obtained for three specific

plate problems, namely, a square plate clamped at all four edges, a square plate clamped along two adjacent edges and free along the other two edges and a square plate clamped along one edge and free along the other three edges. Warburton [37] considered the free vibrations of rectangular plates with all possible boundary conditions obtained by combining free, freely supported, and fixed edges. The Rayleigh method, assuming waveforms similar to those of beams, was used to derive a simple approximate frequency expression for all modes of vibration. Rajalingham *et al.* [38] used the eigenfunctions of a clamped Poisson-Kirchoff plate as the basis functions in a Rayleigh-Ritz formulation of a clamped rectangular plate. The results showed that the specific choice of basis functions enhances the effectiveness of the Rayleigh-Ritz method.

An attempt has been made by Baz [39] to select the optimal geometrical parameters and locations of the piezoelectric elements on a beam under known static loading conditions. A modified independent modal space control method has been presented to select the optimal location, control gains and excitation voltage of the piezoelectric actuators. The method minimizes the vibration amplitudes of beams to which these actuators are bonded, as well as the input control effort necessary to suppress the vibrations. The results are applicable only to beams and cannot be directly used to optimize the locations of the actuators and sensors in plate applications.

The problem of model reduction has received considerable attention over the last two decades. The approximation of high-order plant and controller systems by lower order models is an integral part of the control system design process. The problem can be characterized by the availability of a high order parameterized model to which an appropriate low order approximation is sought. The aim is to provide a low order model which retains the effect of parameter changes. Various

properties of linear systems such as transfer functions, output correlations and cost functions, can be considered to preserve the exact properties of interest. Friswell [40] considered the problems of using high order finite element models to identify physical structural parameters with the time and frequency domain methods. Modal approximations, based either on current estimated eigenvectors or a first order eigenvector expansion in the parameter variations, have been recommended as the most suitable order reduction methods. The main reason for this recommendation is that modal truncation is the only method that guarantees no change in the natural frequencies of interest. Hankel norm model reduction with fixed modes is presented by Hung *et al.* [41]. This method can be described as a partial eigenvalue preservation method. The reduced order transfer function is allowed to have a set of free poles in addition to eigenvalues which are present from the original system due to physical considerations. This method can be used in conjunction with the dominant mode concept. It is equally feasible to retain some eigenvalues of particular interest and let the free poles take care of the dominant characteristics of the system. The frequency response matching is based on a minimum Hankel-norm criterion. Hughes *et al.* [42] discussed a technique for model reduction which simultaneously attempts to match a specified number of output covariance derivatives. The COVariance Equivalent Realizations which match q+1 covariance derivatives are called "q-COVERS". In general, q-COVERS are not unique and the additional freedom is so that the q-COVERS obtained also match q Markov parameters. The truncation technique uses a form of the observability matrices of the full order system to determine *a priori* the order required of the reduced order model to match a specified number of output covariance derivatives and Markov parameters. Yousuff *et al.* [43] developed a method for controller reduction, based upon the participation of the controller states in the value of a quadratic performance metric. The

controller states which have the smallest contribution to the performance metric are truncated to produce the reduced controllers. In this work an error index is also defined to evaluate the reduced controller compared to the optimal LQG controller and bounds on this index are derived.

In the following, the Poisson-Kirchoff plate theory will be used to study the transverse vibrations of a rectangular simply supported plate with attached piezoelectric actuators.

3.2 Theoretical Formulation

The mathematical model of the classical Poisson-Kirchoff plate is developed. Following the development of the Kirchoff plate equation, the plate eigenfunctions are used in a Galerkin formulation to study vibrations of rectangular plates.

3.2.1 Classical Plate-Bending Theory

Consistent with the assumptions for an Poisson-Kirchoff theory of plates it is assumed that axial loads and rotatory inertia are negligible, and that plane sections remain plane and normal (Figure 4.4). The governing differential equation of free vibration for a Poisson-Kirchoff plate is [32]:

$$D\nabla^4 w(x,y,t) + \rho h\ddot{w}(x,y,t) = 0 \qquad 0 \le x \le L_x \quad 0 \le y \le L_y \tag{3.1}$$

where $D = \frac{Eh^3}{12(1-\nu^2)}$ is the bending rigidity, E is the modulus of elasticity, h is the plate thickness, ν is Poisson's ratio and ρ is the mass density. The Galerkin method is one of several possible procedures for solving this equation. Assume that w is

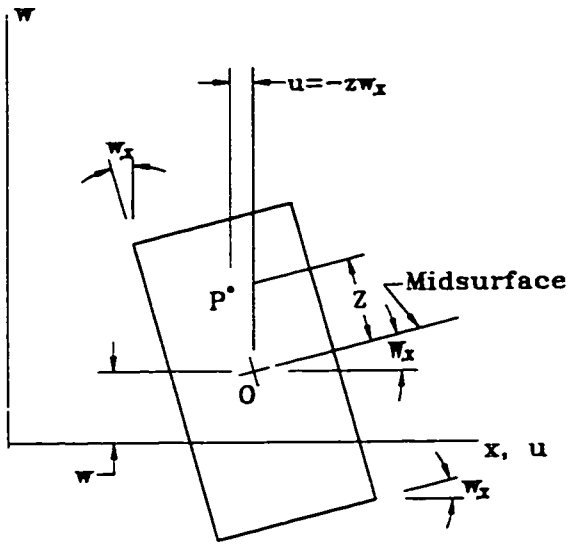

Figure 3.1: Kirchoff plate element after loading.

separable in space and time, such that:

$$w(x,y,t) = \phi_x(x)\phi_y(y)Z(t) \tag{3.2}$$

where ϕ_x and ϕ_y are the shape functions depending on x and y respectively and Z is a time dependent function. This may be substituted into equation (3.1) to yield:

$$D(\phi_x{}^{\mathrm{IV}}\phi_y + 2\phi_x{}^{\mathrm{II}}\phi_y{}^{\mathrm{II}} + \phi_x\phi_y{}^{\mathrm{IV}})Z + \rho h\phi_x\phi_y\ddot{Z} = 0 \quad 0 \le x \le L_x \quad 0 \le y \le L_y \tag{3.3}$$

where superscripts $^{\mathrm{II}}$ and $^{\mathrm{IV}}$ are the second and the fourth derivatives of the shape functions with respect to the subscript. Dividing through by $\rho h\phi_x\phi_y Z$, setting $\alpha = \frac{D}{\rho h}$, and equating the result to the separation constant λ yields separate equations in time and space expressed in symmetrical form by:

$$\alpha\left(\frac{\phi_x{}^{\mathrm{IV}}}{\phi_x} + 2\frac{\phi_x{}^{\mathrm{II}}\phi_y{}^{\mathrm{II}}}{\phi_x\phi_y} + \frac{\phi_y{}^{\mathrm{IV}}}{\phi_y}\right) = -\frac{\ddot{Z}}{Z} = \lambda \quad 0 \le x \le L_x \quad 0 \le y \le L_y \tag{3.4}$$

The spatial equation is readily shown to lead to an eigenvalue problem which, under various boundary conditions, has been formulated by Rajalingham *et al* [38]. For

simply supported plates the boundary conditions can be expressed as:

$$\begin{aligned} \phi_x(0) &= 0 \quad & \phi_y(0) &= 0 \\ \phi_x^{II}(0) &= 0 \quad & \phi_y^{II}(0) &= 0 \\ \phi_x(L_x) &= 0 \quad & \phi_y(L_y) &= 0 \\ \phi_x^{II}(L_x) &= 0 \quad & \phi_y^{II}(L_y) &= 0 \end{aligned} \tag{3.5}$$

For rectangular plates, with edges parallel to the x- and y- axes, it is expedient [31] to take the series approximation for w in the form

$$w(x,y,t) = \sum_{n=1}^{R} \sum_{m=1}^{S} \phi_{nx}(x)\phi_{my}(y)Z_{nm}(t) \tag{3.6}$$

where the infinite series is truncated at R and S modes and (x,y) are the coordinates with origin at a corner of the rectangular plate which spans the domain $x \in [0 \quad L_x]$ and $y \in [0 \quad L_y]$. In (3.6), ϕ_{nx} and ϕ_{my} must satisfy the essential and the natural boundary conditions. Substituting (3.6) into (3.1) and dropping the summations to consider only the pqth mode results in an equation in the form of (3.3). Now take the inner product of (3.3) with respect to $\phi_{mx}\phi_{ny}$, and use integration by parts, boundary conditions (3.5), and recognizing that (pq) and (mn) are interchangeable, the mass orthogonality relation may be found to be:

$$\int_0^{L_x} \int_0^{L_y} \rho\phi_{px}\phi_{qy}\phi_{nx}\phi_{my}dxdy = 0 \qquad p \neq n, \; q \neq m \tag{3.7}$$

Introducing an external forcing term $F(x,y,t)$ and an external moment per unit length $T(x,y,t)$ into (3.1) and assuming the series solutions (3.6) gives:

$$[\mathbf{m}]\{\ddot{Z}\} + [\mathbf{k}]\{Z\} = F(x,y,t) + T(x,y,t) \tag{3.8}$$

where $[\mathbf{m}]$, $[\mathbf{k}]$ are row vectors such that

$$\mathbf{m}_j = \rho h(\phi_{nx}\phi_{my}) \qquad j = R \times (m-1) + n \tag{3.9}$$

$$\mathbf{k}_j = D(\phi_{nx}{}^{\mathrm{IV}}\phi_{my} + 2\phi_{nx}{}^{\mathrm{II}}\phi_{my}{}^{\mathrm{II}} + \phi_{nx}\phi_{my}{}^{\mathrm{IV}}) \quad j = R \times (m-1) + n \tag{3.10}$$

and $\{Z\}$ is the time function vector in separation of variables. Now take the inner product of (3.8) with respect to $\frac{1}{\rho h}[\mathrm{m}]^T$ and integrate over the area to find:

$$[\mathcal{M}]\{\ddot{Z}\} + [\mathcal{K}]\{Z\} = [\overline{\mathcal{F}}] + [\overline{\mathcal{T}}] \tag{3.11}$$

where

$$\mathcal{M}_{ij} = \int_0^{L_x}\int_0^{L_y} \phi_{px}\phi_{qy} m_j dx dy \tag{3.12}$$

$$\mathcal{K}_{ij} = \int_0^{L_x}\int_0^{L_y} \phi_{px}\phi_{qy} k_j dx dy \tag{3.13}$$

$$\overline{\mathcal{F}}_i = \int_0^{L_x}\int_0^{L_y} \phi_{px}\phi_{qy} F(x,y,t) dx dy \tag{3.14}$$

$$\overline{\mathcal{T}}_i = \int_0^{L_x}\int_0^{L_y} \phi_{px}\phi_{qy} T(x,y,t) dx dy \tag{3.15}$$

where $i = R \times (q-1) + p$. For a simply supported plate the deflections $w(x,y)$ can be expressed by the double sine series [31], such that

$$\phi_{nx}(x) = \mathcal{A}\sin(\frac{n\pi x}{L_x}) \qquad \phi_{my}(y) = \mathcal{B}\sin(\frac{m\pi y}{L_y}) \tag{3.16}$$

Upon substituting (3.16) into equation (3.11), and normalizing the mass matrix to identity by choosing $\mathcal{A} = \left[\frac{4}{\rho h L_x^2}\right]^{\frac{1}{4}}$ and $\mathcal{B} = \left[\frac{4}{\rho h L_y^2}\right]^{\frac{1}{4}}$ we obtain

$$\{\ddot{Z}\} + \lceil\Omega\rfloor\{Z\} = [\mathcal{F}] + [\mathcal{T}] \tag{3.17}$$

where $\lceil\cdot\rfloor$ denotes a diagonal matrix and

$$\lceil\Omega\rfloor = \lceil\omega^2\rfloor \qquad \lceil\omega\rfloor = \lceil\omega_{11},\cdots,\omega_{ij},\cdots\rfloor \qquad \omega_{ij} = \sqrt{\frac{D}{\rho h}}\left[\left(\frac{i\pi}{L_x}\right)^2 + \left(\frac{j\pi}{L_y}\right)^2\right] \tag{3.18}$$

By introducing Rayleigh damping, the system equation (3.17) can be rewritten as

$$\{\ddot{Z}\} + \lceil\mathcal{C}\rfloor\{\dot{Z}\} + \lceil\Omega\rfloor\{Z\} = [\mathcal{F}] + [\mathcal{T}] \tag{3.19}$$

where

$$\lceil\mathcal{C}\rfloor = 2\lceil\zeta\rfloor\lceil\omega\rfloor = \lceil 2\zeta_{11}\omega_{11},\cdots,2\zeta_{ij}\omega_{ij},\cdots\rfloor, \qquad \lceil\zeta\rfloor = \lceil\zeta_{11},\cdots,\zeta_{ij},\cdots\rfloor \tag{3.20}$$

and ζ_{ij} is the damping factor for mode ij.

The forcing term may now be addressed. Assuming a point load applied at $x = \xi$ and $y = \eta$ (3.14) yields:

$$\mathcal{F}_i(\xi, \eta, t) = \int_0^{L_x} \int_0^{L_y} \phi_{px}(x)\phi_{qy}(y)W(t)\delta(x - \xi, y - \eta)dxdy \tag{3.21}$$

where, δ is Dirac delta function and $W(t)$ is the magnitude of the point force at time t. Therefore the modal forcing term can be written as:

$$\mathcal{F}_i(\xi, \eta, t) = \phi_{px}(\xi)\phi_{qy}(\eta)W(t) = \gamma_{f_i}W(t) \tag{3.22}$$

where, γ_{f_i} is a parametric gain depending on the location of the load and $W(t)$ is the magnitude of the point force at time t. In the case of simply supported plates the parametric gain is equal to

$$\gamma_{f_i} = \sqrt{\frac{4}{\rho h L_x L_y}} \sin(\frac{p\pi\xi}{L_x}) \sin(\frac{q\pi\eta}{L_y}) \tag{3.23}$$

Under an assumption of perfect bonding, the piezoelectric actuators produce a bending moment on the plate. In that case, the forcing terms may be treated as a superposition of point moments acting at the edges of the piezoelectric elements. In all the currently avaiable piezoelectric actuators, the moments are applied about x and y axes simultaneously. The moments are either equal (ceramic) or anisotropic (PVDF). In this work, since we assume a large aspect ratio between length of piezoelectric element in two diffent directions, the effect of piezoelectric element in the shorter direction will be ignored.

Assuming a point moment with the magnitude of $U(t)$ applied at $x = \xi$, $y = \eta$ and replacing the moment with a coupled force $U(t) = W(t)\epsilon$, the modal effect of the point moment can be written as:

$$\mathcal{T}_i(\xi, \eta, t) = \lim_{\epsilon \to 0} \int_0^{L_x} \int_0^{L_y} \phi_{px}\phi_{qy}W(t) \left[\delta(x - \xi, y - \eta) - \delta(x - \xi, y - \eta + \epsilon)\right] dxdy \tag{3.24}$$

where ϵ is the moment arm between the forces and the point moment assumed to be applied around x axis.

Now, the modal contribution of the point moment can be computed as:

$$\mathcal{T}_i(\xi,\eta,t) = \phi_{px}(\xi)\phi'_{qy}(\eta)U(t) \tag{3.25}$$

where ϕ'_{qy} is the derivative of the shape function with respect to y.

When an actuator is located at $x = \xi$, $y = \eta$ and is oriented in the x direction the modal effect of the piezoelectric element can be written as:

$$\left[\mathcal{T}_i(\xi - \frac{L_p}{2},\eta,t) - \mathcal{T}_i(\xi + \frac{L_p}{2},\eta,t)\right] = \gamma_{xu_i}U(t) \tag{3.26}$$

where, L_p is the length of the piezoelectric actuator, $U(t)$ is the magnitude of the moment applied at either end of the piezoelectric and $\gamma_{xu_{pq}}$ is a parametric gain term in the x direction resulting from the modal contribution of the point moments. $\gamma_{xu_{pq}}$ will be implemented electrically as a piezoelectric gain and is defined by

$$\gamma_{xu_i} = \left[\phi'_{px}(\xi - \frac{L_p}{2}) - \phi'_{px}(\xi + \frac{L_p}{2})\right]\phi_{qy}(\eta) \tag{3.27}$$

For a simply supported plate $\gamma_{xu_{pq}}$ can be evaluated from

$$\gamma_{xu_i} = \sqrt{\frac{16p^2\pi^2}{\rho h L_x^3 L_y}}\sin(\frac{p\pi\xi}{L_x})\sin(\frac{p\pi L_p}{2L_x})\sin(\frac{q\pi\eta}{L_y}) \tag{3.28}$$

When the actuator is oriented in the y direction the effect of the piezoelectric can be found by interchanging x and y, and ξ and η in (3.28).

3.2.2 Solution of the State Equations

A dynamical system of a finite number of lumped elements may be described by ordinary differential equations in which time is the independent variable. By use

of vector matrix notation, an nth-order differential equation may be expressed by a first order vector matrix differential equation. If n elements of the vector are a set of state variables, then the vector matrix differential equation is called a state equation. Considering the state equation of a linear, causal and relaxed system of the form

$$\dot{\mathcal{Z}}(t) = A(t)\mathcal{Z}(t) + B(t)\mathcal{U}(t) + D(t)\mathcal{W}(t) \tag{3.29}$$

$$w(x,y,t) = C(x,y,t)\mathcal{Z}(t) + H(x,y,t)\mathcal{U}(t) + J(x,y,t)\mathcal{W}(t) \tag{3.30}$$

The unique solution of (3.30) is given as [23]

$$w(x,y,t) = C\varphi(t_0,t) + C\int_{t_0}^{t}\varphi(t,\tau)[B\mathcal{U}(\tau) + D\mathcal{W}(\tau)]d\tau + H\mathcal{U}(t) + J\mathcal{W}(t) \tag{3.31}$$

where $\varphi(t_0,t)$ is the state transition matrix for A, and t_0 and t are any specified times.

Considering the second order linear time invariant system (3.19) with no direct transformation, the state equation can be written as

$$\begin{aligned} \dot{\mathcal{Z}}(t) &= A\mathcal{Z}(t) + B\mathcal{U}(t) + D\mathcal{W}(t) \\ w(x,y,t) &= C\mathcal{Z}(t) \end{aligned} \tag{3.32}$$

where

$$\mathcal{Z}(t) = \begin{Bmatrix} Z(t) \\ \dot{Z}(t) \end{Bmatrix} \quad A = \begin{bmatrix} 0 & I \\ -\Omega & -C \end{bmatrix} \quad B = \begin{bmatrix} 0 \\ \gamma_u \end{bmatrix} \quad D = \begin{bmatrix} 0 \\ \gamma_f \end{bmatrix} \tag{3.33}$$

By applying the linear transformation E, the matrix A can be written in Jordan canonical form as:

$$[J] = [\mathsf{E}]^{-1}[A][\mathsf{E}] = \begin{bmatrix} \Lambda & 0 \\ 0 & \overline{\Lambda} \end{bmatrix} \tag{3.34}$$

where

$$[\mathsf{E}] = \begin{bmatrix} I & I \\ \Lambda & \overline{\Lambda} \end{bmatrix} \quad [\mathsf{E}]^{-1} = \begin{bmatrix} [\overline{\Lambda} - \Lambda]^{-1}\overline{\Lambda} & -[\overline{\Lambda} - \Lambda]^{-1} \\ -[\overline{\Lambda} - \Lambda]^{-1}\Lambda & [\overline{\Lambda} - \Lambda]^{-1} \end{bmatrix} \tag{3.35}$$

where $\Lambda = [-\zeta\omega + j\omega\sqrt{I-\zeta^2}]$, $\overline{\Lambda} = [-\zeta\omega - j\omega\sqrt{I-\zeta^2}]$ and the natural frequency matrix ω and the damping factor matrix ζ are defined in (3.18) and (3.20) respectively.

Now, by choosing the damped frequency matrix $\omega_d = \omega\sqrt{I-\zeta^2}$ the state transition matrix of A can be computed as follows:

$$e^{At} = \mathsf{E}e^{Jt}\mathsf{E}^{-1} = \begin{bmatrix} e^{-\zeta\omega t}[\cos(\omega_d t) + \frac{\zeta\omega}{\omega_d}\sin(\omega_d t)] & \frac{e^{-\zeta\omega t}}{\omega_d}\sin(\omega_d t) \\ -\frac{\omega^2 e^{-\zeta\omega t}}{\omega_d}\sin(\omega_d t) & e^{-\zeta\omega t}[\cos(\omega_d t) - \frac{\zeta\omega}{\omega_d}\sin(\omega_d t)] \end{bmatrix} \tag{3.36}$$

where the following matrix relations have been used

$$e^{\Lambda t} + e^{\overline{\Lambda} t} = 2e^{-\zeta\omega t}\cos(\omega_d t) \qquad e^{\Lambda t} - e^{\overline{\Lambda} t} = 2je^{-\zeta\omega t}\sin(\omega_d t) \tag{3.37}$$

For lightly damped structures, $\zeta \ll I$, in which case

$$e^{At} = \mathsf{E}e^{\Lambda t}\mathsf{E}^{-1} = \begin{bmatrix} e^{-\zeta\omega t}[\cos(\omega t) + \zeta\sin(\omega t)] & \frac{e^{-\zeta\omega t}}{\omega}\sin(\omega t) \\ -\omega e^{-\zeta\omega t}\sin(\omega t) & e^{-\zeta\omega t}[\cos(\omega t) - \zeta\sin(\omega t)] \end{bmatrix} \tag{3.38}$$

For the case of no direct transformation and $t_0 = 0$, the system dynamic response can be written as

$$w(x,y,t) = Ce^{At}\mathcal{Z}(0) + C\int_0^t e^{A(t-\tau)}B\mathcal{U}(\tau)d\tau \tag{3.39}$$

Now position and velocity states can be separated by defining C as

$$C = \begin{bmatrix} P & 0 \\ 0 & R \end{bmatrix} \tag{3.40}$$

The impulse response can be found as

$$w(x,y,t) = Ce^{At}B = \begin{bmatrix} P\frac{e^{-\zeta\omega t}}{\omega}\sin(\omega t)\gamma_f \\ Re^{-\zeta\omega t}[\cos(\omega t) - \zeta\sin(\omega t)]\gamma_f \end{bmatrix} \tag{3.41}$$

The above state space solution will be employed to illustrate a numerical example. In the following, an analytical method will be considered to find the optimal location of sensors/actuators.

3.3 Optimization of Actuator/Sensor Locations

The size and the location of the piezoelectric actuators are two important issues to guarantee the highest energy efficiency and controllability of the system. As well, the appropriate location of the sensors has to be considered for system observability and minimum noise-sensor output ratio. In the following a process of optimization for sensor/actuator placement is described.

3.3.1 Formulation of the Problem

The governing differential equation of forced vibration for a Poisson-Kirchoff plate is:

$$D\nabla^4 w(x,y,t) + \rho h \frac{\partial^2 w(x,y,t)}{\partial t^2} = T(x,y,t) \tag{3.42}$$

where $T(x,y,t)$ is the external bending moment applied to the unit length of the plate. Now consider a simply supported plate, subject to a concentrated moment, which varies harmonically with time at point $A(\xi,\eta)$ as illustrated in Figure 4.5, *i.e.*

$$T(x,y,\xi,\eta,t) = \psi(x,y,\xi,\eta)U(t) = \psi(x,y,\xi,\eta)\sin\omega_f t \tag{3.43}$$

We seek the solution for (3.42) in two parts as follow:

$$w(x,y,t) = w_H(x,y,t) + w_P(x,y,t) \tag{3.44}$$

where suffix H denotes the complementary solution and P the particular solution. The time invariant part of the forcing function can be represented by the double trigonometric series [31]:

$$\psi(x,y) = \sum_{n=1}^{\infty}\sum_{m=1}^{\infty} \Gamma_{nm}(\xi,\eta)\sin(\frac{m\pi x}{L_x})\sin(\frac{n\pi y}{L_y}) \tag{3.45}$$

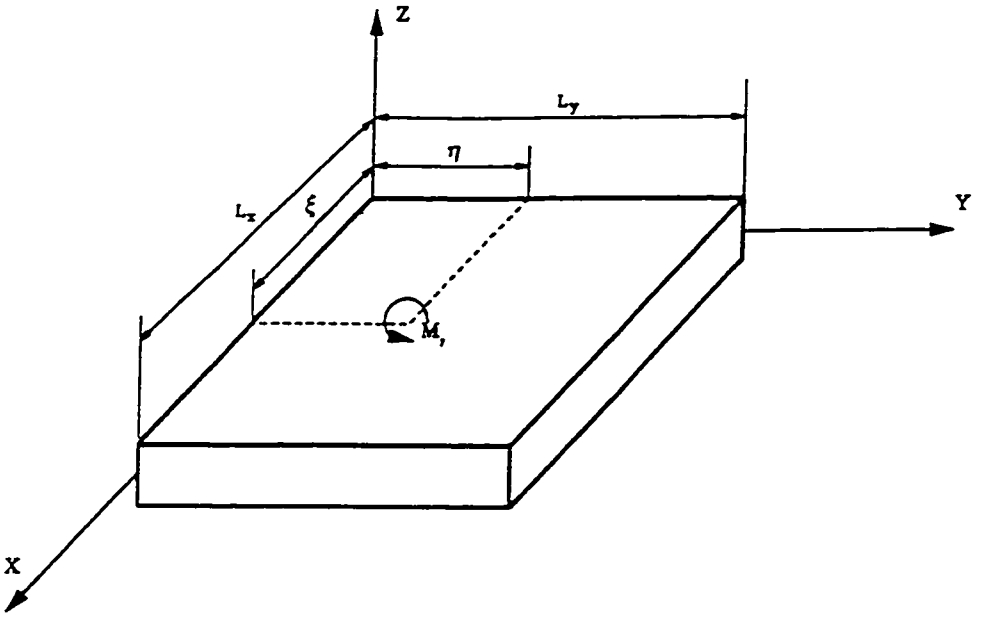

Figure 3.2: Simply Supported Plate with a Concentrated Moment

where the constants of the Fourier expansion of the load are [31]

$$\Gamma_{nm}(\xi,\eta) = \frac{4M_y n}{\pi^3 L_x^2 L_y D}\cos(\frac{n\pi\xi}{L_x})\sin(\frac{m\pi\eta}{L_y}) = \overline{\Gamma}_{nm}\cos(\frac{n\pi\xi}{L_x})\sin(\frac{m\pi\eta}{L_y}) \qquad (3.46)$$

n, m are the mode numbers, L_x, L_y are dimensions of the plate and M_y is the moment applied to the plate. In accordance with Navier's method we shall look for the particular solution in the form:

$$w_p(x,y,t) = \sin\omega_f t \sum_{n=1}^{\infty}\sum_{m=1}^{\infty} D_{nm}\sin(\frac{m\pi x}{L_x})\sin(\frac{n\pi y}{L_y}) \qquad (3.47)$$

The substitution of (3.47) into the governing differential equation of motion (3.42), using a specific set of n,m values, yields:

$$D_{nm}[D\pi^4(\frac{m^2}{L_x^2}+\frac{n^2}{L_y^2})^2 - \rho h\omega_f^2] = \Gamma_{nm} \qquad (3.48)$$

The first term inside the square brackets in equation (3.48) can be expressed in terms of the free vibration frequency (3.18) to yield:

$$D_{nm} = \frac{\Gamma_{nm}}{\rho h \omega_{nm}^2 (1 - \frac{\omega_f^2}{\omega_{nm}^2})} \tag{3.49}$$

If the time dependent changes of the excitation are very slow, ω_f will be small in comparison with ω_{nm} and the displacements will correspond to those obtained from the static loading.

The lateral deflection of a freely vibrating simply supported plate can be expressed by:

$$w_H = \sum_{n=1}^{\infty} \sum_{m=1}^{\infty} A_{nm} \sin \frac{n\pi x}{L_x} \sin \frac{m\pi y}{L_y} \sin(\omega_{mn} t - \phi) \tag{3.50}$$

where A_{nm} is amplitude, and ϕ represents the phase angle and can be determined from the initial conditions. If the initial conditions are $w = 0$ and $\dot{w} = 0$ at $t = 0$, for instance, then ϕ is zero.

We now assume the simultaneous action of free and forced vibrations. The superposition of free and forced vibration can be written as

$$w(x,y,t) = \sum_{n=1}^{\infty} \sum_{m=1}^{\infty} \sin(\omega_f t) \times [D_{nm} \sin(\frac{m\pi x}{L_x}) \sin(\frac{n\pi y}{L_y})] + A_{nm} \sin \frac{n\pi x}{L_x} \sin \frac{m\pi y}{L_y} \sin(\omega_{mn} t - \phi) \tag{3.51}$$

Under the assumption of a velocity initial condition of $\dot{w} = 0$ we obtain

$$A_{mn} = -\frac{\omega_f}{\omega_{mn}} D_{nm} \tag{3.52}$$

By substituting (3.52) into (3.51) the solution for (3.42) can be rewritten as:

$$w(x,y,t) = \sum_{n=1}^{\infty} \sum_{m=1}^{\infty} [\sin(\omega_f t) - \frac{\omega_f}{\omega_{nm}} \sin(\omega_{nm} t)] D_{nm} \sin(\frac{n\pi x}{L_x}) \sin(\frac{m\pi y}{L_y}) \tag{3.53}$$

where D_{nm} is calculated from equation (3.49). A similar approach can be taken when the excitation is not a simple harmonic but is of arbitrary period or even

transient. For such conditions, we express the time dependent parts in a Fourier series and obtain the dynamic response of the system by using superposition. The response of the system for an actuator with the influence length of L_p is given by

$$w = \sum_{n=1}^{\infty}\sum_{m=1}^{\infty}[\sin(\omega_f t) - \frac{\omega_f}{\omega_{nm}}\sin(\omega_{nm}t)]\frac{\Gamma_{mn}(\xi,\eta)}{\rho h(\omega_{nm}^2 - \omega_f^2)}\sin(\frac{n\pi x}{L_x})\sin(\frac{m\pi y}{L_y}) \quad (3.54)$$

where

$$\Gamma_{nm}(\xi,\eta) = \Gamma_{1nm}(\xi - \frac{L_p}{2},\eta) - \Gamma_{2nm}(\xi + \frac{L_p}{2},\eta) \quad (3.55)$$

Now the deflection shapes can be expressed as separable functions of actuator location, actuator length and deflection coordinates and time as

$$w(\xi,\eta,x,y,t) = \sum_{n=1}^{\infty}\sum_{m=1}^{\infty}\overline{w}(x,y,t)\sin(\frac{n\pi L_p}{2L_x})\sin(\frac{n\pi\xi}{L_x})\sin(\frac{m\pi\eta}{L_y}) \quad (3.56)$$

It is clear that to maximize the effect of the control inputs on the system one should maximize the sine functions in (3.56). For instance the optimal location function for the first mode has a half sine distribution in the x and y directions. This means that to control the first mode, the best location for a piezoelectric actuator is at $\frac{L_x}{2}$ and $\frac{L_y}{2}$. However, by doing this, there is no participation of the even modes of either direction and the system is not controllable. At least one more actuator is needed to control an even mode. Similar to the problem of controllability, the observability of the system can be investigated, where now ξ and η in (3.56) are the location of the sensor. If one needs the (n,m)th mode to be observable, ξ and η must be chosen such that the two participating sine functions in that mode do not go to zero.

When M_x is applied, the plate deflection shapes can be found by interchanging ξ and η, m and n, and L_x and L_y in (3.56). Therefore the optimal size and location

of the piezoelectric actuator for applied M_x gives similar results as when M_y has been applied.

Now we consider only one term in (3.53), when the frequency of the forcing function, ω_f, is approximately the same magnitude as one of the free vibration frequencies, ω_{mn}.

$$\omega_{nm} - \omega_f = 2\delta_{nm} \tag{3.57}$$

Since the two frequencies are nearly equal, δ_{nm} represents a small quantity and $\frac{\omega_f}{\omega_{mn}} \approx 1$. Therefore a selected set of values for n and m in (3.53) can be written as:

$$w_{nm} = -2D_{nm}\sin(\delta_{nm}t)\cos(\frac{(\omega_f + \omega_{nm})t}{2})\sin(\frac{n\pi x}{L_x})\sin(\frac{m\pi y}{L_y}) \tag{3.58}$$

Since δ_{nm} is a small quantity $\sin(\delta_{nm}t)$ varies slowly, with the large period $2\pi/\delta_{nm}$. Whenever the frequency of the excitation is close to the natural frequency of the system we will have a beat phenomenon and when $\omega_f = \omega_{nm}$ the amplitude will increase without bound (Figure 4.6). The beating phenomena can be employed to transfer energy between coupled oscillatory systems for the purpose of vibration suppression [44].

3.4 Modal Cost Analysis

It is a common practice in the control design and analysis of mechanical systems to construct a mathematical model which ignores some of the dynamic feedback paths or couplings in the physical system. This is often due to a desire to work with a finite dimensional model.

As a measure of system performance a quadratic control objective composed of those error variables that are of importance to the design is introduced. The

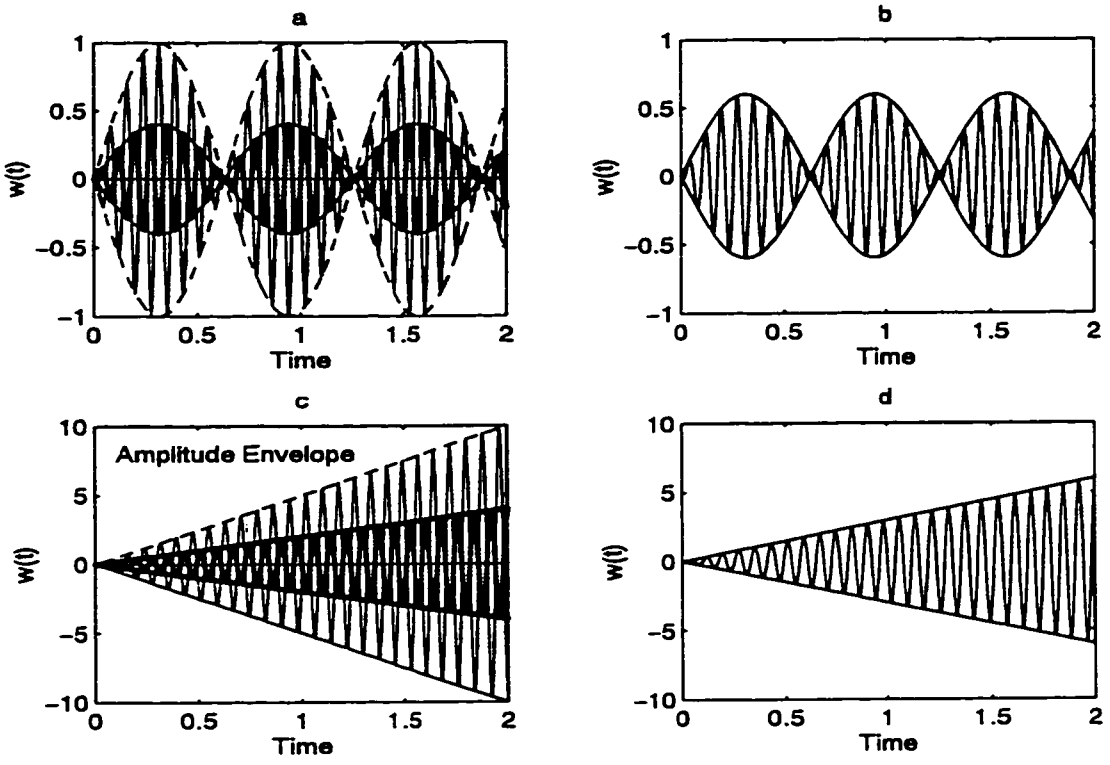

Figure 3.3: a) Beat phenomenon in plate and actuator ($\omega_{mn} \approx \omega_f$), b) Resultant response of the plate and actuator in a, c) Beat phenomenon in plate and actuator ($\omega_{mn} = \omega_f$), d) Resultant response of the plate and actuator in c

.

smaller the error variables, the better is the performance and hence the norm of the vector of error variables is an important measure of performance. Consider the linear state space system (3.19)

$$\dot{\mathcal{Z}}(t) = A\mathcal{Z}(t) + B\mathcal{U}(t) + D\mathcal{W}(t) \tag{3.59}$$

$$w(x,y,t) = C\mathcal{Z}(t) \tag{3.60}$$

where $\mathcal{U}$ is the "control" vector with its ith input given as $\mathcal{U}_i(t) = \overline{u}_i\delta(t)$ and where $\mathcal{W}$ is a vector of "disturbances" with its ith input given as $\mathcal{W}_i(t) = \overline{w}_i\delta(t)$. Both are

impulses of strength $\overline{u}_i$ and $\overline{w}_i$ respectively. By considering the root mean square (RMS) of the error as an important performance measure, the "cost function" V is defined by:

$$V = \sum_{i=1}^{n} \int_0^\infty w^{i^T}(t) Q w^i(t) dt \tag{3.61}$$

where $w^i(t)$, $i = 1, 2, ..., n_z + n_w + n_U$ are the responses from the sequence of excitations from initial conditions, disturbances and inputs acting alone. Q is a weighting matrix. Defining the state covariance matrix X as:

$$X = \sum_{i=1}^{n} \int_0^\infty \mathcal{Z}^i(t) \mathcal{Z}^{i^T}(t) dt = \sum_{i=1}^{n} C_{zz}(0) \tag{3.62}$$

and the output covariance as:

$$R_0 = \sum_{i=1}^{n} \int_0^\infty w^i(t) w^{i^T}(t) dt = CXC^T \tag{3.63}$$

the value of the cost function is given by [28]:

$$V = trXC^TQC = trK\Gamma \tag{3.64}$$

where X and K satisfy

$$0 = KA + A^TK + C^TQC \tag{3.65}$$

$$0 = X_{zwU}A^T + AX_{zwU} + \Gamma \tag{3.66}$$

with

$$\Gamma = (\Gamma_{z_0} + D\Gamma_w D^T + B\Gamma_U B^T) \tag{3.67}$$

$$\Gamma_{z_0 ij} = \mathcal{Z}_i^2(0)\delta_{ij} \tag{3.68}$$

$$\Gamma_{w_{ij}} = \overline{w}_i^2 \delta_{ij} \tag{3.69}$$

$$\Gamma_{U_{ij}} = \overline{u}_i^2 \delta_{ij} \tag{3.70}$$

The contribution of each state to the controlled (or disturbance) part of the cost function is

$$V_{z_i} = \frac{1}{2}\int_0^\infty [\sum_{\alpha=1}^{n_U(n_W)} (\frac{\partial Z^\alpha Q Z^\alpha}{\partial Z_i^\alpha}) Z_i^\alpha] dt = [CXC^T Q]_{ii} \tag{3.71}$$

where V_{z_i} is called the ith component of cost [42] and represents the contribution of state variable Z_i in the cost function. The contribution of the αth input (control input or disturbance) to the output cost V_{z_i} is given by [45]

$$V_{z_i}^\alpha = [CC_{zz}(0)C^T Q]_{ii} \tag{3.72}$$

Theorem 1 *(Skelton [46]) For the asymptotically stable, nondefective system*

$$\dot{\mathcal{Z}}_i(t) = \lambda_i \mathcal{Z}_i + b_i^* \mathcal{U}(t) \tag{3.73}$$

$$w(x,y,t) = \sum_{i=1}^{n_x} C_i \mathcal{Z}_i \tag{3.74}$$

where $i = 1, \ldots, n_x$, define ζ_i, ω_i by

$$\lambda_i = -\zeta_i\omega_i + j\omega_i\sqrt{1-\zeta_i^2}, \qquad \zeta_i > 0, \qquad \omega_i > 0 \tag{3.75}$$

and let $\lambda_{i+1} = \bar{\lambda}_i$, for some i. Suppose $b_i \neq 0$, $c_i \neq 0$. Then, if any of the following hold

$$\begin{aligned} &i) && b_i^* \Gamma_U b_k = 0 && k \neq i, \\ &ii) && c_k^* Q c_i = 0 && k \neq i, \\ &iii) && \zeta_i \ll \tfrac{|\omega_i - \omega_k|}{2\omega_i} && k \neq i \end{aligned} \tag{3.76}$$

the ith modal cost is given by

$$V_{z_i} = V_{z_{ii}} = \frac{||b_i||^2 \mathcal{U} ||c_i||^2 Q}{2\zeta_i\omega_i} + O(\zeta_i) \tag{3.77}$$

where $O(\zeta_i)$ is zero under conditions (i) or (ii) and is of order ζ_i otherwise.

Corollary 1 *(Skelton [46]) For the asymptotically stable system described by*

$$\ddot{Z}_i + 2\zeta_i\omega_i\dot{Z}_i + \omega_i^2 Z_i = b_i^* U \qquad i = 1, \ldots, N \tag{3.78}$$

$$w = \sum_{i=1}^{N} \phi_{ixy} Z_i \qquad \dot{w} = \sum_{i=1}^{N} \phi_{ixy} \dot{Z}_i \tag{3.79}$$

the modal cost associated with $Z_i(t)$ for the cost function

$$V = \sum_{i=1}^{N} \int_0^\infty \left\{ \begin{array}{cc} w^{i^T} & \dot{w}^{i^T} \end{array} \right\} \left[\begin{array}{cc} Q_p & 0 \\ 0 & Q_v \end{array} \right] \left\{ \begin{array}{c} w^{i^T} \\ \dot{w}^{i^T} \end{array} \right\} dt \tag{3.80}$$

with impulsive inputs is given by

$$V_{z_i} \cong \frac{b_i^* \Gamma_U b_i [\phi_{ixy}^T (Q_p + \omega_i^2 Q_v) \phi_{ixy}]}{4\zeta_i \omega_i^3} \tag{3.81}$$

where $\Gamma_{U_{ij}} = \gamma_{U_{ij}}^2 \delta_{ij}$.

For a simply supported plate, the modes of vibrations are described by (3.16). Considering an impulsive point force $\gamma_f W(t)$ at (L_{xf}, L_{yf}), the impulsive control inputs $\gamma_{xu1}U(t)$, $\gamma_{xu2}U(t)$, $\gamma_{xu3}U(t)$, $\gamma_{yu4}U(t)$, $\gamma_{yu5}U(t)$, and $\gamma_{yu6}U(t)$ at locations $(\frac{L_x}{2}, \frac{L_y}{2})$, $(\frac{L_x}{4}, \frac{L_y}{2})$, $(\frac{3L_x}{4}, \frac{L_y}{2})$, $(\frac{L_x}{2}, \frac{L_y}{2})$, $(\frac{L_x}{2}, \frac{L_y}{4})$, $(\frac{L_x}{2}, \frac{3L_y}{4})$ respectively (the optimal locations obtained in section 3.3 to control the first three modes), and the unit weight function $Q = I$, the modal cost analysis is given as

$$b_i = \left\{ \begin{array}{ccccccc} \gamma_f & \gamma_{xu1} & \gamma_{xu2} & \gamma_{xu3} & \gamma_{yu4} & \gamma_{yu5} & \gamma_{yu6} \end{array} \right\} \tag{3.82}$$

$$\Gamma_u = \left[\begin{array}{ccccccc} \overline{w}_i^2 & \overline{u}_{i1}^2 & \overline{u}_{i2}^2 & \overline{u}_{i3}^2 & \overline{u}_{i4}^2 & \overline{u}_{i5}^2 & \overline{u}_{i6}^2 \end{array} \right] \tag{3.83}$$

$$V_{z_i} \cong \frac{||b_i \Gamma_U^{\frac{1}{2}}||^2 ||\phi_{ixy}||^2}{4\zeta_i \omega_i^3} \tag{3.84}$$

The contribution of all the impulses yields

$$V_z = \sum_{i=1}^{N} V_{z_i} \cong \sum_{i=1}^{N} \frac{||b_i \Gamma_U^{\frac{1}{2}}||^2 ||\phi_{ixy}||^2}{4\zeta_i \omega_i^3} \tag{3.85}$$

The impact of pqth mode on the performance function when a unit impulse is applied to the plate, is shown in Figure 4.7; Figure 4.7-a shows the effect when the unit impulse applied through actuator located at $(\frac{L_x}{2}, \frac{L_y}{4})$, Figure 4.7-b shows the effect when the the unit impulse applied through actuator located at $(\frac{L_x}{2}, \frac{L_y}{2})$, Figure 4.7-c shows the effect of applying the unit impulse at all four actuator locations, and Figure 4.7-d shows the effect of an external disturbance to the cost function when applying a unit impulse. These Figures indicate that the contribution of the pqth mode to the cost function is drastically decreased for the higher modes.

To determine the number of modes N required to be retained in the model to guarantee that the error in the finite sum $\sum_{i=1}^{N} \mid V_{z_i} \mid$ is smaller than a specified value, an upper bound can be found for the cost function in (3.85). By using the Schwartz inequality (3.85) can be written as

$$V_z \leq \sum_{i=1}^{N} \frac{||b_i||^2 ||tr\Gamma_U|| ||\phi_{ixy}||^2}{4\zeta_i \omega_i^3} \tag{3.86}$$

With reference to the denominator of (3.86) we observe that the use of a Rayleigh damping model implies that

$$\zeta_i = \frac{\overline{\zeta}[\omega_{11}\omega_{12} + \omega_{pq}^2]}{\omega_{pq}(\omega_{11} + \omega_{12})} \tag{3.87}$$

Considering $L_x \leq L_y$, a lower bound for the natural frequency can be found by replacing L_x with L_y in (3.18) and an upper bound for the natural frequency can be found by replacing L_y with L_x in (3.18)

$$\min \omega_{pq} = \sqrt{\frac{D}{\rho h}} \frac{\pi^2}{L_y^2}(p^2 + q^2) \qquad \max \omega_{pq} = \sqrt{\frac{D}{\rho h}} \frac{\pi^2}{L_x^2}(p^2 + q^2) \tag{3.88}$$

using (3.88) a lower bound for the damping factor can be found as

$$\inf \zeta_i = \bar{\zeta} \frac{\inf[\omega_{11}\omega_{12} + \omega_{pq}^2]}{\sup[\omega_{pq}(\omega_{11} + \omega_{12})]} = \bar{\zeta} \frac{L_x^4[10 + (p^2 + q^2)^2]}{7L_y^4(p^2 + q^2)} \tag{3.89}$$

The supremum of the b_i in (3.86) components can be found by maximizing the sine functions in (3.23) and (3.28) as

$$\sup \gamma_f = \sqrt{\frac{4}{\rho h L_x L_y}} \qquad \sup \gamma_{xu} = \sqrt{\frac{16p^2\pi^2}{\rho h L_x^3 L_y}} \qquad \sup \gamma_{yu} = \sqrt{\frac{16q^2\pi^2}{\rho h L_x L_y^3}} \tag{3.90}$$

then upon substituting (3.90) into (3.82), and taking the vector norm of b_i, leads to

$$\sup ||b_i||^2 = \frac{4}{\rho h L_x^3 L_y}[L_x^2 + 12\pi^2(p^2 + q^2)] \tag{3.91}$$

The supremum of the shape function vector norm in (3.86) can be found by maximizing the sine functions in (3.16) as

$$\sup ||\phi_{ixy}||^2 = \frac{4}{\rho h L_x L_y} \tag{3.92}$$

By substituting (3.88), (3.89), (3.91) and (3.92) into (3.86) a supremum for the cost function can be found to be

$$\sup V_z = \frac{28L_y^2||tr\Gamma_U||}{\bar{\zeta}\pi^6 L_x^2\sqrt{\rho h D^3}} \sum_{p=1}^{\infty}\sum_{q=1}^{\infty} \frac{[L_x^2 + 12\pi^2(p^2 + q^2)]}{[10 + (p^2 + q^2)^2](p^2 + q^2)^2} \tag{3.93}$$

Using (3.93), a new supremum for V_z can be defined as

$$\sup V_z = K \sum_{p=1}^{\infty}\sum_{q=1}^{\infty} \frac{1}{(p^2 + q^2)^3} < K \sum_{p=1}^{\infty}\sum_{q=1}^{\infty} \frac{1}{p^6 q^6} \tag{3.94}$$

where

$$K = \frac{28L_y^2||tr\Gamma_U||(L_x^2 + 12\pi^2)}{\bar{\zeta}\pi^6 L_x^2\sqrt{\rho h D^3}} \tag{3.95}$$

Now, if f(p,q) is a nonincreasing function of p and q then (Naylor, 1982)

$$\sup \sum_{p=R+1}^{\infty} \sum_{q=S+1}^{\infty} f(p,q) \leq \int_R^{\infty} \int_S^{\infty} f(p,q)dpdq \tag{3.96}$$

The cost function truncation error ϵ can be formed as

$$\epsilon = \frac{\sup \sum_{i=N+1}^{\infty} V_{z_i}}{\sup \sum_{i=1}^{\infty} V_{z_i}} = \frac{\sum_{p=R+1}^{\infty} \sum_{q=S+1}^{\infty} \frac{1}{p^6 q^6}}{\sum_{p=1}^{\infty} \sum_{q=1}^{\infty} \frac{1}{p^6 q^6}} \leq \frac{\int_R^{\infty} \int_S^{\infty} \frac{1}{p^6 q^6} dpdq}{\sum_{p=1}^{\infty} \sum_{q=1}^{\infty} \frac{1}{p^6 q^6}} \tag{3.97}$$

From algebra and with reference to (3.94) and (3.96) we observe that

$$\int_R^{\infty} \int_S^{\infty} \frac{1}{p^6 q^6} dpdq = \frac{1}{25R^5 S^5} \qquad \sum_{p=1}^{\infty} \sum_{q=1}^{\infty} p^{-6} q^{-6} = \frac{\pi^{12}}{893025} \tag{3.98}$$

and therefore a supremum for ϵ can be defined as

$$\sup \epsilon = \frac{893025}{25\pi^{12} R^5 S^5} \tag{3.99}$$

Sample values of (R, S) versus ϵ as a percent are given in Table 3.1. It may be observed that for $R \geq 2$ and $S \geq 2$ the error ϵ is always less than 0.004%.

Table 3.1: Number of Modes Required in Plate Model to Satisfy the Error requirements

Percent Error		R or S				
		1	2	3	4	5
S or R	1	3.86E00	1.21E-1	1.59E-2	3.77E-3	1.23E-3
	2	1.21E-1	3.77E-3	4.97E-4	1.18E-4	3.86E-5
	3	1.59E-2	4.97E-4	6.54E-5	1.55E-5	5.09E-6
	4	3.77E-3	1.18E-4	1.55E-5	3.68E-6	1.21E-6
	5	1.23E-3	3.86E-5	5.09E-6	1.21E-6	3.96E-7

Example: Consider a simply supported plate subjected to a point load $\gamma_f W(t)$ at $(\frac{L_x}{5}, \frac{L_y}{7})$. In order to suppress the vibrations six thin piezoelectric actuators are bonded to the plate. The actuators $\gamma_{xu}U(t)$ (or control inputs one to three) are located at $(\frac{L_x}{2}, \frac{L_y}{2})$, $(\frac{L_x}{4}, \frac{L_y}{2})$, $(\frac{3L_x}{4}, \frac{L_y}{2})$, and the actuators $\gamma_{yu}U(t)$ (or control inputs four to six) are located at $(\frac{L_x}{2}, \frac{L_y}{2})$, $(\frac{L_x}{2}, \frac{L_y}{4})$, $(\frac{L_x}{2}, \frac{3L_y}{4})$. The material characteristics and dimensions of the plate and piezoelectric elements are given in Tables 3.2 and 3.3. It should be noted that to simulate the reality a 5% propotonal damping is considered for each mode.

Table 3.2: Material characteristics and dimensions of the Plate

Length in x direction	$L_x = 0.68\ m$
Length in y direction	$L_y = 0.77\ m$
Thickness	$h = 0.815\ mm$
Young's Modulus	$E = 70\ GPa$
Poisson's ratio	$\nu = 0.3$
Mass density	$2710\ \frac{kg}{m^3}$
Damping ratio	$\overline{\zeta} = \zeta_{11} = \zeta_{12} = \zeta_{21} = \zeta_{22} = 0.05$

Now if the maximum desired truncation error in the cost function is 0.004%, from Table 3.1 the minimum required number of modes in the plate model will be R=2 and S=2. However from this table it is clear that also R=1 and S=4, or R=4 and S=1 satisfy the error requirements but would result in an asymmetrical modelling situation.

Considering R=2 and S=2, from (3.18) and (3.20) the undamped natural frequency

Table 3.3: Material characteristics and dimensions of the Piezoelectric

Dimension $cm \times cm \times mm$	$5 \times 2 \times 0.3$
Composition	Lead Zirconate Titanate
Material Designation	PSI-5H-S4ENH
Dielectric Constant (1KHz)	3800
Strain Coefficient $\frac{Meters}{Volt}$	$d_{33} = 650E{-}12$, $d_{31} = -320E{-}12$
Density $\frac{Kg}{m^3}$	6800
Elastic Modulus	$E_3 = 5.0 \times 10^{10}$, $E_1 = 6.2 \times 10^{10}$

matrix and damping matrix are

$$\lceil \omega \rfloor = \begin{bmatrix} 47.62 \\ 110.22 \\ 127.89 \\ 190.48 \end{bmatrix} \qquad \lceil C \rfloor = \begin{bmatrix} 4.76 \\ 11.02 \\ 12.79 \\ 19.05 \end{bmatrix} \tag{3.100}$$

By using (3.35) the components of the Jordan canonical form of matrix A can be evaluated as

$$\lceil \Lambda \rfloor = \begin{bmatrix} -\zeta_{11}\omega_{11} + j\omega_{11}\sqrt{1-\zeta_{11}^2} \\ -\zeta_{12}\omega_{12} + j\omega_{12}\sqrt{1-\zeta_{12}^2} \\ -\zeta_{21}\omega_{21} + j\omega_{21}\sqrt{1-\zeta_{21}^2} \\ -\zeta_{22}\omega_{22} + j\omega_{22}\sqrt{1-\zeta_{22}^2} \end{bmatrix} = \begin{bmatrix} -2.38 + 47.56j \\ -5.51 + 110.08j \\ -6.39 + 127.73j \\ -9.52 + 190.25j \end{bmatrix} \tag{3.101}$$

The state transion matrix of A can be evaluated from (3.38) and is defined in appendix B. Upon substitution of the natural frequencies and damping factors, the

state transition matrix can be rewritten as

$$e^{At} = \begin{bmatrix} \lceil a_{11} \rfloor & \lceil a_{12} \rfloor \\ \lceil a_{21} \rfloor & \lceil a_{22} \rfloor \end{bmatrix} \tag{3.102}$$

where a_{11}, a_{12}, a_{21} and a_{22} are defined in appendix B.

Considering the point load force applied at $\xi_1 = \frac{L_x}{5}$, $\eta_1 = \frac{L_y}{7}$, the parametric gain vector of the disturbance force can be from (3.23) as

$$[\gamma_f] = \sqrt{\frac{4}{\rho h L_x L_y}} \begin{bmatrix} \sin(\frac{\pi\xi_1}{L_x})\sin(\frac{\pi\eta_1}{L_y}) \\ \sin(\frac{\pi\xi_1}{L_x})\sin(\frac{2\pi\eta_1}{L_y}) \\ \sin(\frac{2\pi\xi_1}{L_x})\sin(\frac{\pi\eta_1}{L_y}) \\ \sin(\frac{2\pi\xi_1}{L_x})\sin(\frac{2\pi\eta_1}{L_y}) \end{bmatrix} = \begin{bmatrix} 0.47 \\ 0.85 \\ 0.77 \\ 1.38 \end{bmatrix} \tag{3.103}$$

Therefore the disturbance vector can be formed as

$$D = \begin{bmatrix} 0 & 0 & 0 & 0 & 0.47 & 0.85 & 0.77 & 1.38 \end{bmatrix}^T \tag{3.104}$$

The piezoelectric gains γ_{xu} and γ_{yu}, are obtained from (3.28), and are defined in appendix B. Upon evaluation the parametric gain matrix is

$$[\gamma_u] = \begin{bmatrix} 1.98 & 1.40 & 1.40 & 1.55 & 1.09 & 1.09 \\ 0.00 & 0.00 & 0.00 & 0.00 & 6.15 & -6.15 \\ 0.00 & 7.87 & -7.87 & 0.00 & 0.00 & 0.00 \\ 0.00 & 0.00 & 0.00 & 0.00 & 0.00 & 0.00 \end{bmatrix} \tag{3.105}$$

The control matrix B can be formed as specified in (3.33) and the matrix C can be found from (3.40) where

$$[P] = [R] = \begin{bmatrix} \phi_{1x}\phi_{1y} \\ \phi_{1x}\phi_{2y} \\ \phi_{2x}\phi_{1y} \\ \phi_{2x}\phi_{2y} \end{bmatrix}^T = \sqrt{\frac{4}{\rho h L_x L_y}} \begin{bmatrix} \sin(\frac{\pi x}{L_x})\sin(\frac{\pi y}{L_y}) \\ \sin(\frac{\pi x}{L_x})\sin(\frac{2\pi y}{L_y}) \\ \sin(\frac{2\pi x}{L_x})\sin(\frac{\pi y}{L_y}) \\ \sin(\frac{2\pi x}{L_x})\sin(\frac{2\pi y}{L_y}) \end{bmatrix}^T \tag{3.106}$$

By having collocated piezoelectric actuators and sensors (the sensors measure the deflection) matrices P and R can be formed as shown in appendix B. Upon substitution of the $\xi_1 \ldots \xi_6$ and $\eta_1 \ldots \eta_6$ in (B.4), P and R matrices become

$$[P] = [R] = \begin{bmatrix} 1 & 0.71 & 0.71 & 1 & 0.71 & 0.71 \\ 0 & 0 & 0 & 0 & 1 & -1 \\ 0 & 1 & -1 & 0 & 0 & 0 \\ 0 & 0 & 0 & 0 & 0 & 0 \end{bmatrix}^T \tag{3.107}$$

If an impulse is applied to the plate through the point load, from (3.40) the impulse response of the plate can be found as

$$w(x,y,t) = 1.86 \begin{bmatrix} \sin(\frac{\pi x}{L_x})\sin(\frac{\pi y}{L_y}) \\ \sin(\frac{\pi x}{L_x})\sin(\frac{2\pi y}{L_y}) \\ \sin(\frac{2\pi x}{L_x})\sin(\frac{\pi y}{L_y}) \\ \sin(\frac{2\pi x}{L_x})\sin(\frac{2\pi y}{L_y}) \end{bmatrix}^T \begin{bmatrix} \frac{e^{-2.38t}}{47.62}\sin(47.62t) \\ \frac{e^{-5.51t}}{110.22}\sin(110.22t) \\ \frac{e^{-6.39t}}{127.89}\sin(127.89t) \\ \frac{e^{-9.52t}}{190.48}\sin(190.48t) \end{bmatrix} \begin{bmatrix} 0.47 \\ 0.85 \\ 0.77 \\ 1.38 \end{bmatrix} \overline{f} \tag{3.108}$$

where $\overline{f}$ is the magnitude of the impulse.

In the case of force response with zero initial conditions the system dynamic response can be written as

$$w(x,y,t) = 1.86 \begin{bmatrix} \sin(\frac{\pi x}{L_x})\sin(\frac{\pi y}{L_y}) \\ \sin(\frac{\pi x}{L_x})\sin(\frac{2\pi y}{L_y}) \\ \sin(\frac{\pi x}{L_x})\sin(\frac{2\pi y}{L_y}) \\ \sin(\frac{2\pi x}{L_x})\sin(\frac{2\pi y}{L_y}) \\ 0 \\ 0 \\ 0 \\ 0 \end{bmatrix} \times$$

$$\int_0^t e^{A(t-\tau)} \begin{bmatrix} 0 & 0 & 0 & 0 & 0 & 0 & 0 \\ 0 & 0 & 0 & 0 & 0 & 0 & 0 \\ 0 & 0 & 0 & 0 & 0 & 0 & 0 \\ 0 & 0 & 0 & 0 & 0 & 0 & 0 \\ 0.47 & 1.98 & 1.40 & 1.40 & 1.55 & 1.09 & 1.09 \\ 0.85 & 0.00 & 0.00 & 0.00 & 0.00 & 6.15 & -6.15 \\ 0.77 & 0.00 & 7.87 & -7.87 & 0.00 & 0.00 & 0.00 \\ 1.38 & 0.00 & 0.00 & 0.00 & 0.00 & 0.00 & 0.00 \end{bmatrix} \begin{bmatrix} \mathcal{F}(\tau) \\ \mathcal{T}_1(\tau) \\ \mathcal{T}_2(\tau) \\ \mathcal{T}_3(\tau) \\ \mathcal{T}_4(\tau) \\ \mathcal{T}_5(\tau) \\ \mathcal{T}_6(\tau) \end{bmatrix} d\tau \quad (3.109)$$

From (3.107) the deflections observed through the collocated sensors can be estimated as shown in appendix B. The integration in (3.109) will be performed numerically in the next chapter.

The responses of a linear time-invariant dynamical equation are dictated mainly by its modes, or equivalently, the eigenvalues of A. If an eigenvalue has a negative real part, its mode will approach zero exponentially as time goes to infinity. Depending on whether its imaginary part is zero or not the approach to zero is either monotonic or oscillatory. If an eigenvalue has a positive real part, its mode will approach infinity exponentially. In the case of zero real part with index one, its mode is a pure sinusoid, and by having zero real part with index n_i higher than one, the mode will approach infinity at the rate of t^{n_i-1}. In this example, the eigenvalues of matrix A have negative real parts and non-zero imaginary parts therefore all the modes approach zero monotonically.

A dynamical system of the form (3.34) is controllable if and only if the set of vectors in the matrix $(\mathsf{E}^{-1}B)^T$ are linearly independent, and the system is observable if and only if the set of vectors in the matrix $(C\mathsf{E})$ are linearly independent. Examining this condition, it is observed that the above system is not state controllable and state observable.

3.5 Conclusion and Summary

Towards the goal of establishing an active vibration absorber for a simply supported plate all important issues associated with modelling the problem were addressed. Initially the classical plate theory has been considered to develop the mathematical model of the system. The plate characteristic functions have been used to study the plate vibrations analytically.

The separation of variables and Fourier expansion coupled with Navier's method is used to optimize size of piezoelectric actuators, the actuation voltage, and appropriate location of the sensors,

In order to work with a finite dimensional model and ignoring some of the feedback paths in the physical system a quadratic control objective has been introduced. The number of modes required in the plate model to guarantee that the error in the objective function is smaller than a specified error has been derived.

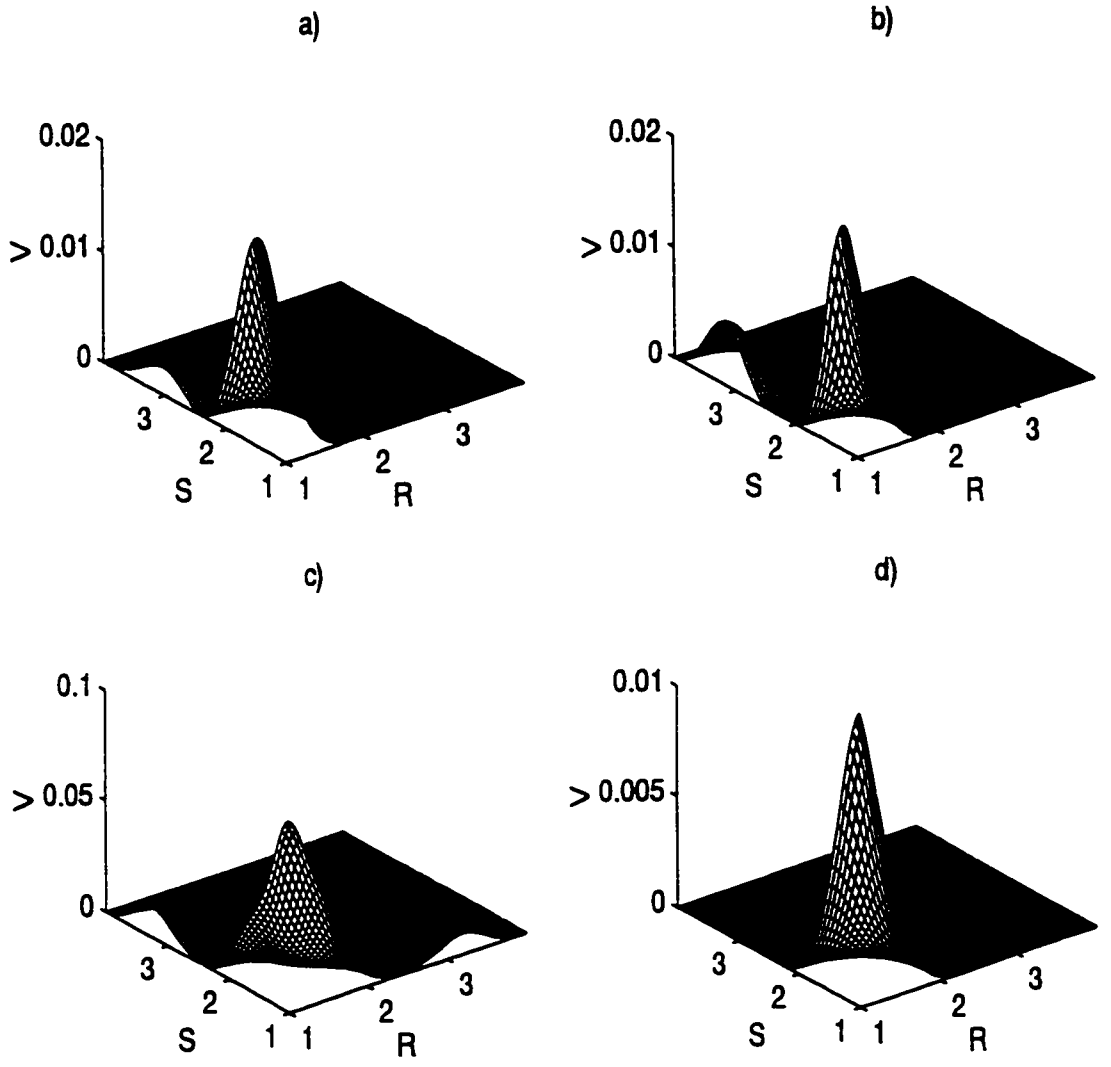

Figure 3.4: Contribution of inputs to the cost function at observation point $(\frac{5L_x}{12}, \frac{5L_y}{12})$ (a)Effect of piezo located at $(\frac{L_x}{2}, \frac{L_y}{4})$ (b)Effect of piezo located at $(\frac{L_x}{2}, \frac{L_y}{2})$. (c)Effect of all piezos (d)Effect of external point load

Chapter 4

Optimal Controller

The energy based control strategy "Linear Coupling Control (LCC)" [47] is used for controlling free and forced vibrations in a simply supported plate. The control strategy is implemented by coupling a virtual second order linear system (controller) to an oscillatory plant and creating an energy exchange between the two systems [47]. The energy transfer phenomena from the plant to the controller is maximized by coupling the appropriate states. Once the transfer of energy has taken place it is dissipated via linear damping. To provide a basis for comparing the results of the proposed control algorithm and the conventional control methods, the linear quadratic optimal control method also was implemented.

4.1 Introduction

Recently, there has been a great deal of research in the area of passive and active vibration control of flexible structures [48, 49]. There are a number of mechanisms that can be used for the element of smart structures. They are piezoelectricity

[50, 51], thermal expansion [52], electrostriction [53, 54], magnetostriction [55], and material phase change [56, 57]. Piezoelectricity has been especially recognized as a favorable mechanism over the others because the integration with load-bearing structures can be easily accomplished by surface bonding or embedding. It does not significantly alter the static or dynamic stiffness and mass characteristics of the structures. It is capable of operating in a wide frequency range. An overview of various active noise and vibration control methods is given in a recent review paper by Stevens [58]. The present work focuses on the control of plate vibration via piezoelectric actuators. It addresses the development of the control law.

In the past decade, the control of free and forced vibration has been accomplished largely in practice by classical control techniques such as PID or state feedback [59, 60]. Burke [61] presented an energy based technique for the design and analysis of distributed transducers used for the observation and control of thin plates. The technique assumes that the requisite transducers can be modelled as separable in space and time, i.e. degenerate distributed transducers. The limitations of a uniform spatial weighting as applied to a simply supported plate were explored. By matching the spatial distributions of both sensing and actuating transducers it was shown that guaranteed stability is achieved in the Lyapunov sense.

Tzou [62] used the conventional elastic shell to develop generic theory for the intelligent shell systems. From the theory derived, it was concluded that the distributed sensor is capable of sensing all vibration modes and the distributed actuator controlling all modes. Two feedback control algorithms, namely direct feedback control and Lyapunov control, were proposed and the control moments for each control algorithm were also derived. However the modal gains and time delay in feedback systems were not explored.

Lee *et al.* [63] used laminated plate theory to first derive theoretically and then examine experimentally the modal sensors/actuators. A point sensor/actuator, had been developed which bypasses the need for extensive signal processing because the surface electrode and the polarization profile of a distributed sensor/actuators can be used to integrate sensor/actuator signals in the special domain. A mode one and mode two sensor for a one-dimensional cantilever plate were constructed and tested to examine the applicability of the modal sensors/actuators.

Dworak and Falangas [64] modelled mechanical and electrical behavior of a thin plate with attached piezoelectrics. Two control system configurations were considered in which an accelerometer was used as feedback to a collocated piezoelectric actuator and a cross coupled configuration in which the accelerometers were combined to form the feedback to a particular piezoelectric. Two control design methods were considered for closing the loops between the accelerometers and the piezoelectric actuators, rate feedback obtained by integrating the accelerometer signals and the H_∞ design methodology.

Fariborzi *et al.* [65] have presented a mathematical model of the transverse vibration of a plate to be used for free and forced vibration control purposes. A quadratic control objective had been defined as a measure of system performance. The control objective is composed of those error variables that are important to the design and they are used to approximate the high order plant system by a lower order model. To guarantee that the error in the reduced model is smaller than the desired error, a minimum required number of modes in the plate model is specified.

The notion of using an energy based controller has been considered by Golnaraghi [66] and later extended to forced vibrations by Fariborzi *et al.* [44]. Tuer *et al.* [67] extended this work by utilizing the energy transfer phenomena precipitated by linear and nonlinear state coupling as paradigms in the formulation of vibration

suppression laws. In his work Tuer investigated the performance of both linear and nonlinear coupling controllers on a numerical level. Fariborzi *et al.* [44] investigated the theoretical modeling and simulation of piezoelectric actuators and used a linear coupling control strategy to control free and forced vibration in a cantilever beam. The controller was modelled as a single degree of freedom linear oscillator which was coupled to the plant via a linear term. The system was solved as a linear eigenvalue problem. The experimental verification of this approach to vibration suppression was presented. In the forced vibration the control law provided over 98% improvement in amplitude over the uncontrolled responses.

4.2 Optimal Control

For an asymptotically stable system, there exists some function that is decreased during the natural trajectory of the states. This function, which is called the Liapunov function might, represent a physical entity such as system energy. The particular Liapunov function might not be the function the designer wishes to decrease, and one may ask if it might be possible to decrease this function even faster with some choice of control input. Therefore, the task can be proposed as: given a function of the designer's choice, find a control input that will keep the Liapunov function as small as possible. This is the philosophy of optimal control.

4.2.1 LQ "Linear Quadratic" Optimal Control

A dynamical system of a finite number of lumped elements may be described by ordinary differential equations in which time is the independent variable. By use of vector matrix notation, an nth-order differential equation may be expressed in

state space form. Considering the state equation of a causal and relaxed second order linear time invariant system with no direct transformation, the state equation can be written as

$$\begin{aligned} \dot{\mathcal{Z}}(t) &= A\mathcal{Z}(t) + B\mathcal{U}(t) + D\mathcal{W}(t) \\ w(x,y,t) &= C\mathcal{Z}(t) \end{aligned} \tag{4.1}$$

where

$$\mathcal{Z}(t) = \begin{Bmatrix} Z(t) \\ \dot{Z}(t) \end{Bmatrix} \quad A = \begin{bmatrix} 0 & I \\ -\Omega & -C \end{bmatrix} \quad B = \begin{bmatrix} 0 \\ \gamma_u \end{bmatrix} \quad D = \begin{bmatrix} 0 \\ \gamma_f \end{bmatrix} \tag{4.2}$$

and $\mathcal{U}$ is the "control" vector with its ith input given as $\mathcal{U}_i(t) = \overline{u}_i\delta(t)$ and where $\mathcal{W}$ is a vector of "disturbances" with its ith input given as $\mathcal{W}_i(t) = \overline{w}_i\delta(t)$. Both are impulses of strength $\overline{u}_i$ and $\overline{w}_i$ respectively.

In the linear quadratic optimal control problem the order of the controller is equal to the order of the plant, and it is desired to minimize a quadratic function of the outputs and the control inputs. the "cost function" V is defined by:

$$V = \sum_{i=1}^{n} \int_0^\infty \left[w^{i^T}(t) Q w^i(t) + \mathcal{U}^{i^T}(t) R\, \mathcal{U}^i(t) \right] dt \tag{4.3}$$

where $w^i(t), i = 1, 2, \ldots, n_w + n_U$ are the responses from the sequence of excitations from disturbances and inputs acting alone. Q and R are the weighting matrix. Now the objective is to minimize the cost function using a choice of state feedback gain G.

$$\begin{aligned} z(t) &= M\mathcal{Z}(t) \\ \mathcal{U}(t) &= Gz(t) \end{aligned} \tag{4.4}$$

where z is the measured states

Theorem 2 *(Skelton [68]) The measurement feedback problem described by (4.1) and (4.2) has a unique solution if*

a) M has linearly independent rows, $R > 0$,

b) The controllable modes of $(A+BGM, D)$ and observable modes of $(A+BGM, C)$ are asymptotically stable,

c) $[A + BGM]$ has no eigenvalues symmetric about the imaginary axis.

The solution must satisfy

$$G = -R^{-1}B^T K X M^T (M X M^T)^{-1} \tag{4.5}$$

where X and K satisfy

$$0 = K(A + BGM) + (A + BGM)^T K + M^T G^T R G M + C^T Q C, \tag{4.6}$$

$$0 = X(A + BGM)^T + (A + BGM)X + DWD^T + X_0 \tag{4.7}$$

and the minimum value of the cost function is

$$V = trX(C^T Q C + M^T G^T R G M) = trK(DWD^T + X_0) \tag{4.8}$$

The uniqueness follows from conditions for unique solutions of Liapunov equations (4.6) and (4.7). b), c) and condition a) imply that the measurements $z_1(t), z_2(t), \ldots$ are linearly independent. The equations (4.5) through (4.7) have no analytical solution and numerical iteration is required. A special case of this theorem is much simpler to solve. The special case can be defined when $\mathcal{U} = G\mathcal{Z}(t)$ as the "state feedback control."

Corollary 2 *The optimal state feedback control is*

$$\mathcal{U} = G\mathcal{Z}(t), \qquad G = -R^{-1}B^T K, \tag{4.9}$$

$$0 = KA + A^T K - KBR^{-1}B^T K + C^T Q C, \tag{4.10}$$

$$V = trK(D\Gamma_w D + \Gamma_{z_0}) = trX(C^T Q C + G^T R G), \tag{4.11}$$

where

$$0 = X(A+BG)^T + (A+BG)X + D\Gamma_W D^T + \Gamma_{z_0} \tag{4.12}$$

Theorem 3 *(Skelton [68]) If (A,B) is stabilizable and (A,C) is detectable, then solution of the nonlinear equation*

$$0 \;=\; KA + A^TK - KBR^{-1}B^TK + C^TQC \tag{4.13}$$

is

$$K = E_2E_1^{-1} \tag{4.14}$$

where E_1,E_2 are the eigenvector of the left half-plane eigenvalues of the matrix

$$\begin{bmatrix} A & -BR^{-1}B^T \\ -C^TQC & -A^T \end{bmatrix} \tag{4.15}$$

4.2.2 Stability Margin of the LQ Optimal Control

In the study of the state feedback system (4.1), where the feedback control input is given as (4.9), the eigenvalues of the system are in the left half plane if the following inequality holds

$$[I + L^T(j\omega)][I + L(j\omega)] \geq I \tag{4.16}$$

where

$$L^T(j\omega) = -R^{-\frac{1}{2}}B^T[-A^T - j\omega I]^{-1}G^TR^{\frac{1}{2}} \tag{4.17}$$

It can be shown that such control designs have an infinite gain margin and a phase margin $\geq 60°$ [68]. The inequality (4.16) implies that the Nyquist plot for the optimal state feedback system never penetrates the unit circle centered around the $-1 + j0$ point.

4.3 Controller Design

Linear and nonlinear coupling methods [67] represent a relatively new approach to control of flexible structures. Use of these techniques involves dynamically linking components within a system or creating external supplementary dynamic links. This coupling creates a global system between which energy can be exchanged within vibrational modes or coordinates.

The plant under consideration consists of a flexible simply supported plate exhibiting planar vibration due to a concentrated load located at $(\frac{L_x}{5}, \frac{L_y}{7})$. To control oscillations, piezoelectric elements are rigidly bonded to the plate as described in the previous section. Using a four term Rayleigh-Ritz approximation the system is of the form:

$$\begin{aligned}
\ddot{Z}_{11_p} + 2\zeta_{11_p}\omega_{11_p}\dot{Z}_{11_p} + \omega_{11_p}^2 Z_{11_p} &= \gamma_{11_f} W_{11}(t) + U_{11} \\
\ddot{Z}_{12_p} + 2\zeta_{12_p}\omega_{12_p}\dot{Z}_{12_p} + \omega_{12_p}^2 Z_{12_p} &= \gamma_{12_f} W_{12}(t) + U_{12} \\
\ddot{Z}_{21_p} + 2\zeta_{21_p}\omega_{21_p}\dot{Z}_{21_p} + \omega_{21_p}^2 Z_{21_p} &= \gamma_{21_f} W_{21}(t) + U_{21} \\
\ddot{Z}_{22_p} + 2\zeta_{22_p}\omega_{22_p}\dot{Z}_{22_p} + \omega_{22_p}^2 Z_{22_p} &= \gamma_{22_f} W_{22}(t) + U_{22}
\end{aligned} \tag{4.18}$$

where ω_{pq} is the pqth natural frequency of the plant, $\gamma_{rs_f} W_{rs}(t)$ is a disturbance input and U_{rs} is a general function representing the control signal. In (3.19) it has been shown that each mode of vibration can be represented by an ordinary differential equation similar to (4.18). Using superposition the control strategy can be implemented as a superposition of the control for each mode.

A successful control strategy [67], incorporates four virtual systems such that

$$\begin{aligned}
\ddot{Z}_{11_c} + 2\zeta_{11_c}\omega_{11_c}\dot{Z}_{11_c} + \omega_{11_c}^2 Z_{11_c} &= \alpha_{11_p} M_{11_p}(Z_{11_p}, \dot{Z}_{11_p}, \ddot{Z}_{11_p}, t) \\
\ddot{Z}_{12_c} + 2\zeta_{12_c}\omega_{12_c}\dot{Z}_{12_c} + \omega_{12_c}^2 Z_{12_c} &= \alpha_{12_p} M_{12_p}(Z_{12_p}, \dot{Z}_{12_p}, \ddot{Z}_{12_p}, t) \\
\ddot{Z}_{21_c} + 2\zeta_{21_c}\omega_{21_c}\dot{Z}_{21_c} + \omega_{21_c}^2 Z_{21_c} &= \alpha_{21_p} M_{21_p}(Z_{21_p}, \dot{Z}_{21_p}, \ddot{Z}_{21_p}, t) \\
\ddot{Z}_{22_c} + 2\zeta_{22_c}\omega_{22_c}\dot{Z}_{22_c} + \omega_{22_c}^2 Z_{22_c} &= \alpha_{22_p} M_{22_p}(Z_{22_p}, \dot{Z}_{22_p}, \ddot{Z}_{22_p}, t)
\end{aligned} \tag{4.19}$$

where Z_{rs_c} is a time dependent generalized controller co-ordinate, ζ_{rs_c} is the controller damping ratio, ω_{rs_c} is the controller natural frequency and $M_{rs_p}(Z_{rs_p}, \dot{Z}_{rs_p}, \ddot{Z}_{rs_p}, t)$ is a generalized forcing input which is a linear or nonlinear function of the plant acceleration $(\ddot{Z}_{rs_p})$, velocity $(\dot{Z}_{rs_p})$ or position (Z_{rs_p}) and is proportional to the parametric gain α_{rs_p}. The control inputs U_{rs}, in (4.18) are defined as

$$\begin{aligned} U_{11} &= \alpha_{11_c} M_{11_c}(Z_{11_c}, \dot{Z}_{11_c}, \ddot{Z}_{11_c}, t) \\ U_{12} &= \alpha_{12_c} M_{12_c}(Z_{12_c}, \dot{Z}_{12_c}, \ddot{Z}_{12_c}, t) \\ U_{21} &= \alpha_{21_c} M_{21_c}(Z_{21_c}, \dot{Z}_{21_c}, \ddot{Z}_{21_c}, t) \\ U_{22} &= \alpha_{22_c} M_{22_c}(Z_{22_c}, \dot{Z}_{22_c}, \ddot{Z}_{22_c}, t) \end{aligned} \tag{4.20}$$

where $M_{rs_c}(Z_{rs_c}, \dot{Z}_{rs_c}, \ddot{Z}_{rs_c}, t)$ is a linear or nonlinear function of the controller acceleration $(\ddot{Z}_{rs_c})$, velocity $(\dot{Z}_{rs_c})$ or position (Z_{rs_c}) and is proportional to the parametric gain α_{rs_c}.

In the Linear Coupling Control (LCC) technique there are up to nine possible coupling parameters [69]. Six of these are complementary pairs; for example, the coupling of controller velocity and plant position have similar characteristics to the coupling of controller position and plant velocity. Here the plant position and the controller position have been used as coupling terms between the plant and the controller [67].

$$\begin{aligned} M_{rs_p}(Z_{rs_p}, \dot{Z}_{rs_p}, \ddot{Z}_{rs_p}, t) &= Z_{rs_p} \\ M_{rs_c}(Z_{rs_c}, \dot{Z}_{rs_c}, \ddot{Z}_{rs_c}, t) &= -Z_{rs_c} \end{aligned} \tag{4.21}$$

Assuming an undamped plant in (4.18) and coupling the system of the equation with the corespondance virtual system in (4.19), the Laplace transform of the coupled system yields

$$Z_{rs_p}(s) = \frac{s^2 + a_1 s + a_0}{s^4 + b_3 s^3 + b_2 s^2 + b_1 s + b_0} W_{rs}(s) \tag{4.22}$$

where

$$\begin{aligned} a_0 &= \omega_{rs_c}^2 & a_1 &= 2\zeta_{rs_c}\omega_{rs_c} \\ b_0 &= \omega_{rs_p}^2\omega_{rs_c}^2 + \alpha_{rs_p}\alpha_{rs_c} & b_1 &= 2\zeta_{rs_c}\omega_{rs_c}\omega_{rs_p}^2 \\ b_2 &= (\omega_{rs_p}^2 + \omega_{rs_c}^2) & b_3 &= 2\zeta_{rs_c}\omega_{rs_c} \end{aligned} \tag{4.23}$$

In the case of harmonic forcing in which all of the forcing is considered to be of a single frequency Ω_{rs} (4.22) can be converted to the corresponding frequency response function via the substitution $s = j\Omega_{rs}$. Hence,

$$Z_{rs_p}(\Omega_{rs}) = \frac{R_n + I_n j}{R_d + I_d j} W_{rs}(\Omega_{rs}) \tag{4.24}$$

where

$$\begin{aligned} R_n &= (a_0 - \Omega_{rs}^2) & I_n &= a_1\Omega_{rs} \\ R_d &= \Omega_{rs}^4 - b_2\Omega_{rs}^2 + b_0 & I_d &= b_1\Omega_{rs} - b_3\Omega_{rs}^3 \end{aligned} \tag{4.25}$$

The coefficient of $W_{rs}(\Omega_{rs})$ represents the frequency response function of the total system. The amplitude of the plant response can be obtained as

$$\frac{||Z_{rs_p}(\Omega)||^2}{||W_{rs}(\Omega_{rs})||^2} = \frac{R_n^2 + I_n^2}{R_d^2 + I_d^2} \tag{4.26}$$

A successful vibration suppression strategy minimizes the function described by (4.26). In (4.26), the parameters ω_{rs_p} and Ω_{rs} are fixed features of the system, and α_{rs_p} and α_{rs_c} are variables controlling the rate of energy exchange. They are used to maximize the flow of energy from one coupling coordinate to the other. Finally, both ζ_{rs_c} and ω_{rs_c} are adjustable parameters that can be used for vibration suppression. The gain described in (4.26) is shown in Figure 4.1 as ζ_{rs_c} is varied, where (4.26) becomes an undamped system with two degrees of freedom when $\zeta_{rs_c} = 0$, and an undamped system with one degree of freedom when $\zeta_{rs_c} = \infty$. Notice that for two points, I and J, the gain does not change regardless of the damping ratio, ζ_{rs_c}. Using I and J as design conditions, the optimum system can be found when the gains at these two points are equal and are at the neighborhood

of a local maxima. The location of these points can be found by equating the two limits of (4.26)

$$\frac{(\omega_{rs_c}^2 - \Omega_{rs}^2)^2}{[\Omega_{rs}^4 - (\omega_{rs_p}^2 + \omega_{rs_c}^2)\Omega_{rs}^2 + \omega_{rs_p}^2\omega_{rs_c}^2 + \alpha_{rs_p}\alpha_{rs_c}]^2} = \frac{1}{(\omega_{rs_p}^2 - \Omega_{rs}^2)^2} \tag{4.27}$$

where the left-hand-side represents the amplitude of the coupled system when $\zeta_{rs_c} = 0$ and the right hand side is the amplitude when $\zeta_{rs_c} = \infty$. This can be expanded into a quadratic form to give,

$$\Omega_{rs}^4 - (\omega_{rs_p}^2 + \omega_{rs_c}^2)\Omega_{rs}^2 + \omega_{rs_p}^2\omega_{rs_c}^2 + \frac{\alpha_{rs_p}\alpha_{rs_c}}{2} = 0 \tag{4.28}$$

and the roots of this equation represent the "fixed" points. These are given by,

$$\Omega_{rs_{I,J}} = \frac{(\omega_{rs_p}^2 + \omega_{rs_c}^2)}{2} \pm \sqrt{(\frac{\omega_{rs_p}^2 - \omega_{rs_c}^2}{2})^2 - \frac{\alpha_{rs_p}\alpha_{rs_c}}{2}} \tag{4.29}$$

The optimization process involves ensuring the two fixed points to have the same amplitudes. This constraint may be met by placing a restriction on ω_{rs_c}. Since the amplitude at the fixed points is independent of the damping ratio, ω_{rs_c} can be found by using the right hand side of (4.27),

$$\frac{1}{\omega_{rs_p}^2 - \Omega_{rs_I}^2} = \frac{1}{\Omega_{rs_J}^2 - \omega_{rs_p}^2} \tag{4.30}$$

giving

$$\Omega_{rs_I}^2 + \Omega_{rs_J}^2 = 2\omega_{rs_p}^2 \tag{4.31}$$

Then, because the sum of the roots of a quadratic are equal to its second coefficient, (4.29) gives

$$\Omega_{rs_1}^2 + \Omega_{rs_2}^2 = \omega_{rs_p}^2 + \omega_{rs_c}^2 \tag{4.32}$$

which means,

$$\omega_{rs_c}^2 = \omega_{rs_p}^2 \tag{4.33}$$

The second of two conditions for optimum design is when the amplitude ratio in (4.27) is maximized in the neighborhood of $\Omega_{rs_{IJ}}$. (4.27) is partially differentiated with respect to Ω_{rs} in order to obtain the optimum damping ratio as

$$\zeta_{rs_{c_{Opt}}} = \frac{1}{4}\sqrt{|1 - (\frac{\Omega_{rs}}{\omega_{rs_c}})^2|} \tag{4.34}$$

Realizing a plant/controller beat phenomena relies on tuning two frequencies to be near each other and we will require that $\omega_{rs_p} \approx \omega_{rs_c} = \omega_{rs}$ [65]. This then yields

$$Z_{rs_p}(\Omega) = \frac{R_n + I_n j}{R_d + I_d j} W_{rs}(\Omega_{rs}) \tag{4.35}$$

where

$$\begin{aligned} R_n &= (\omega_{rs}^2 - \Omega_{rs}^2) & I_n &= 2\zeta_{rs_c}\omega_{rs}\Omega_{rs} \\ R_d &= \Omega_{rs}^4 - 2\omega_{rs}^2\Omega_{rs}^2 + \omega_{rs}^4 + \alpha_{rs_p}\alpha_{rs_c} & I_d &= 2\zeta_{rs_c}\omega_{rs}\Omega_{rs}(\omega_{rs}^2 - \Omega_{rs}^2) \end{aligned} \tag{4.36}$$

The stability of the closed loop system under the linear canonical control law can be examined by Routh's stability criterion [70]. Since the closed loop system is linear and time invariant, system stability can be ascertained by examining the product of the coupling parameters, where the stability condition can be found as

$$-\omega_{rs}{}^4 < \alpha_{rs_p}\alpha_{rs_c} < 0 \tag{4.37}$$

Example: Consider a simply supported plate subjected to a point load $\gamma_f W(t)$ at $(\frac{L_x}{5}, \frac{L_y}{7})$. In order to suppress the vibrations six thin piezoelectric actuators are bonded to the plate. The actuators $\gamma_{zu}U(t)$ (or control inputs one to three) are located at $(\frac{L_x}{2}, \frac{L_y}{2})$, $(\frac{L_x}{4}, \frac{L_y}{2})$, $(\frac{3L_x}{4}, \frac{L_y}{2})$, and the actuators $\gamma_{yu}U(t)$ (or control inputs four to six) are located at $(\frac{L_x}{2}, \frac{L_y}{2})$, $(\frac{L_x}{2}, \frac{L_y}{4})$, $(\frac{L_x}{2}, \frac{3L_y}{4})$. The material characteristics and dimensions of the plate and piezoelectric elements are given in Tables 3.2 and 3.3. Now if the maximum desired truncation error in the cost function is 0.004%,

from Table 3.1 of chapter 3, the minimum required number of modes in the plate model will be R=2 and S=2. However from this table it is clear that also R=1 and S=4, or R=4 and S=1 satisfy the error requirements but would result in an asymmetrical situation.

Considering R=2 and S=2, from (3.18) and (3.20) the natural frequency matrix and damping matrix are

$$\lceil \omega_p \rfloor = \begin{bmatrix} 47.62 \\ 110.22 \\ 127.89 \\ 190.48 \end{bmatrix} \qquad \lceil C_p \rfloor = \begin{bmatrix} 4.76 \\ 11.02 \\ 12.79 \\ 19.05 \end{bmatrix} \tag{4.38}$$

Considering the point load force applied at $\xi_1 = \frac{L_x}{5}$, $\eta_1 = \frac{L_y}{7}$, the parametric gain vector of the disturbance force can be from (3.23) as

$$[\gamma_f] = \sqrt{\frac{4}{\rho h L_x L_y}} \begin{bmatrix} \sin(\frac{\pi\xi_1}{L_x})\sin(\frac{\pi\eta_1}{L_y}) \\ \sin(\frac{\pi\xi_1}{L_x})\sin(\frac{2\pi\eta_1}{L_y}) \\ \sin(\frac{2\pi\xi_1}{L_x})\sin(\frac{\pi\eta_1}{L_y}) \\ \sin(\frac{2\pi\xi_1}{L_x})\sin(\frac{2\pi\eta_1}{L_y}) \end{bmatrix} = \begin{bmatrix} 0.47 \\ 0.85 \\ 0.77 \\ 1.38 \end{bmatrix} \tag{4.39}$$

Therefore the disturbance vector can be formed as:

$$D = \begin{bmatrix} 0 & 0 & 0 & 0 & 0.47 & 0.85 & 0.77 & 1.38 \end{bmatrix}^T \tag{4.40}$$

The piezoelectric gains obtained from (3.28), and are defined in the appendix. Upon evaluation the parametric gain matrix is

$$[\gamma_u] = \begin{bmatrix} 1.98 & 1.40 & 1.40 & 1.55 & 1.09 & 1.09 \\ 0.00 & 0.00 & 0.00 & 0.00 & 6.15 & -6.15 \\ 0.00 & 7.87 & -7.87 & 0.00 & 0.00 & 0.00 \\ 0.00 & 0.00 & 0.00 & 0.00 & 0.00 & 0.00 \end{bmatrix} \tag{4.41}$$

The control matrix B can be formed as specified in 3.33 and the matrix C can be found from 3.40 where

$$[P] = [R] = \begin{bmatrix} \phi_{1x}\phi_{1y} \\ \phi_{1x}\phi_{2y} \\ \phi_{2x}\phi_{1y} \\ \phi_{2x}\phi_{2y} \end{bmatrix}^T = \sqrt{\frac{4}{\rho h L_x L_y}} \begin{bmatrix} \sin(\frac{\pi x}{L_x})\sin(\frac{\pi y}{L_y}) \\ \sin(\frac{\pi x}{L_x})\sin(\frac{2\pi y}{L_y}) \\ \sin(\frac{2\pi x}{L_x})\sin(\frac{\pi y}{L_y}) \\ \sin(\frac{2\pi x}{L_x})\sin(\frac{2\pi y}{L_y}) \end{bmatrix}^T \tag{4.42}$$

By having collocated piezoelectric actuators and sensors (the sensors measure the deflection) matrices P and R can be formed as shown in equation (B.4). Upon substitution of the $\xi_1 \ldots \xi_6$ and $\eta_1 \ldots \eta_6$ in B.4 of, P and R matrices become

$$[P] = [R] = \begin{bmatrix} 1 & 0.71 & 0.71 & 1 & 0.71 & 0.71 \\ 0 & 0 & 0 & 0 & 1 & -1 \\ 0 & 1 & -1 & 0 & 0 & 0 \\ 0 & 0 & 0 & 0 & 0 & 0 \end{bmatrix}^T \tag{4.43}$$

The optimal state feedback control matrix can be obtained from (4.14) as

$$[K] = 10^2 \times \begin{bmatrix} 6.84 & 0.00 & 0.00 & 0.00 & 0.00 & 0.00 & 0.00 & 0.00 \\ 0.00 & 8.82 & 0.00 & 0.00 & 0.00 & 0.00 & 0.00 & 0.00 \\ 0.00 & 0.00 & 9.89 & 0.00 & 0.00 & 0.00 & 0.00 & 0.00 \\ 0.00 & 0.00 & 0.00 & 0.00 & 0.06 & 0.00 & 0.00 & 0.00 \\ 0.00 & 0.00 & 0.00 & 0.00 & 0.00 & 0.02 & 0.00 & 0.00 \\ 0.00 & 0.00 & 0.00 & 0.00 & 0.00 & 0.00 & 0.01 & 0.00 \end{bmatrix} \tag{4.44}$$

where $E_1 = E_{1R} + iE_{1I}$ and $E_2 == E_{2R} + iE_{2I}$ obtained from (4.15) as

$$[E_{1R}] = 10^{-2} \times$$

$$\begin{bmatrix} -0.04 & -0.04 & 0.00 & 0.00 & 0.00 & 0.00 & 0.00 & 0.00 \\ 0.00 & 0.00 & -0.11 & -0.11 & 0.00 & 0.00 & 0.00 & 0.00 \\ 0.00 & 0.00 & 0.00 & 0.00 & 0.08 & 0.08 & 0.00 & 0.00 \\ 0.00 & 0.00 & 0.00 & 0.00 & 0.00 & 0.00 & 0.47 & 0.47 \\ -6.49 & -6.49 & 0.00 & 0.00 & 0.00 & 0.00 & 0.00 & 0.00 \\ 0.00 & 0.00 & 5.21 & 5.21 & 0.00 & 0.00 & 0.00 & 0.00 \\ 0.00 & 0.00 & 0.00 & 0.00 & -8.22 & -8.22 & 0.00 & 0.00 \\ 0.00 & 0.00 & 0.00 & 0.00 & 0.00 & 0.00 & -50.10 & -50.10 \end{bmatrix} \tag{4.45}$$

$$[E_{1I}] = 10^{-2} \times$$

$$\begin{bmatrix} 0.14 & -0.14 & 0.00 & 0.00 & 0.00 & 0.00 & 0.00 & 0.00 \\ 0.00 & 0.00 & -0.04 & 0.04 & 0.00 & 0.00 & 0.00 & 0.00 \\ 0.00 & 0.00 & 0.00 & 0.00 & 0.06 & -0.06 & 0.00 & 0.00 \\ 0.00 & 0.00 & 0.00 & 0.00 & 0.00 & 0.00 & 0.24 & -0.24 \\ -2.48 & 2.48 & 0.00 & 0.00 & 0.00 & 0.00 & 0.00 & 0.00 \\ 0.00 & 0.00 & -11.25 & 11.25 & 0.00 & 0.00 & 0.00 & 0.00 \\ 0.00 & 0.00 & 0.00 & 0.00 & 9.84 & -9.04 & 0.00 & 0.00 \\ 0.00 & 0.00 & 0.00 & 0.00 & 0.00 & 0.00 & 86.54 & -86.54 \end{bmatrix} \tag{4.46}$$

$$[E_{2R}] = 10^{-2} \times$$

$$\begin{bmatrix} -27.11 & -27.11 & 0.00 & 0.00 & 0.00 & 0.00 & 0.00 & 0.00 \\ 0.00 & 0.00 & -92.91 & -92.91 & 0.00 & 0.00 & 0.00 & 0.00 \\ 0.00 & 0.00 & 0.00 & 0.00 & 80.92 & 80.92 & 0.00 & 0.00 \\ 0.00 & 0.00 & 0.00 & 0.00 & 0.00 & 0.00 & 0.00 & 0.00 \\ -1.96 & -1.96 & 0.00 & 0.00 & 0.00 & 0.00 & 0.00 & 0.00 \\ 0.00 & 0.00 & 0.38 & 0.38 & 0.00 & 0.00 & 0.00 & 0.00 \\ 0.00 & 0.00 & 0.00 & 0.00 & -0.50 & -0.50 & 0.00 & 0.00 \\ 0.00 & 0.00 & 0.00 & 0.00 & 0.00 & 0.00 & 0.00 & 0.00 \end{bmatrix} \quad (4.47)$$

$$[E_{2I}] = 10^{-2} \times$$

$$\begin{bmatrix} 95.98 & -95.98 & 0.00 & +0.00 & 0.00 & 0.00 & 0.00 & 0.00 \\ 0.00 & 0.00 & -34.84 & 34.84 & 0.00 & 0.00 & 0.00 & 0.00 \\ 0.00 & 0.00 & 0.00 & 0.00 & 57.33 & -57.33 & 0.00 & 0.00 \\ 0.00 & 0.00 & 0.00 & 0.00 & 0.00 & 0.00 & 0.00 & 0.00 \\ -0.75 & +0.75 & 0.00 & 0.00 & 0.00 & 0.00 & 0.00 & 0.00 \\ 0.00 & 0.00 & -0.82 & -0.82 & 0.00 & 0.00 & 0.00 & 0.00 \\ 0.00 & 0.00 & 0.00 & 0.00 & 0.60 & -0.60 & 0.00 & 0.00 \\ 0.00 & 0.00 & 0.00 & 0.00 & 0.00 & 0.00 & 0.00 & 0.00 \end{bmatrix} \quad (4.48)$$

where the controllable left half-plane eigenvalues of the matrix $\mathcal{H}$ are

$$\begin{bmatrix} -4.28 + 47.43i \\ -4.28 - 47.43i \\ -8.26 + 109.91i \\ -8.26 - 109.91i \\ -9.52 + 190.24i \\ -9.52 - 190.24i \\ -10.14 + 127.49i \\ -10.14 - 127.49i \end{bmatrix} \tag{4.49}$$

The performance of the LQ controller have been numerically simulated. Figures (4.2) and (4.3) show the impulse response and forced response of the plant at $(\frac{5L_x}{12}, \frac{7L_x}{12})$ respectively. As shown in the FFT of the uncontrolled impulse response and forced response of the simply supported plate, the observation point was chosen such that the contributions of the all modes are evident in the output signal. For the uncontrolled impulse response, it takes over 10 seconds to suppress the vibration. By implementing the LQ controller this period can be cut down to 3 seconds. In the controlled forced case the vibration amplitude shows a 50% reduction of amplitude in comparison to the uncontrolled case. It was observed that magnification of the feedback matrix does not help to further reduce the vibration amplitude in the forced case or oscillation period in transient response.

In LCC method the controller frequencies have been selected to ensure the necessary beat phenomenon is present and are

$$[\omega_c] = \begin{bmatrix} 47.62 & 0 & 0 & 0 \\ 0 & 110.22 & 0 & 0 \\ 0 & 0 & 127.89 & 0 \\ 0 & 0 & 0 & 190.48 \end{bmatrix} \tag{4.50}$$

Considering the disturbance input has four harmonics $48s^{-1}, 110s^{-1}, 128s^{-1}$, and $190s^{-1}$, From (3.20) and (4.34) the controller optimal damping can be found as

$$[C_c] = \begin{bmatrix} 2.13 & 0 & 0 & 0 \\ 0 & 2.46 & 0 & 0 \\ 0 & 0 & 1.87 & 0 \\ 0 & 0 & 0 & 4.78 \end{bmatrix} \tag{4.51}$$

To investigate the performance of this control method the plant and the controller have been numerically simulated. A damping $\zeta_p = 0.05$ is introduced for each mode to reflect the true simulation of the plant. Figures (4.4) and (4.5) show the numerical results of the free vibration. As it is shown in Figure (4.5)b, the FFT of the output signal shows the contributions of the four modes. Figure (4.4) shows the plant response for a set of nonoptimal and nonmaximized α_c and α_p. As is clearly evident in Figure (4.4), the energy exchange between the coordinates, and furthermore this energy exchange may be maximized by appropriate coupling parameters. Observe that the beat period is entirely dependent of the product of the coupling parameters [69]. This means that to change the system, we need only change one of the parameters, leaving the other unaltered. This is a valuable tool where coupling coefficients may be restricted due to physical limitations of the chosen actuator. The best results were obtained when the controller damping ratio was optimum and the link between the plant and the controller was maximized with respect to physical limitation and stability limitation. In the forced case setting the controller damping factor is a compromise between plant/controller rate of energy modulation and the controlled steady state value. By increasing the controller damping factor the exchange and dissipation of energy between the plant and the controller was achieved in a shorter time but the steady state error increased. Figure (4.7) indicates that the product of coupling parameters define

the beat period as well as the control response improvement [69]. Defining the percentage of improvement over the uncontrolled response as one minus the ratio of the controlled amplitude to the uncontrolled amplitude, Figure (4.7) shows 70% improvement of the response. The effect of increasing the the coupling parameters depicted in Figure (4.8), which shows the force response of the system at $(\frac{5L_x}{12}, \frac{7L_x}{12})$ for an optimal damping and maximized $\alpha_c\alpha_p$. Here, the percentage of improvement over the uncontrolled response is over 80%. Figure (4.9) shows the force response of the system for an optimal damping and maximized $\alpha_c\alpha_p$, where the observation point is somehow that forth mode is not observable. It can be seen that in all cases, the frequency of the beat is entirely dependent on the product of the coupling parameters.

4.4 Conclusion and Summary

To study distributed actuators, we implemented a control law to quantify the characteristics of the controlled system. To investigate the performance of the control method, a laminated simply supported plate and the controller have been numerically simulated. Initially a LQ controller was employed to control a simply supported plate. The use of this strategy assisted in solving problems associated with the control of the plate. The results were also used to estimate the effectiveness of the other controller strategy. Examination of the LCC strategy indicated that the results did not generally improve relative to the LQ controller. However the LCC method can be furthermore improved by monitoring the energy of the plant as a criteria to connect/disconnect the link between the parameter of plant with the controller. In this method, the rate of energy modulation between plant and controller can be increased, compared to the LCC method, and the steady state controlled

value can be achieved in shorter time [44]. In the developed LCC technique the steady state vibration was reduced by over 80%.

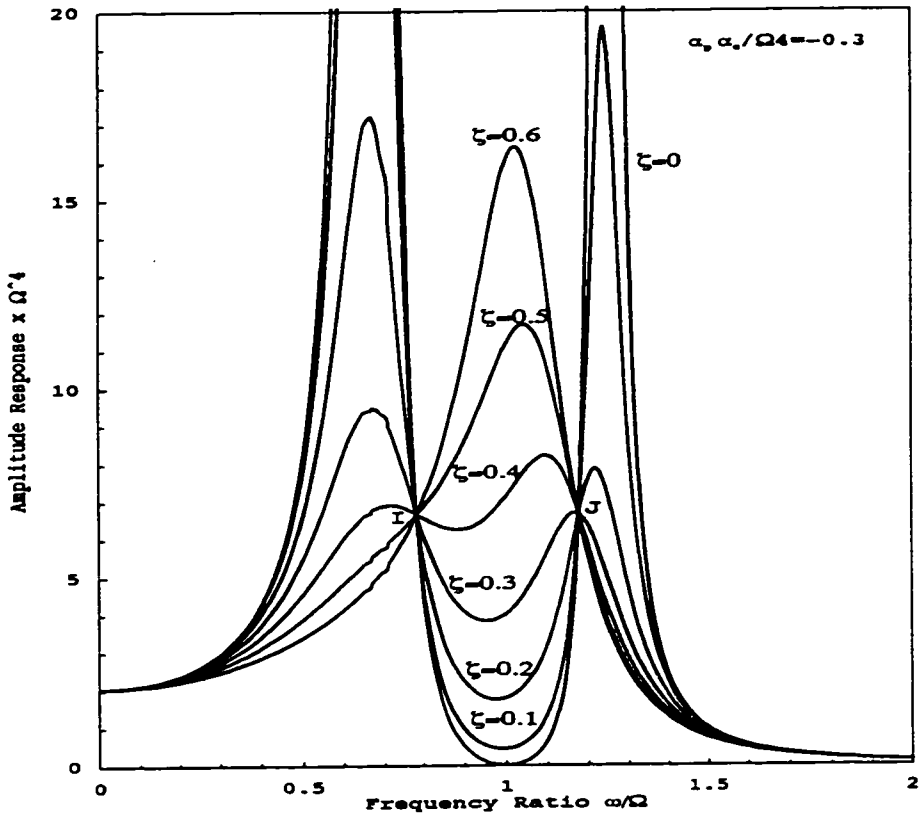

Figure 4.1: Damping Effects on the Forced Coupled System

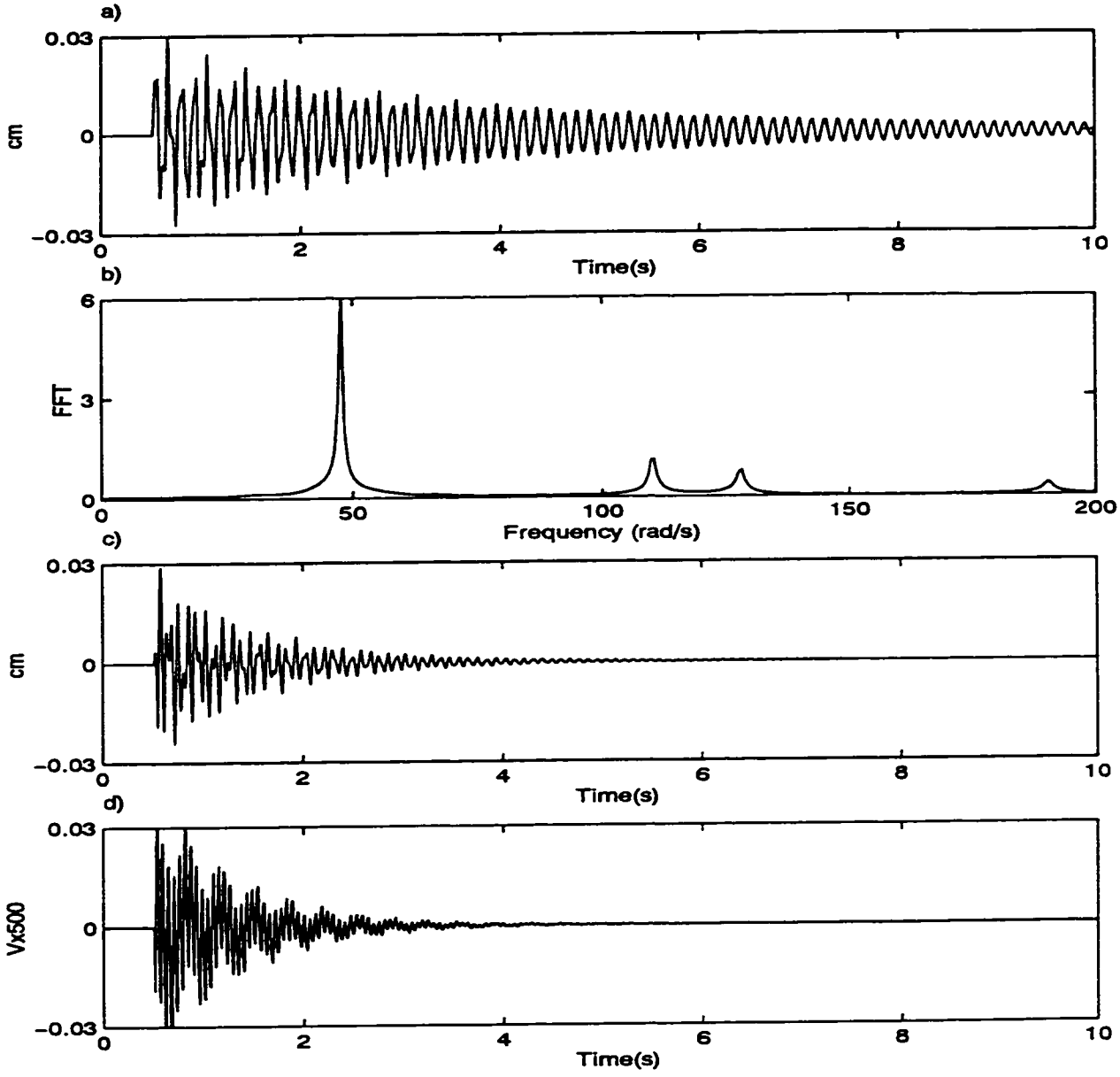

Figure 4.2: Oscillatory response of a simply supported plate to a pulse input a)Uncontrolled plant response at $(\frac{5L_x}{12}, \frac{7L_y}{12})$ b)FFT of the uncontrolled plant c) Controlled plant response at $(\frac{5L_x}{12}, \frac{7L_y}{12})$ using LQ d)Controller Input using LQ

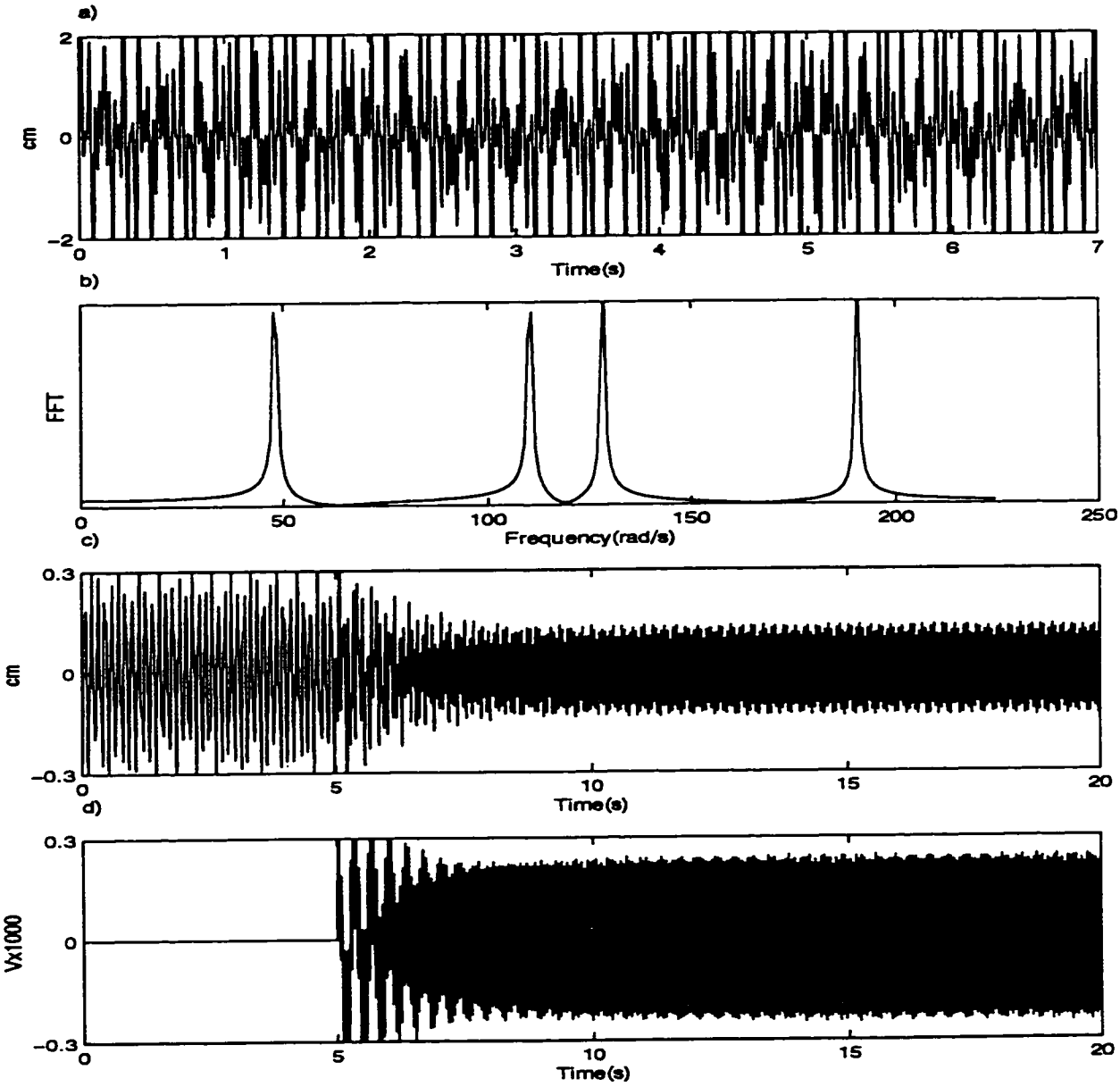

Figure 4.3: Oscillatory response of a simply supported plate to four harmonic inputs a)Disturbance b)FFT of the disturbance c)Plant response at $(\frac{L_x}{2}, \frac{7L_y}{12})$ using LQ d)Controller Input using LQ

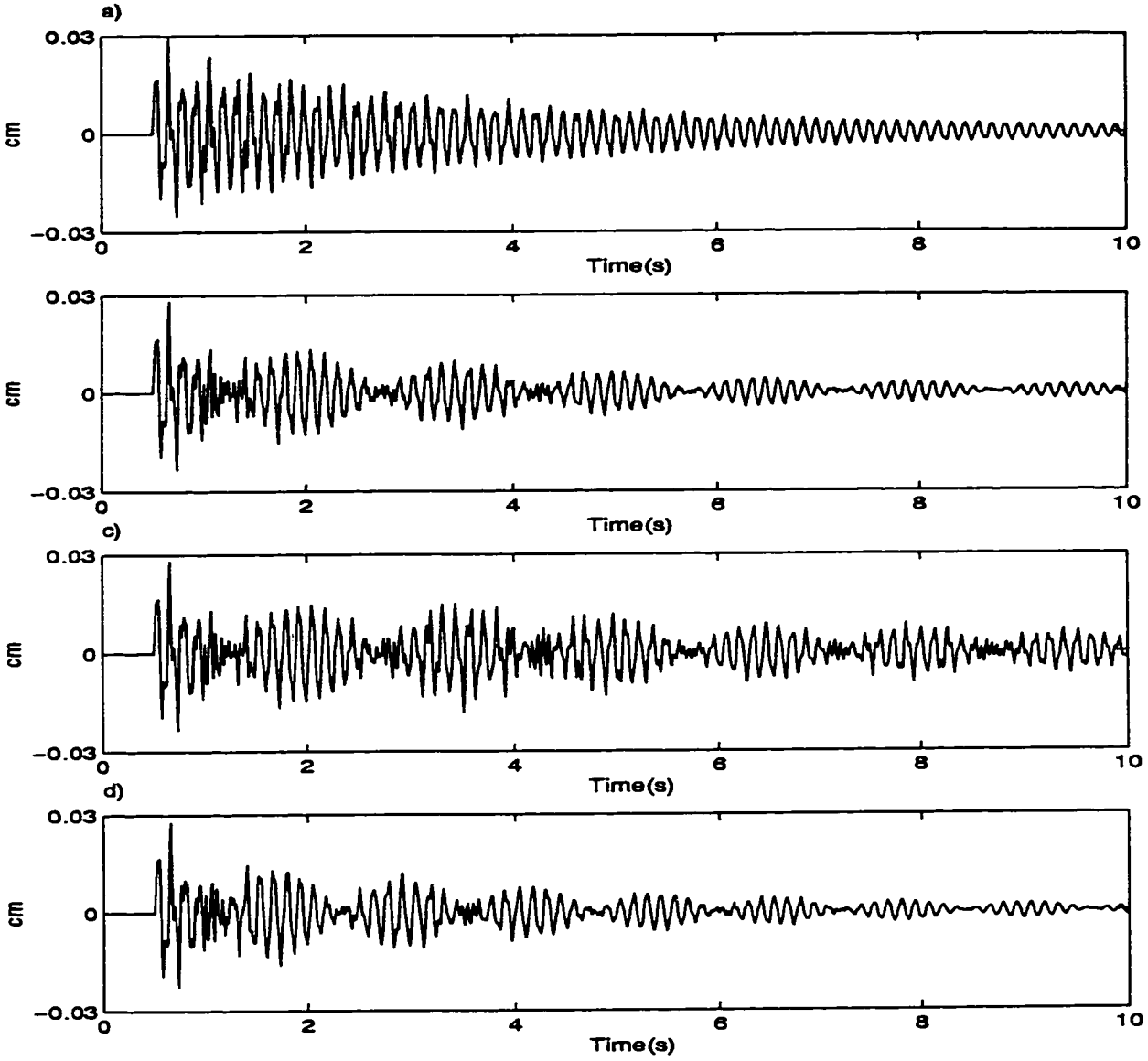

Figure 4.4: Oscillatory response of a simply supported plate to a pulse input a)Uncontrolled plant response at $(\frac{5L_x}{12}, \frac{7L_y}{12})$ b) Controlled plant response at $(\frac{5L_x}{12}, \frac{7L_y}{12})$ for $\alpha_p = -1500, \alpha_c = 750$ and $\xi_c = 0.05$ c)Controlled plant response at $(\frac{5L_x}{12}, \frac{7L_y}{12})$ for $\alpha_p = -1000, \alpha_c = 500$ and $\xi_c = 0.05$ d)Controlled plant response at $(\frac{5L_x}{12}, \frac{7L_y}{12})$ for $\alpha_p = -1500, \alpha_c = 750$ and $\xi_c = 0.1$

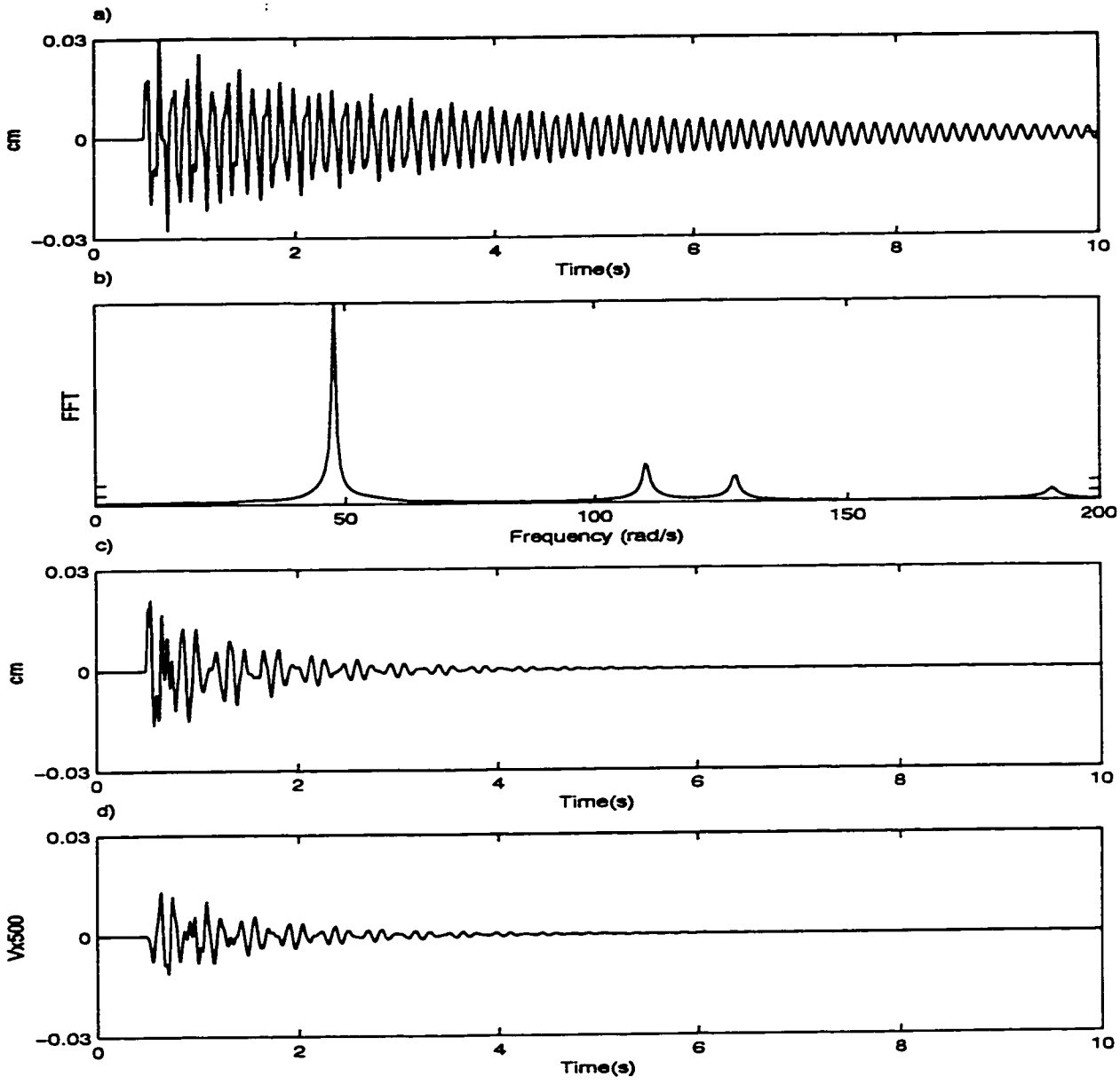

Figure 4.5: Oscillatory response of a simply supported plate to a pulse input a)Uncontrolled plant response at $(\frac{5L_x}{12}, \frac{7L_y}{12})$ b)FFT of the uncontrolled plant c) Controlled plant response at $(\frac{5L_x}{12}, \frac{7L_y}{12})$ for $\alpha_p = -2000, \alpha_c = 1000$ and optimal ξ_c c)Controlled plant response at $(\frac{5L_x}{12}, \frac{7L_y}{12})$ for $\alpha_p = -1000, \alpha_c = 500$ and $\xi_p = \xi_c = 0.05$ d)Controller input

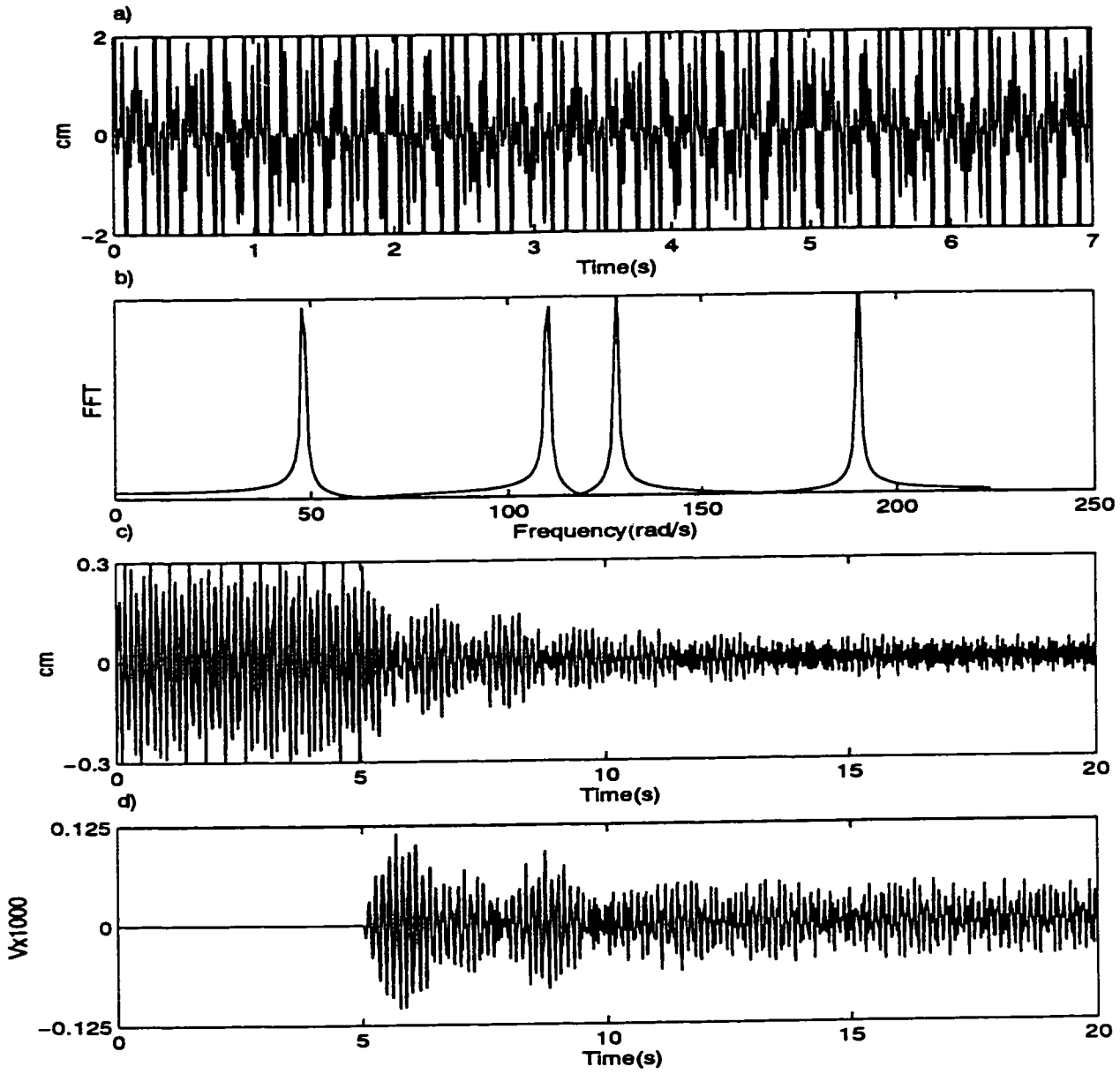

Figure 4.6: Oscillatory response of a simply supported plate to four harmonic inputs a)Disturbance b)FFT of the disturbance c)Plant response at $(\frac{5L_x}{12}, \frac{7L_y}{12})$ for $\alpha_p = -2000, \alpha_c = 1000$ and $\xi_c = .15$ d)Controller Input

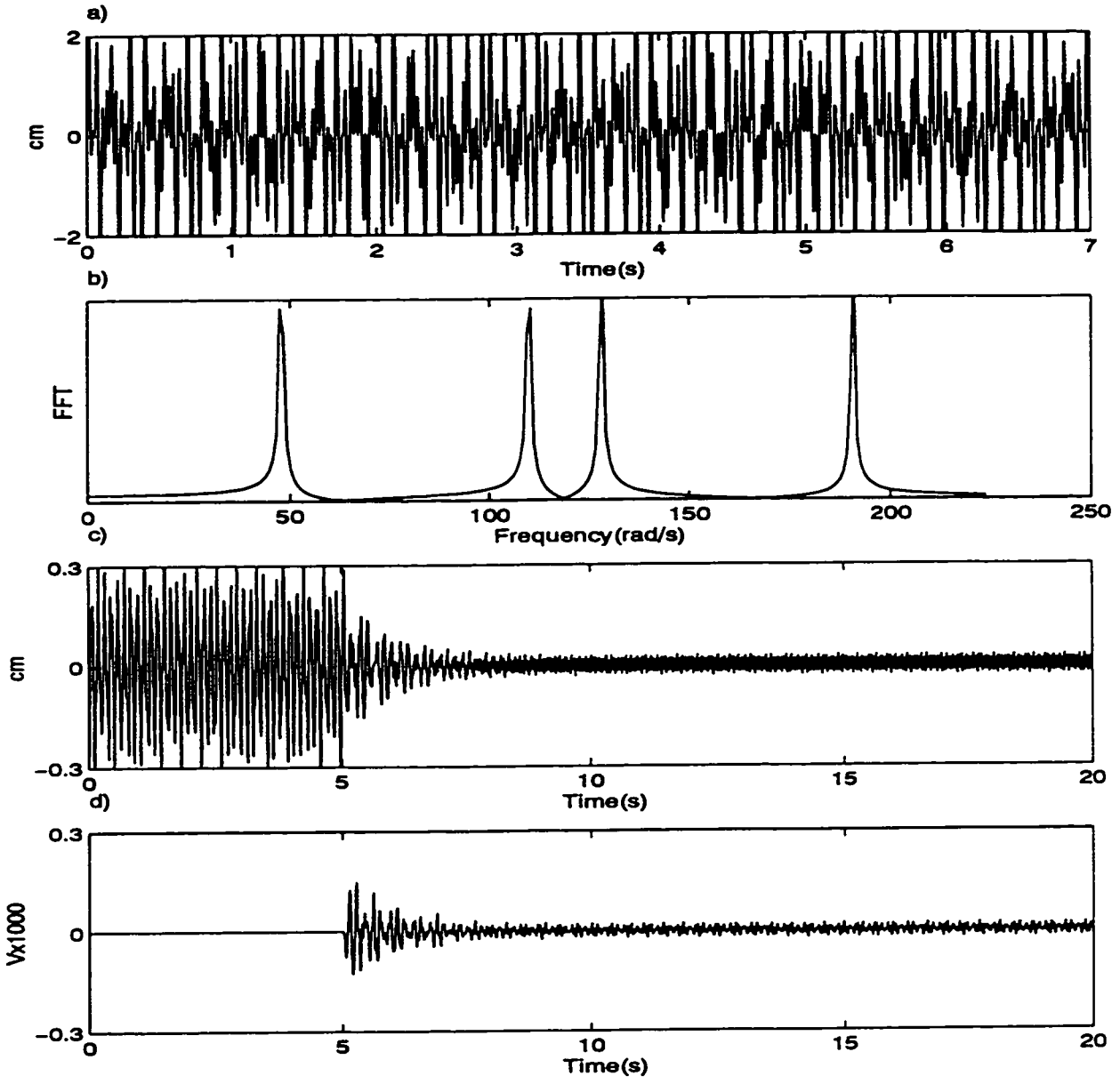

Figure 4.7: Oscillatory response of a simply supported plate to four harmonic inputs a)Disturbance b)FFT of the disturbance c)Plant response at $(\frac{L_x}{2}, \frac{7L_y}{12})$ for $\alpha_p = -1500, \alpha_c = 500$ and optimal ξ_c d)Controller Input

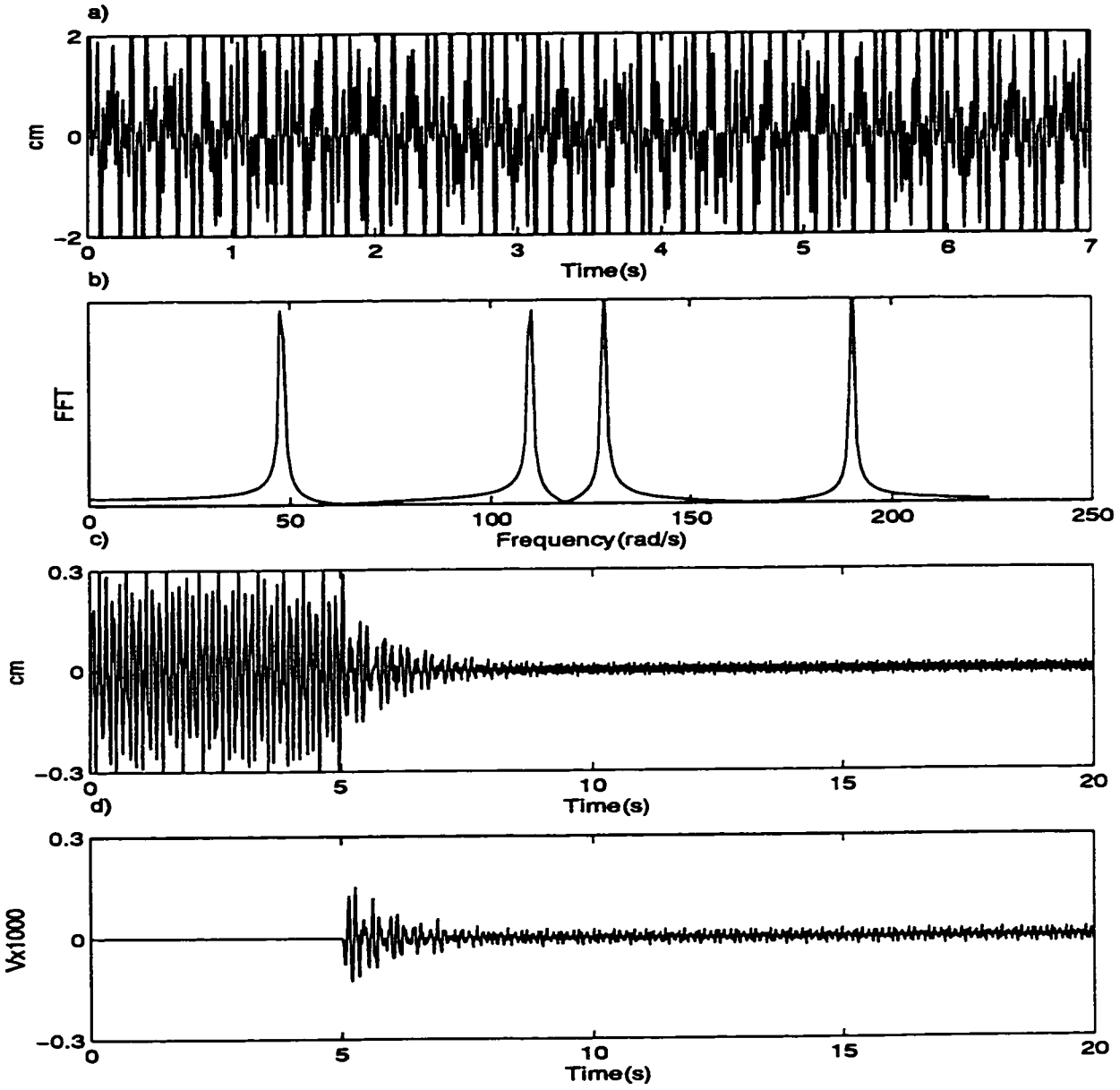

Figure 4.8: Oscillatory response of a simply supported plate to four harmonic inputs a)Disturbance b)FFT of the disturbance c)Plant response at $(\frac{5L_x}{12}, \frac{7L_y}{12})$ for $\alpha_p = -2000, \alpha_c = 500$ and optimal ξ_c d)Controller Input

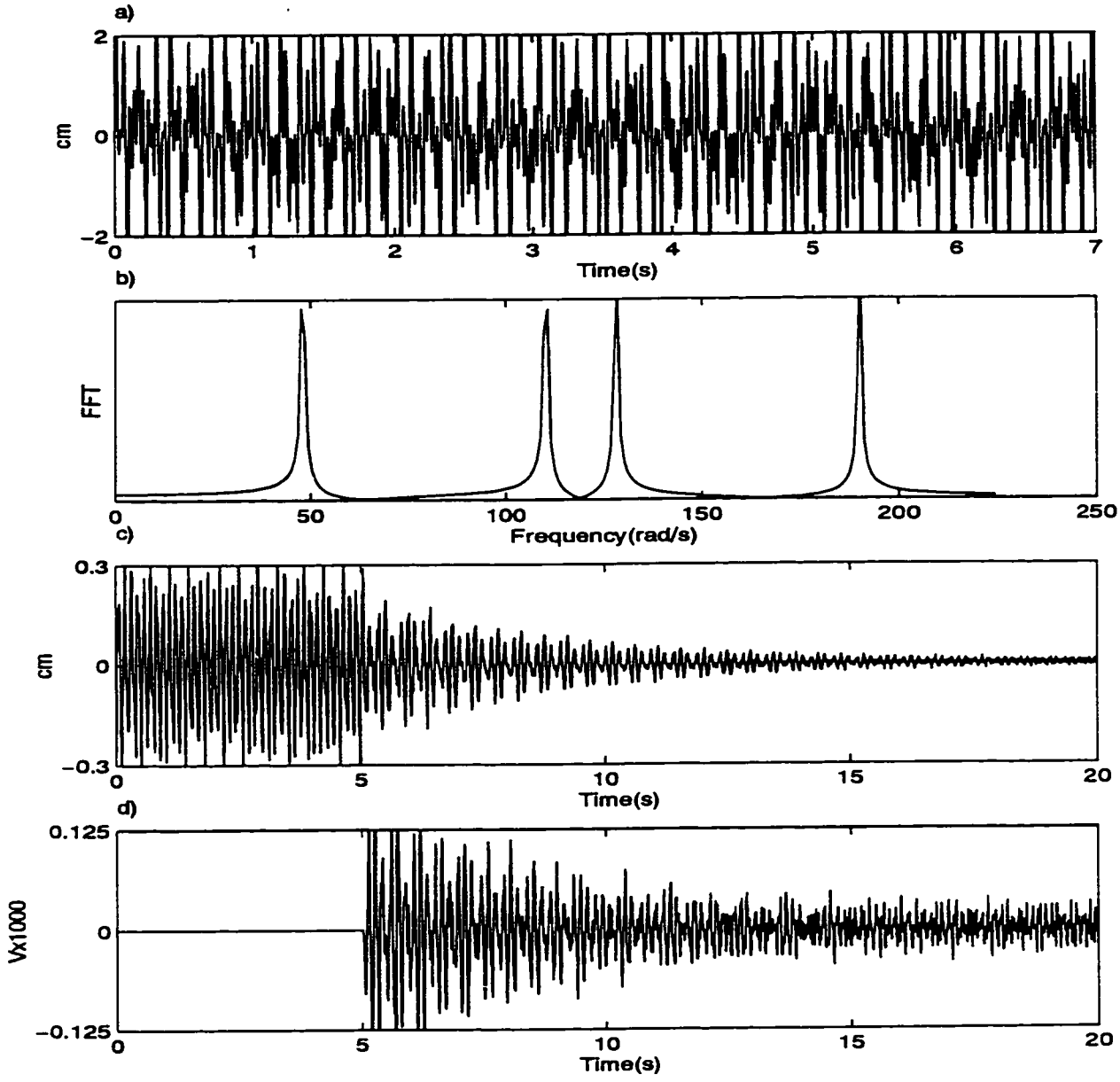

Figure 4.9: Oscillatory response of a simply supported plate to four harmonic inputs a)Disturbance b)FFT of the disturbance c)Plant response at $(\frac{5L_x}{12}, \frac{7L_y}{12})$ for $\alpha_p = -1000, \alpha_c = 500$ and optimal ξ_c d)Controller Input

Chapter 5

Experimental Implementation

The experimental study of structural vibration control is a key component of this research. Experimental observations have been made to determine the nature and extent of vibration and to verify the theoretical models and predictions. We have used Modal Testing with an objective to estimate the dynamic and vibration behavior of a simply supported plate. This phase of the modal test procedure is often referred to as experimental modal analysis and leads to derivation of the system's modal properties. In addition, the control models suggested by the theory developed in Chapters 3 and 4 are verified experimently. The experimental verification of these approaches to vibration suppression is presented for a simply supported plate with attached piezoelectric actuators at optimum locations according to the method described in Chapter 3. The virtual controller has been built into a Pentium based personal computer with a clock rate of 100 MHz. The Matlab software, Real-Time Workshop Toolbox, WatCom C^{++} compiler, and WinCon software in conjunction with an Analog-Digital/Digital-Analog card are employed to implement the control law.

5.1 Introduction

A review of the recent developments in the analysis of laminated plates shows a significant amount of research conducted on the numerical and analytical modeling of the plate. However, to the best knowledge of the author, there are not many experimental investigations on active control of plates.

Fuller *et al.* [71] experimentally studied the control of sound radiation from a simply supported rectangular plate with a single piezoelectric actuator as the control input. In that study, control of a far-field sound was achieved by "modal suppression," meaning that during control, all of the modal amplitudes were reduced. The alternative to modal suppression is "modal restructing." In modal restructing, the modal amplitudes can increase; however, the residual structural response has a lower overall radiation efficiency leading to a reduction in far-field sound level [72]. As an extension to the work conducted by Fuller *et al.* [71], Clark [73] studied the distributed control of the structure, utilizing up to three piezoelectric actuators as control inputs, in conjunction with an adaptive controller. In this work Clark considered a simply supported rectangular plate excited by a steady-state harmonic point force. Based on results of this study, the adaptive lms algorithm [71] is shown to be effective narrow-band controller. As a future work Fuller and Clark both recommend the optimization of the location of the piezoelectric actuators.

An experiment has been performed by Gu *et al.* [74] to investigate the implementation of shaped polyvinylidene fluoride (PVDF) modal sensors on a simply supported rectangular plate to control specific modes of the vibration. A comparative test was performed by using two accelerometers as error sensors. Results indicated that for both on and off resonance excitations, the shaped PVDF modal sensors are superior to point error sensors, such as accelerometers for controlling

specific structural modes.

Dworak [64] considered two configurations to experiment the vibration control of a rectangular clamped plate. A localized configuration in which an accelerometer is used as feedback to a collocated PZT actuator and a cross coupled configuration in which the accelerometers combined to form the feedback to a particular PZT. Two control design method considered for closing the loops between the accelerometers and PZT actuators, rate feedback obtained by integrating the accelerometer signals and the H_∞ design methodology. The experimental comparison shows superior performance of rate feedback over H_∞ controllers for a broad band disturbance. However, the advantage of the H_∞ design over the rate feedback is its ability to concentrate the attenuation at specific frequencies.

The experimental application of a linear coupling control strategy to control free and forced vibrations of a cantilever beam was investigated by Fariborzi *et al.* [44] which will also be discussed in this chapter. In this work the overall effectiveness of three different strategies for vibration suppression of a cantilever beam was examined. Initially a state feedback controller was employed. The results of this method of control were used to estimate the effectiveness of the other control strategies. Examination of the linear coupling control strategy by using position as coupling state indicated that the results were generally comparable to a conventional state-feedback controller. Furthermore the linear coupling control method was improved by monitoring the energy of the plant as criterion to connect/disconnect the link between the parameter of the plant and the controller. In the forced vibration the control law provided over 98% improvement in amplitude over the uncontrolled responses.

5.2 Experimental Apparatus

In this section the control models suggested by Tuer [75] are evaluated experimentally and the results of the proposed control algorithm are compared with the linear quadratic optimal control. The experimental setup is comprised of two components, the physical structure (the plant) and the virtual system (the controller). The physical system is a simply supported aluminum plate. The control apparatus consists of a Pentium computer with an internal Analog-Digital/Digital-Analog module. The piezoelectric elements bonded to the optimal locations of the plate are used to couple the plant and the controller [65]. The collocated strain gauges have been placed on the opposite face of the plate to measure the plate vibration.

5.2.1 Aluminum Plate

The simply supported plate under study is a thin aluminum plate which is attached to a massive test-bed (with cutoff frequency of 100Hz) in order to isolate the plate from external excitations (Figure 5.1). The simply supported boundary conditions were achieved by attaching the plate to the rigid frame with cloth duct tape (Figure 5.2). This method of implementation of simply supported boundary allows the plate to bend relatively freely but restricts out of plane motion at the boundaries. The piezoelectric actuators consist of 8 thin piezoelectric elements, which are used for disturbance inputs and the control inputs (Figure 5.3). The piezoelectric material is a PZT ceramic H4E-602 series produced by Piezo Systems, Inc. These piezoelectric elements are bonded to the plate with TRA-DUCT 2919 epoxy, and are arranged such that the dielectric poles of all elements are pointing in the same direction. TRA-DUCT 2919 is a non-bleeding, electrically conductive, silverfilled epoxy recommended for electronic bonding. Since the epoxy is conduc-

tive, it permits current to flow to the undersides of the elements. The material characteristics and dimensions of the plate and piezoelectric elements are outlined in Tables 3.2 and 3.3. The plate deflections are measured using a bidirectional strain gauge (Measurement Group Gauge, type EA-B-125TQ-350) bonded near the piezoelectric layers as in Figure 5.4. The strain gauge signal is amplified by a signal conditioning instrument "CIO-EXP-GP" made by National Instruments Corporation (Figure 5.5), and was sent to a data collection device "A/D card".

5.2.2 Control System

A personal computer containing a Pentium processor with a clock rate of 100 MHz is used to design the controller Figure 5.6. The controller is implemented on Matlab software in conjunction with Simulink, Real-Time Workshop, DSP Blockset toolboxes, and WinCon software. Matlab is a technical computing environment for high-performance numeric computation and visualization.

5.2.3 Data Acquisition

The proposed control algorithm requires signal conditioning instruments, a data collection device and a control signal mechanism. Figure 5.5 shows the strain gauge signal conditioner. Initial data is acquired using an EA series strain gauge from Measurements Group, Inc. (see Figure 5.2). The strain gauge is a 300Ω resistor that changes resistance when it is stretched or compressed. In order to measure the resistance change, a CIO-EXP-GP is used. The CIO-EXP-GP manufactured by ComputerBoards, Inc is an amplification, signal conditioning and multiplexing accessory for DAS boards. The inputs are suitable for connecting a voltage to the DAS board so it may be measured. An analog to digital converter "ADC" is used to

interpret the beam response signal and a digital to analog converter "DAC" is used to provide a control voltage back to the piezoelectric actuators. These two functions are implemented using circuitry on the same acquisition card, CIO-DAS1600. This board is manufactured by Computer Boards, Inc. and can achieve 12 bit resolution with speeds of up to 10^5 samples per second. The card is set with a hardware switch to a maximum output of ± 10 volts to provide the largest possible signal to the piezoelectric elements. Later the calculated control signal is sent via DAC to a 20 times amplifier. This increases the voltage to a level that allows the piezoelectric elements to produce a significant amount of strain in the plate.

5.3 System Identification

The experimental investigation of the structural vibration characteristics is a necessary step prior to the design of a control strategy for vibration regulation. Experimental observations help to determine the nature and extent of the vibration. A preliminary test was conducted to derive the modal properties of the plate. The response of the simply supported plate was tested by using an impulse excitation as an input to the plate and the frequency was sampled (through strain gauges) between 2.00 Hz and 50 Hz. The force signal output and the strain gauge signal were amplified and sent to a HP 35660 Dynamic Signal Analyzer. These two signals are used to plot the frequency response function (FRF) curve of the plate. An average of 15 impulse responses are obtained to reduce the effect of noise. Based on experimental FRF plots the first three damped frequencies are $48.21s^{-1}$, $117.2s^{-1}$, and $137.2s^{-1}$ (Figure 5.7). The comparison between the experimental and predicted natural frequencies obtained in (3.100) shows a good agreement between these two methods. The first predicted mode shows less than 1.3% discrepancy with the first

experimental mode. The trend of the second and third mode appear to be comparable for the experimental and predicted FRF's, but with a larger variation of the natural frequencies. The discrepancy may be due to many factors and imperfections not incorporated in the mathematical model. For example, there exist a possibility of inconsistencies in the boundary condition, material imperfections, or heterogeneous thickness of the plate in the experiment. In addition, the natural frequencies obtained in (3.100) are undamped natural frequencies, while the experimental natural frequencies are damped natural frequencies. Based on these, the experimental natural frequencies are expected to be different from the predicted natural frequencies. There are some methods to adjust the mathematical model of the plate to more accurately predict the measured behavior of the system [76]. There are also methods to measure the damping of the system more precisely [77]. However, model updating and damping measurements are not in the scope of this work.

Because of the aforementioned limitations, the inherent noise in the system (due to the cables, the force transducer, and the strain gauge), and unpredictable response of the supports, some error can be expected between the experimental and the theoretical results of the controlled system.

5.4 Free Vibration Control results

For free vibration control, an impulse input is applied to the center of the plate. After 2 seconds the response of the plate is monitored. For the uncontrolled case, Figure 5.8a, after the pulse is applied to the plate , the vibration takes about 3.6 seconds to disappear. The measured data also reveals that the first mode has the most significant contribution to the response of this specific observation point. A

comparison between the experimental results and the numerical simulation shown in Figure 4.2a show that the actual system, as expected from system identification, has much more than the 5% inherent damping which was assumed in the numerical simulation. If one assumes the effect of higher modes to be negligible, a rough estimate of the damping associated with the first mode may be obtained from the logarithmic decrement method to be $\zeta_{11} = 0.26$. However this method is highly unreliable in this case.

To provide a basis for comparing the results of conventional control methods and the proposed control algorithms, the LQ control method has been implemented as a control algorithm for the simply supported plate. In this method position and velocity were selected as the states to feedback. Therefore $\mathcal{U}$ in equation (4.1) is defined as

$$\mathcal{U} = G\mathcal{Z}(t) \tag{5.1}$$

The controller gain is then set to the optimal state feedback control matrix obtained in (4.44) such that maximum effectiveness (minimum plate deflection) is obtained and saturation of the amplifier does not occur. The ability of the LQ controller to damp the pulse response is shown in Figure 5.8b. A comparison between the theoretical model (Figure 4.2c) and the experimental model (Figure 5.8b) shows similar trends of response; however due to having nonsymmetric piezoelectric actuators (the piezoelectric layers are attached on one face of the plate) the response does not look quite as symmetric as in the numerical simulation. This is due to the fact that in the model, it was assumed that the moments are applied on the neutral axis.

To implement the LCC method, based on desirable pseudo-energy characteristics of the system [75], position (strain gauge output) was chosen (see (4.20), (4.21)) as the coupling term between the plant and the controller. A necessary requirement

for the LCC technique to succeed is the presence of a beat [75]. Through variation of the controller frequency it is possible to manipulate the beating relationship with the plant, and consequently obtain different beat frequencies in the plant. To confirm that this phenomenon could be obtained, coupling parameters were chosen based on the first three modes of the identification result $\omega_{c_{11}} = 48.21s^{-1}$, $\omega_{c_{12}} = 117.2s^{-1}$, and $\omega_{c_{21}} = 137.2s^{-1}$. The controller damping ζ_c was then varied. There is a critical damping parameter that will optimally reduce vibration by maximizing the decay rate of plant energy. The optimal values of the controller damping were experimentally evaluated as $\zeta_{c_{11}} = 0.303$, $\zeta_{c_{12}} = 0.411$, and $\zeta_{c_{21}} = 0.710$. These values were found by sweeping the value of the damping factor over an expected range. The controller initial condition is set by means of giving an initial voltage to the integrator. This voltage is selected as a function of disturbance. The result is that the controller output always starts with the maximum error to suppress the vibration. The position feedback gain is set such that the saturation of the amplifier does not occur. The experimental result of LCC is shown in Figure 5.8c. This Figure shows that in the controlled case the oscillation time has been cut to one third of uncontrolled case. This result (Figure 5.8c) deviates from numerical results because of the same reasons mentioned in the experimental LQ control. However, the controller is very successful in eliminating the plate vibrations. Figures 4.5d and 5.8d present numerical and experimental LCC control input voltages to the piezoelectric actuators. From these results it is obvious that other than simplicity there is no significant advantage/disadvantage of LCC over LQ method.

5.5 Forced Vibration Control results

The problem with forced vibrations that result from a continuous input to the system is that it is not easy to completely suppress the plant vibration in the absence of a strong actuator with a small time constant. Whereas for free vibrations it is possible to entirely eliminate the vibration, with speed being the only limiting factor. In forced vibrations, external excitation is mainly destructive when the driving frequency is close to the resonant frequency of the physical system. Since it is at resonance when this forcing frequency maximizes the vibration amplitude, the first natural frequency of the plate was used in each of the control tests ($\omega_f = 48.21s^{-1}$) as the forcing frequency. Initially the disturbance input was applied to the plate through a VTS 40 vibration shaker. Due to the limitation of the piezoelectric actuators, it was desirable to apply a smaller force at the resonant frequency without adding any traveling constraint at the excitation point. To apply a small force, the peak amplitude of the shaker had to be very small. However by doing this through a shaker, a constraint would be introduced to the system. To achieve the ideal situation (a small force applied at resonance without adding any traveling limitation), the plate was excited through piezoelectric element numbered 1 in Figure 5.5. As a result since the nature of the forcing has been changed, the numerical results may no longer be compared with the experiments. The plate transients were allowed to dissipate and the controller was only turned on when the steady state response was established. Initially an LQ controller was used. The controller gain was set to the optimal state feedback control matrix values (4.44) for maximum controller effectiveness and to avoid saturation. After 4 seconds, the amplitude of the vibration is diminished by 80% (Figure 5.9a). A disadvantage of this system was a control spillover effect where the second mode of the system

was easily stimulated. This was avoided by the use of a second order filter but it introduced a trial and error component. In the LCC method through six coupling mechanisms, a stable pair "plant position and controller position" was used to link the plant and the controller [36]. The frequency of the controller, ω_c, was left at the optimal value, which is equivalent to a forcing frequency $\omega_f = 48.21s^{-1}$. Since the controller is a continuous active vibration absorber, the initial condition of the controller was inconsequential to the overall response, hence it was set to zero. Initially, the optimal damping parameter $\zeta_c = 0.316$ obtained in (4.34) was used. For further tuning of the system, an energy monitoring algorithm was used to tune the damping parameter ζ_c. By estimating the final level of the plant energy, it was found that the damping parameter $\zeta_c = 0.368$ minimized the amplitude in the steady state response. The steady state response amplitude, and the minimal level of energy for the nonoptimal values of the controller natural frequency and damping parameters are shown in Figure 5.9b. Figure 5.9a shows the response of the system for the optimal values of the controller. It is apparent from these plots that the modulation of energy between the plant and the controller takes 3 seconds. After energies transfered from the physical system to the auxiliary system the amplitude of vibration shows an 80% reduction in comparison to the uncontrolled case.

With further improvement of the LCC method, a subsequent control technique can be implemented to increase the rate of energy modulation and to decrease the final energy level of the plant. The principle of the improved controller is based on introducing a disable time for the controller. In the energy exchange between oscillators, there exist periods of time when the virtual controller is importing extra energy to the plant. One alternative to avoid such a phenomena is to monitor the level of the pseudo-energy in either the plant or the controller [44]. When the energy in one of these coordinates passes a local extreme, the plant and the controller are

decoupled ("disable time").

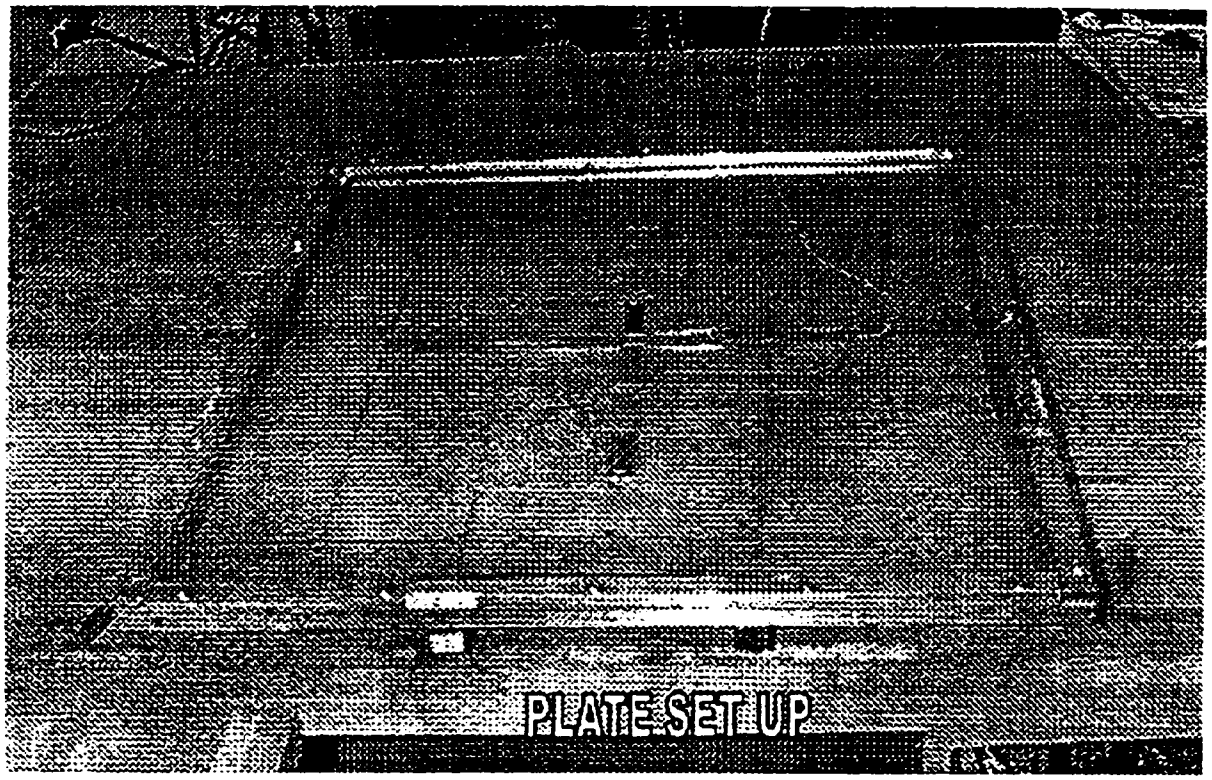

Figure 5.1: Plate in the experimental set-up

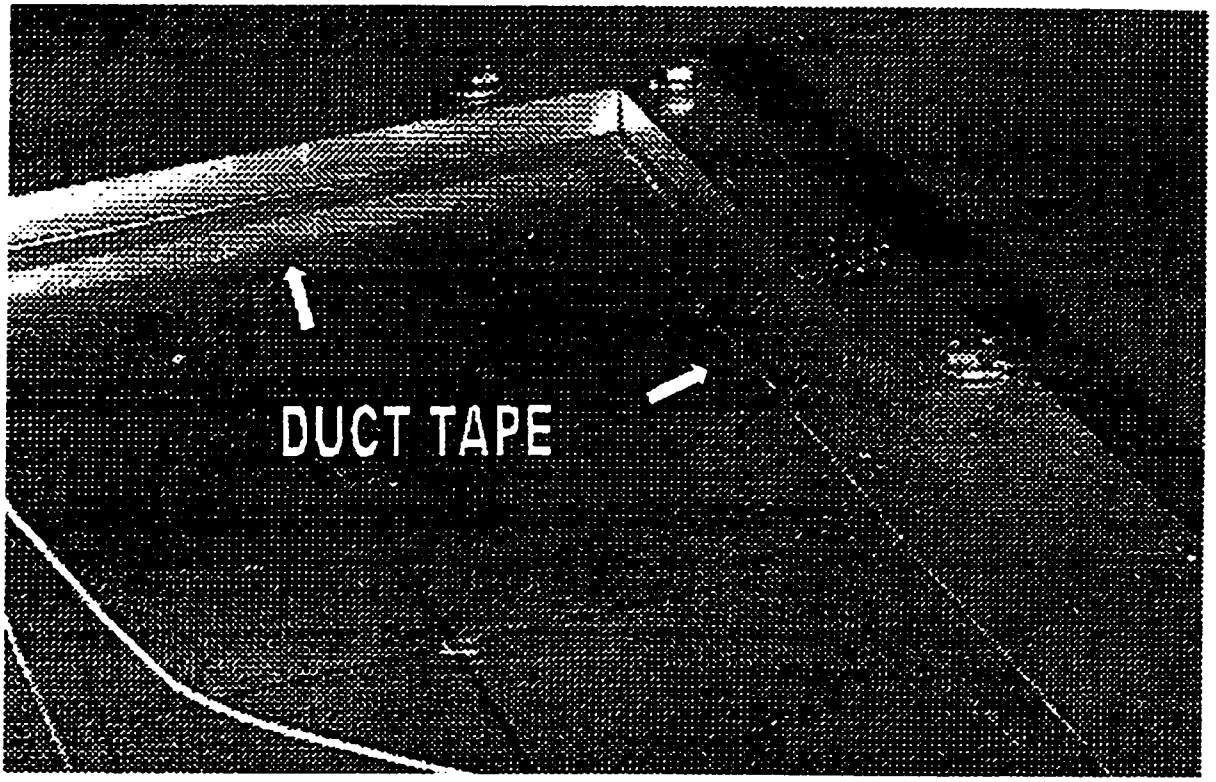

Figure 5.2: Boundary condition in the experimental set-up

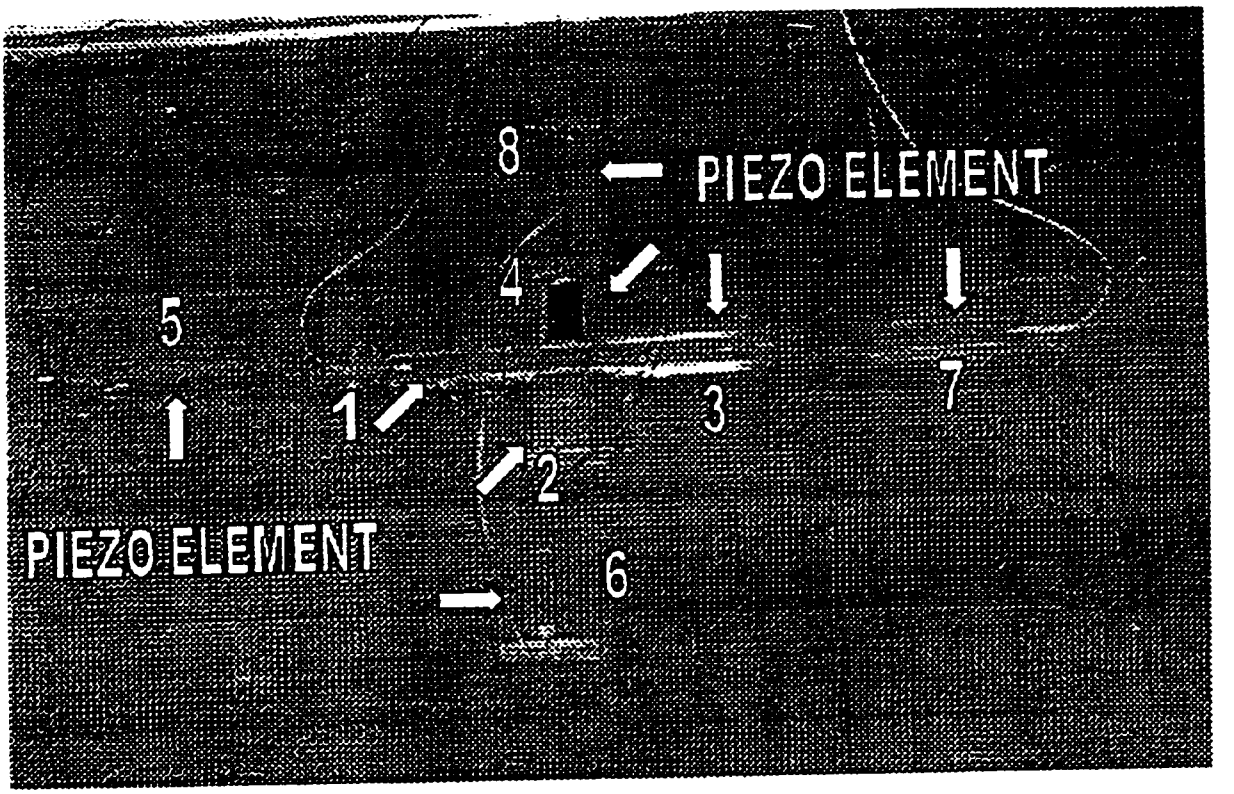

Figure 5.3: Piezoelectric elements in the experimental set-up

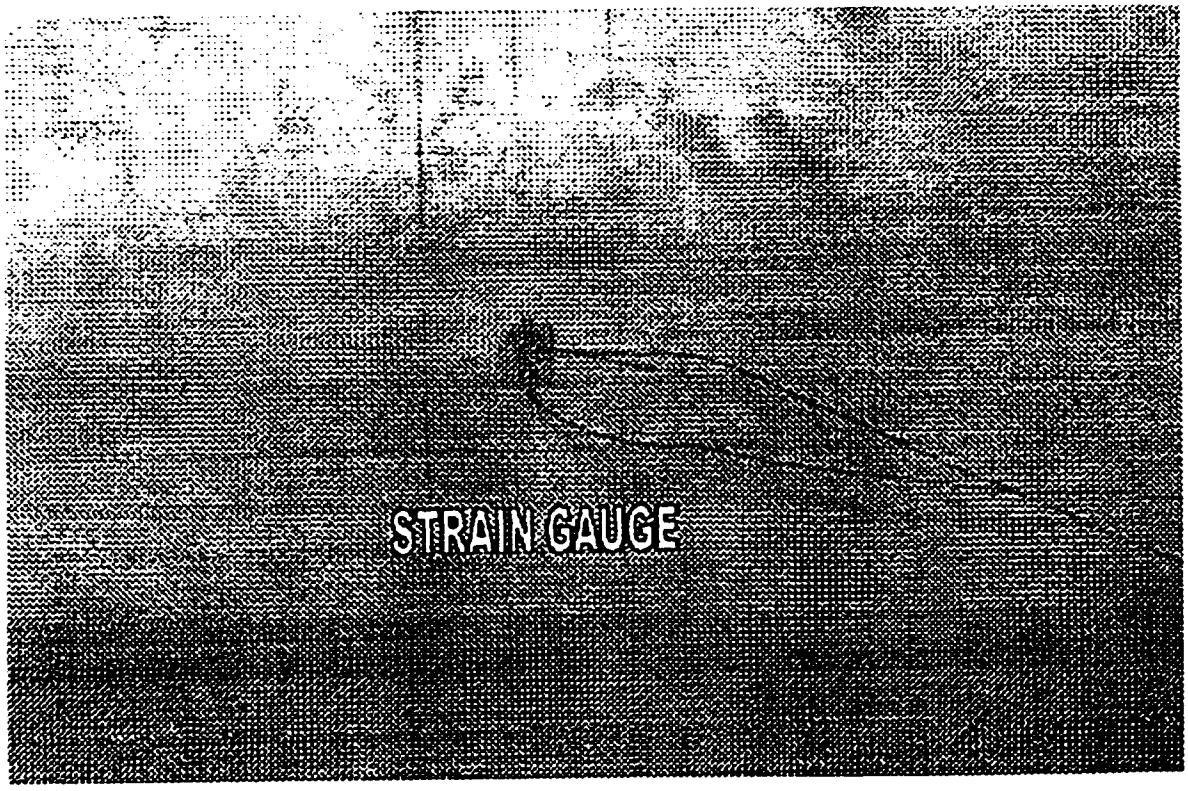

Figure 5.4: Strain gauge in the experimental set-up

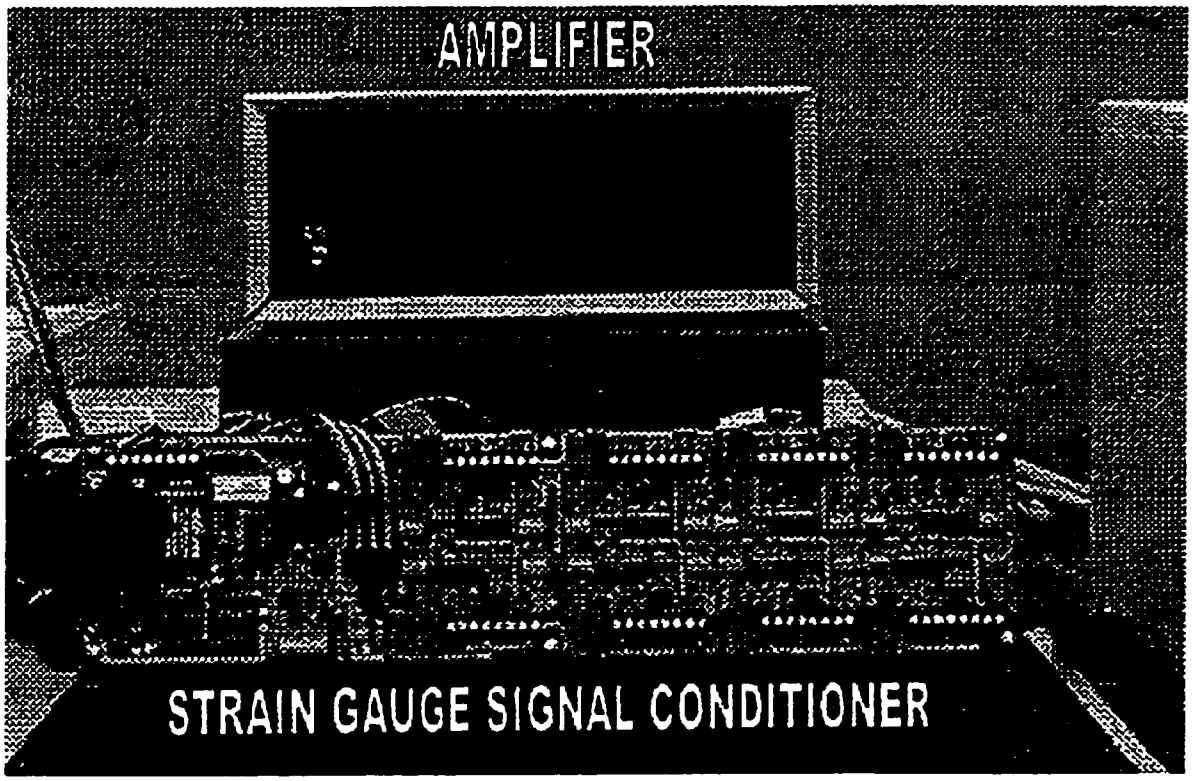

Figure 5.5: Signal conditioner and amplifier in the experimental set-up

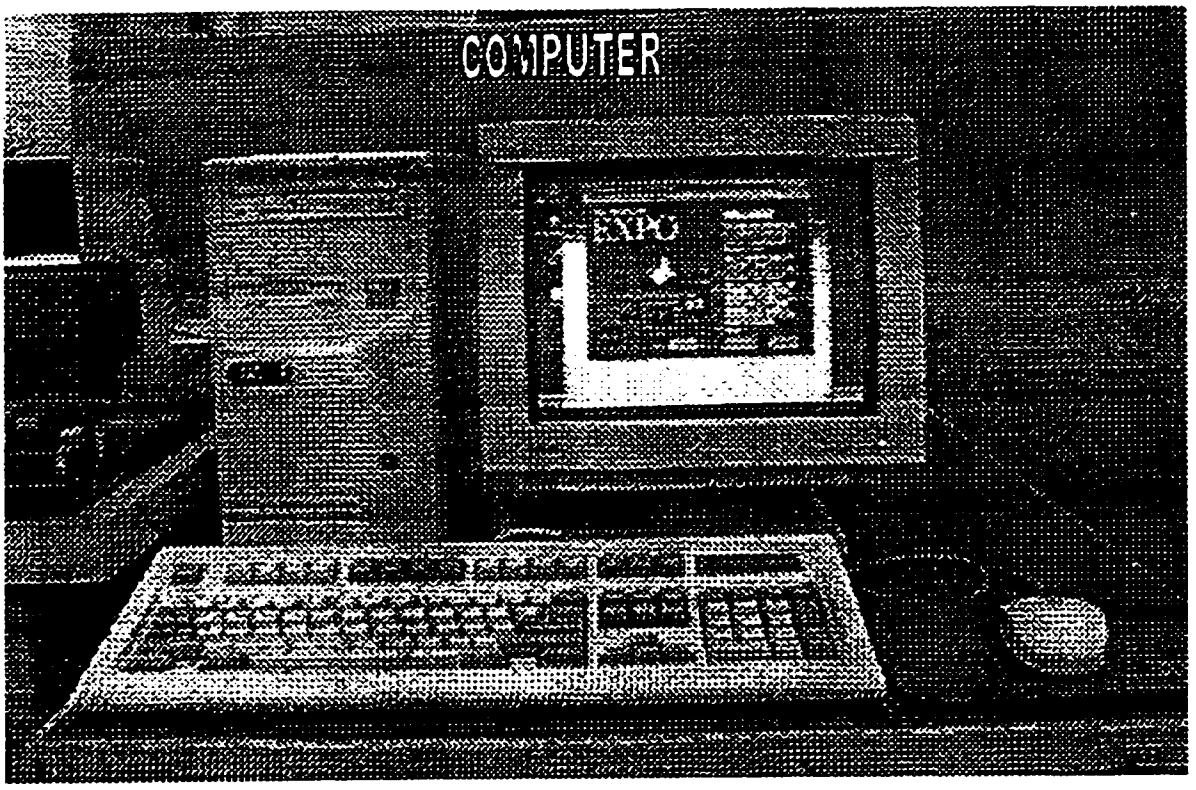

Figure 5.6: Control system in the experimental set-up

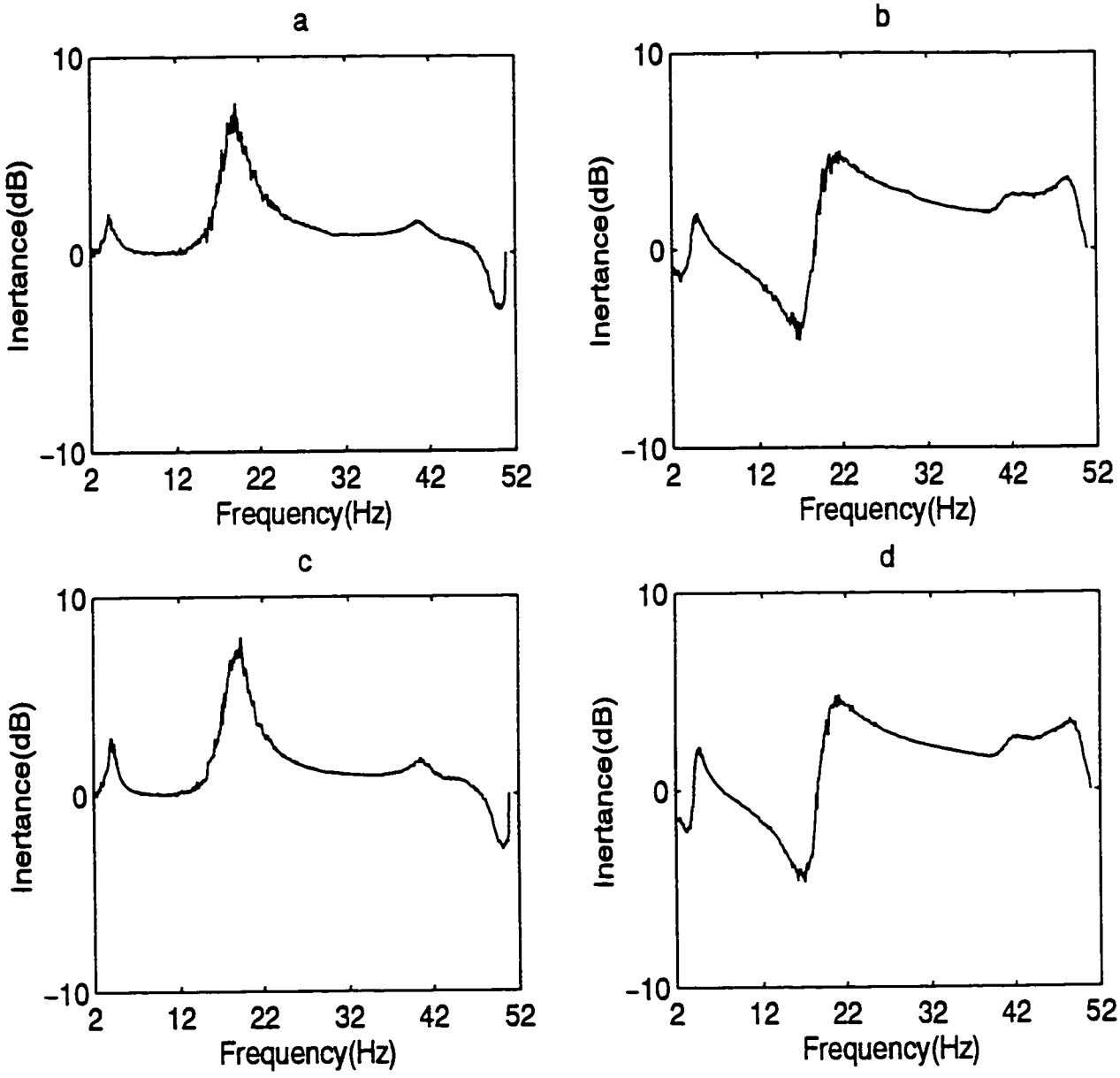

Figure 5.7: Frequency Response Function of Point $(\frac{5L_x}{12}, \frac{5L_x}{12})$ a)Magnitude b)Real, Frequency Response Function of Point $(\frac{7L_x}{12}, \frac{5L_x}{12})$ c)Magnitude d)Real.

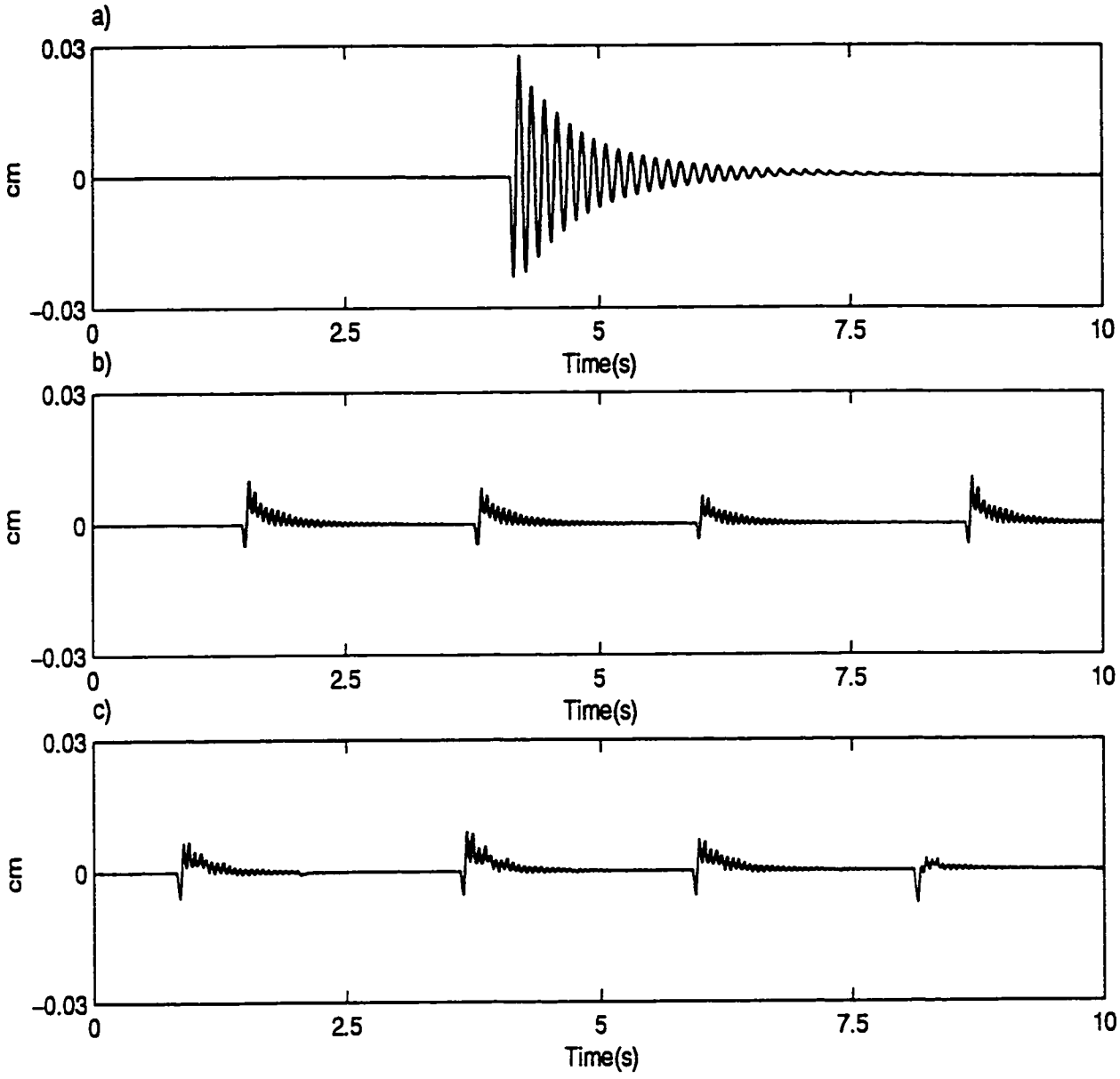

Figure 5.8: Oscillatory response of to a simply supported plate to the pulse inputs a) Uncontrolled plant response at $(\frac{L_x}{2}, \frac{L_y}{2})$ b)Controlled plant response at $(\frac{L_x}{2}, \frac{L_y}{2})$ using LQ c)Controlled plant response at $(\frac{L_x}{2}, \frac{L_y}{2})$ using LCC

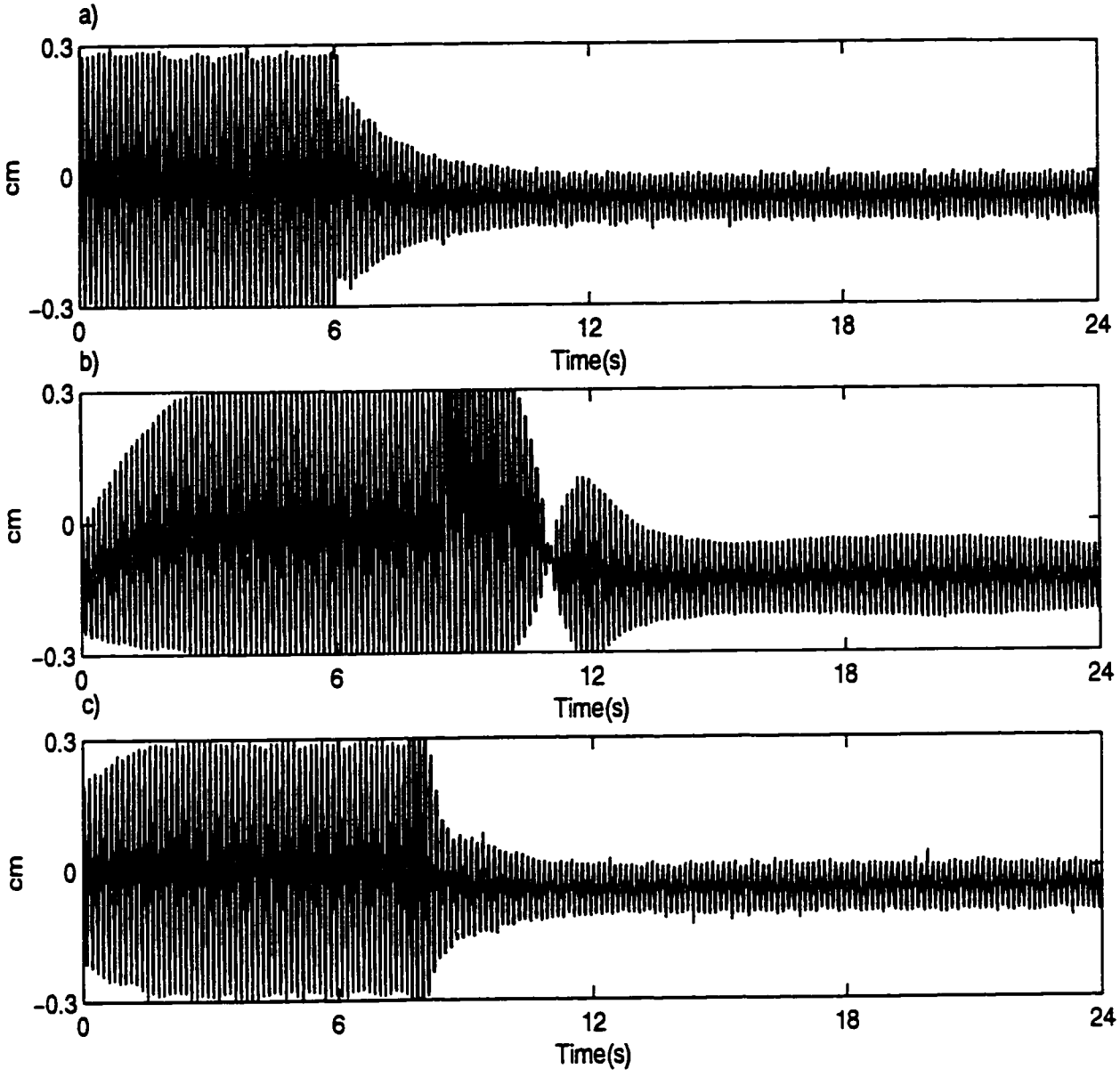

Figure 5.9: Oscillatory response of a simply supported plate to a harmonic input a) Plant response at $(\frac{L_x}{2}, \frac{L_y}{2})$ using LQ b) Plant response at $(\frac{L_x}{2}, \frac{L_y}{2})$ using nonoptimal LCC c)Plant response at $(\frac{5L_x}{12}, \frac{7L_y}{12})$ using optimal LCC

Chapter 6

Conclusion and Summary of the Research

The mathematical modelling of a plate with collocated piezoelectric actuators/sensors to be used for free and forced vibration control purposes is presented. For the analysis of plate flexural vibration, the basic theory of piezoelectricity, Mindlin plate theory and Poisson-Kirchoff theory are described. Then a mathematical model of the flexible structure is developed by considering the interaction between a typical piezoelectric actuator and the plate. In the finite element formulation the classical theory requires C^1 finite element interpolation functions which, in comparison with the C^0 finite element interpolation requirement for the Mindlin theory, is much more complicated. For this reason, we turn away from the Poisson-Kirchoff type of elements to elements based on theories which require C^0 continuity. However in analytical formulations we will use the classical theory to analyze the plate vibrations due to its simplicity.

A finite element formulation of plate elements with thin piezoelectric layers bonded

to the surface as actuators/sensors is formulated in the form of the well known equations of structural dynamics. In this formulation, the Mindlin plate theory is utilized. By applying the Mindlin theory along with an appropriate choice of basis functions, the formulation can be used over a wide range of plate thicknesses, while avoiding shear locking, but still giving excellent accuracy and convergence characteristics. In order to show that the formulation can analyze different range of plate thicknesses, a series of tests on square plates under variety of static loading and boundary conditions were performed. The comparison of the computed solution and the exact thin plate solution shows a good agreement. To validate the mass matrix, the finite element modes of vibration are compared with analytical solutions. In this comparison vibration of a simply supported and cantilever plate is considered. Two compared cases confirmed the model. The frequency response functions of the finite element model for simply supported and clamped plate is plotted. This prediction will be used for a comparison of experimental and theoretical modes of vibration and also can be utilize to adjust the theoretical modal properties.

Following the development of the Kirchoff plate equations one finds that the order of the governing equations derived by neglecting transverse shearing deformations permits only two of the three obvious force conditions to be enforced at a free edge. Since the problem of the plate vibrations deals mainly with thin plates, this shortcoming appears to be largely academic and the elementary plate theory is adequate. So, the classical plate theory has been considered to develop the mathematical model of the system. The plate characteristic functions have been used to study the plate vibrations analytically.

The separation of variables and Fourier expansion coupled with Navier's method is used to optimize size of piezoelectric actuators, the actuation voltage, and ap-

propriate location of the sensors,

In order to work with a finite dimensional model and ignoring some of the feedback paths in the physical system a quadratic control objective have been introduced. The number of modes required in the plate model to guarantee that the error in the objective function is smaller than a specified error have been derived.

Toward the goal of establishing a control strategy for research in distributed actuators, a control law to quantify the characteristic of the controlled system was implemented. To investigate the performance of the control method, a laminated simply supported plate and the controller have been numerically simulated. A prototype active simply supported plate was built and tested. In this work the overall effectiveness of two different strategies for vibration suppression were examined. Initially an LQ controller was employed to control a simply supported plate. The use of this strategy assisted in solving problems associated with the control of the plate. The results were also used to estimate the effectiveness of the other controller strategy. Examination of the LCC strategy indicated that the results were not generally improved as compared to an LQ controller. However the LCC method can be further improved by monitoring the energy of the plant as a criteria to connect/disconnect the link between the parameter of plant with the controller. In this method the rate of energy modulation between plant and controller can be increased compared to the LCC method, and the steady state controlled value can be achieved in shorter time [44]. The LCC controller can be enhanced by automating the parameter setting, that is frequency, damping, initial condition, and disable time are made to be self-tuning. As well the application of Modal Coupling Control (MCC) to vibration control of the oscillatory system can be studied [78]. This method is based on transferring the oscillatory energy from the plant to an auxiliary second order system (controller), coupled to the plant through nonlinear

terms.

Appendix A

Computer program

A computer program, which is written in Matlab environment performs the steps shown in Figure A.1. The main program consist of 9 subroutines DATAF.m, STIFF.m, MKQ.m, EIGV.m, EIGV1.m, PERDIS.m, FRF.m, ZDRAW.m, and RESP.m. The listing of the program is included in appendix A and contains numerous comment statements to explain various subroutine operations. To give insight into the program a brief description is given in the following.

A.1 Subroutine DATAF.m

The nodal data is generated by the subroutine DATAF.m called by the main program. A nodal point is described by the global and local node number, a boundary condition code, the global and local nodal coordinates. Nodal data globally and locally is specified in the Cartesian system. All the nodal point data retain in the DATA.mat file.

A.2 Subroutine STIFF.m and MKQ.m

This subroutine reads the DATA.mat file, and for each element of the plate takes the local nodal data into the MKQ.m subroutine. MKQ.m subroutine uses the nodal data and nodal properties to evaluate the local Mass, Damping, and Stiffness matrices. This local modal properties brought back into the STIFF.m subroutine. STIFF.m subroutine assembles all local Mass, damping, and Stiffness matrices, and generates the global Mass, damping, and Stiffness matrices.

A.3 Subroutine EIGV.m and PERDIS.m

EIGV.m subroutine calls in STIFF.m. This subroutine for incremental thickness takes the global mass, damping, and Stiff.m matrices applies the boundary conditions required. This subroutine also create force vectors, which two force vectors are considered, point load in a middle of the plate force vector, and uniform load on the plate force vector. In the following this subroutine solves two static cases and evaluate the deflection of the center point. The deflection of the center point is also calculated through an analytical method and the result will compare with the finite element results to find the percentage of the error. In the end PERERR.m subroutine will call to plot the percentage of the error for incremental thickness.

A.4 Subroutine EIGV1.m, FRF.m, and ZDRAW.m

This subroutine is also calls in STIFF.m. Initially this subroutine applies the required boundary conditions to the plate's modal properties, and later evaluate the eigen values and eigen vectors of the system. This subroutine also calls two other

subroutines FRF.m and ZDRAW.m. The FRF.m subroutine plot the frequency response function curve and ZDRAW.m subroutine draws the mode shape of the plate.

A.5 Subroutine RESP.m

This routine present the transient and forced response of the plate. The global modal matrices calculated in STIFF.m is passed into this subroutine, and by using the direct integration method the response of the plate is evaluated. This subroutine also graphically demonstrates the transient and the forced response of the plate. In this simulation two cases are considered, first the responses of the plate without interaction of the piezoelectric and second the responses of the plate with effect of the attached piezoelectrics.

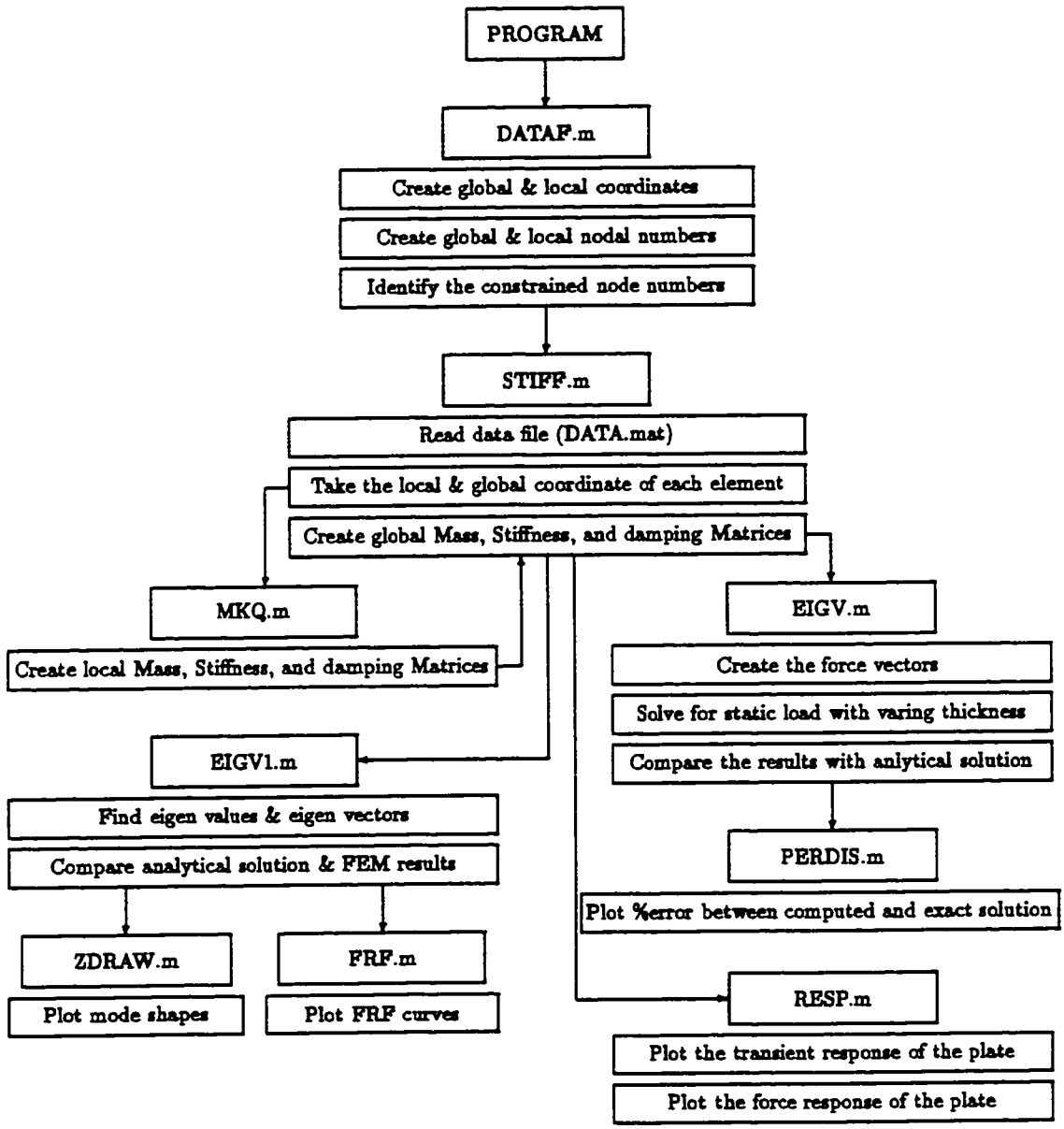

Figure A.1: Flow chart for plate vibration analysis

A.6 DATAF.m

```
% This program only get 2 edges of plate as the simply supported boundary conditions.

% File name is DATAF.m
% node number of applied constrains

% LX=0.4953;
% LY=0.5715;
%NEx=3;
%NEy=3;
LX=0.4;
LY=0.6;
NEx=1;
NEy=1;
[X,Y]=meshgrid(0:LX/(3*NEx):LX,0:LY/(3*NEx):LY);
t=1;            % Indicate the element number
for m=1:NEy
  for n=1:NEx
    P=1;
    for i=1:4
      for j=1:4
        Gx(t,(i-1)*4+j)=X(i+(m-1)*3,j+(n-1)*3);
        Gy(t,(i-1)*4+j)=Y(i+(m-1)*3,j+(n-1)*3);
        Lnod(t,(i-1)*4+j)=P;
        P=P+1;
      end
    end
    t=t+1;
  end
end
h=1;
for m=1:NEy*3+1
  for n=1:NEx*3+1
    nod(m,n)=h;
    h=h+1;
  end
end
Tnn=h-1;                              % Total number of nodes
t=1;
```

```
B=1;
for i=1:NEy*3+1                          % This part the Boundary condition and save the node
  for j=1:NEx*3+1
    if (i==1 | i==sqrt(Tnn))
      Bond(B)=nod(i,j);
      B=B+1;
    end
    if (i~=1 & i~=sqrt(Tnn))
      if (j==1 | j==sqrt(Tnn))
        Bond(B)=nod(i,j);
        B=B+1;
      end
    end
  end
end
NB=B-1;
for i=1:3:NEy*3
  for j=1:3:NEx*3
    Gnod(t,1:4)=nod(i,j:j+3);
    Gnod(t,5:8)=nod(i+1,j:j+3);
    Gnod(t,9:12)=nod(i+2,j:j+3);
    Gnod(t,13:16)=nod(i+3,j:j+3);
    t=t+1;
  end
end
save DATA4esim1 Gx Gy Lnod Gnod NB Bond Tnn X Y NEx NEy LX LY nod
```

A.7 STIFF.m

```
% This file is STIFF.m.
% This program create the stiffness matrix, mass matrix and


load DATA2esim4
% load DATA2ecle4
Lnod=Tnn;

% NEx=1;              % Number of elements in X direction
```

```
% NEy=1;              % Number of elements in Y direction
% LX=0.4953;          % Length of plate in X direction m
% LY=0.5715;

% ts=0.815e-3;        % Thickness of substructure m
ta=0.0;
%ta=0.1e-3;          % Thickness of actuator m
% Es=70E9;            % elastic modulus of aluminum Pa
Ea=0.0;
Es=1e7;
%Ea=6E10;           % Elastic modulus of PZT
d31=-1.15E-10;      % PZT consta
rhos=2710;       % Density of aluminum kg/m^3
rhoa=0.0;
%rhoa=7.6E3;         % Density of PZT
nus=0.3;           % Poisson ratio of substracture
nua=0.0;
%nua=0.25;           % Poisson ratio of PZT

global NEx NEy LX LY Nnode ts ta Es Ea d31 rhos rhoa nus nua ac delta LogLh Bend Tan Bc Cc ned;
step=0.0001;
%  for i=1:NEx*NEy                % ac is an indicator for existence of actuator zero means no
%    ac(i)=0;                      % actuator and one means actuator
%  end
  ac=0.0;

pl=1;
LogLhi=2;
ts=1.01e-6;
while(LogLhi>1.5 & LogLhi<7 )
  for i=1:Nnode*3
    for j=1:Nnode*3
      GK(i,j)=0.0;               % This is making the the global stiffness matrix equal to zero
      GM(i,j)=0.0;               % This is making the the global mass matrix equal to zero
    end
  end
  % ac(11)=1;
  % ac(23)=1;
  % ac(25)=1;
  % ac(27)=1;
```

```
  % ac(39)=1;
  for t=1:NEx*NEy
    t
    [K K]=HEQ(Gx(t,:),Gy(t,:));  % This subroutin create the local stiffness matrix
    for i=1:3:48
      row=(i-1)/3+1;
      for j=1:3:48        % This loops locate the local stiffness matrix in the gloal position
        col=(j-1)/3+1;
        lx=(Gnod(t,row)-1)*3+1;
        ly=(Gnod(t,col)-1)*3+1;
        GK(lx:lx+2,ly:ly+2)=K(i:i+2,j:j+2)+GK(lx:lx+2,ly:ly+2);
        GM(lx:lx+2,ly:ly+2)=M(i:i+2,j:j+2)+GM(lx:lx+2,ly:ly+2);
      end
    end
  end
  [deltai LogLhi delta2 LogLh2]=eigvsim(GK,GM);
%  [deltai LogLhi delta2 LogLh2]=eigvcla(GK,GM);
  A1(pl,1)=LogLhi;
  A1(pl,2)=deltai;
  A2(pl,1)=LogLh2;
  A2(pl,2)=delta2;
  pl=pl+1;
  if(LogLhi<1.8)
     step=0.001;
  end
  if(LogLhi>2 & LogLhi<6)
     step=.1;
  end
  if(LogLhi>6.2)
     step=0.0000001;
  end
  ts=ts+step;
  LogLhi
  deltai
  delta2
end                              % End of the loop for different thickness

save RESUL2esime4 A1 A2
% save RESUL2ecale4 A1 A2
% save GMGK GM GK Gnod X Y
```

A.8 MKQ.m

```
% This file is MKQ.m.
% This subroutin find the local K (Stiffness), M (Mass) and  matrix for each element
% of a two dimensional C^0 problem with 16 nodes per isoparametric element.
% format short e
% load DATA
function [M,K]=MKQ(Gx,Gy)

% Gx and Gy are the global coordinates of each element and ac equal to zero means there
% is no pizoelectric on that element and ac equal to one means there is an piso on the element


global NEx NEy LX LY Nnode ts ta Es Ea d31 rhos rhoa nus nua ac Bond Tnn


%Gx=[-1 -1/3 1/3 1 -1   -1/3  1/3  1  -1  -1/3 1/3 1  -1 -1/3 1/3 1];
%Gy=[-1 -1  -1  -1 -1/3 -1/3 -1/3 -1/3 1/3 1/3 1/3 1/3 1  1   1   1];

% ac=0;
% ts=0.815e-3;
% ta=0.0;
% rhos=2710;
% rhoa=0;
% Es=70E9;
% nus=0.3;

e1=0.86113631159405;
e2=0.33998104358486;
w1=0.34785484513745;
w2=0.65214515486255;

% x & y are coordinate of the quadrature points

x=[-e1 -e2 +e2 +e1 -e1 -e2  +e2  +e1  -e1  -e2  +e2  +e1  -e1  -e2  +e2  +e1];
y=[-e1 -e1 -e1 -e1 -e2 -e2  -e2  -e2  +e2  +e2  +e2  +e2  +e1  +e1  +e1  +e1];

% W is the weighting factors for quadrature points
W=[w1*w1 w2*w1 w2*w1 w1*w1...
   w1*w2 w2*w2 w2*w2 w1*w2...
```

```
   w1*w2 w2*w2 w2*w2 w1*w2...
   w1*w1 w2*w1 w2*w1 w1*w1];

I=[1 1 1 1 1 1 1 1 1 1 1 1 1 1 1 1];


% NP can be changed to increase or decrease number of quadrature points

NP=16;

% P(m,k) is the value of shape functions of each point at quadrature points
% m=1..16 indicate it is the shape function of the m node at quadrature point k

P(1,:)=(-9.*x.^3+9.*x.^2+x-1).*(-9.*y.^3+9.*y.^2+y-1).*(1/256);
P(2,:)=(+3.*x.^3-x.^2-3.*x+1).*(-9.*y.^3+9.*y.^2+y-1).*(9/256);
P(3,:)=(-3.*x.^3-x.^2+3.*x+1).*(-9.*y.^3+9.*y.^2+y-1).*(9/256);
P(4,:)=(+9.*x.^3+9.*x.^2-x-1).*(-9.*y.^3+9.*y.^2+y-1).*(1/256);

P(5,:)=(-9.*x.^3+9.*x.^2+x-1).*(+3.*y.^3-y.^2-3.*y+1).*(9/256);
P(6,:)=(+3.*x.^3-x.^2-3.*x+1).*(+3.*y.^3-y.^2-3.*y+1).*(81/256);
P(7,:)=(-3.*x.^3-x.^2+3.*x+1).*(+3.*y.^3-y.^2-3.*y+1).*(81/256);
P(8,:)=(+9.*x.^3+9.*x.^2-x-1).*(+3.*y.^3-y.^2-3.*y+1).*(9/256);

P(9,:)=(-9.*x.^3+9.*x.^2+x-1).*(-3.*y.^3-y.^2+3.*y+1).*(9/256);
P(10,:)=(+3.*x.^3-x.^2-3.*x+1).*(-3.*y.^3-y.^2+3.*y+1).*(81/256);
P(11,:)=(-3.*x.^3-x.^2+3.*x+1).*(-3.*y.^3-y.^2+3.*y+1).*(81/256);
P(12,:)=(+9.*x.^3+9.*x.^2-x-1).*(-3.*y.^3-y.^2+3.*y+1).*(9/256);

P(13,:)=(-9.*x.^3+9.*x.^2+x-1).*(+9.*y.^3+9.*y.^2-y-1).*(1/256);
P(14,:)=(+3.*x.^3-x.^2-3.*x+1).*(+9.*y.^3+9.*y.^2-y-1).*(9/256);
P(15,:)=(-3.*x.^3-x.^2+3.*x+1).*(+9.*y.^3+9.*y.^2-y-1).*(9/256);
P(16,:)=(+9.*x.^3+9.*x.^2-x-1).*(+9.*y.^3+9.*y.^2-y-1).*(1/256);

% q=[1 5 9 13 2 6 10 14 3 7 11 15 4 8 12 16];
% n=[1 5 9 13 14 15 16 12 8 4 3 2 6 10 11 7];


% P(m,k) is the value of derivative of shape functions in zeta (or x) direction for  each
% quadrature point m=17..32 indicate it is the derivative of shape function in zeta direction
% m=17..32 respond to 1..16 and k indicate the quadrature points
```

```
P(17,:)=(-27.*x.^2+18.*x+1).*(-9.*y.^3+9.*y.^2+y-1).*(1/256);
P(18,:)=(+9.*x.^2-2.*x-3).*(-9.*y.^3+9.*y.^2+y-1).*(9/256);
P(19,:)=(-9.*x.^2-2.*x+3).*(-9.*y.^3+9.*y.^2+y-1).*(9/256);
P(20,:)=(+27.*x.^2+18.*x-1).*(-9.*y.^3+9.*y.^2+y-1).*(1/256);

P(21,:)=(-27.*x.^2+18.*x+1).*(+3.*y.^3-y.^2-3.*y+1).*(9/256);
P(22,:)=(+9.*x.^2-2.*x-3).*(+3.*y.^3-y.^2-3.*y+1).*(81/256);
P(23,:)=(-9.*x.^2-2.*x+3).*(+3.*y.^3-y.^2-3.*y+1).*(81/256);
P(24,:)=(+27.*x.^2+18.*x-1).*(+3.*y.^3-y.^2-3.*y+1).*(9/256);

P(25,:)=(-27.*x.^2+18.*x+1).*(-3.*y.^3-y.^2+3.*y+1).*(9/256);
P(26,:)=(+9.*x.^2-2.*x-3).*(-3.*y.^3-y.^2+3.*y+1).*(81/256);
P(27,:)=(-9.*x.^2-2.*x+3).*(-3.*y.^3-y.^2+3.*y+1).*(81/256);
P(28,:)=(+27.*x.^2+18.*x-1).*(-3.*y.^3-y.^2+3.*y+1).*(9/256);

P(29,:)=(-27.*x.^2+18.*x+1).*(+9.*y.^3+9.*y.^2-y-1).*(1/256);
P(30,:)=(+9.*x.^2-2.*x-3).*(+9.*y.^3+9.*y.^2-y-1).*(9/256);
P(31,:)=(-9.*x.^2-2.*x+3).*(+9.*y.^3+9.*y.^2-y-1).*(9/256);
P(32,:)=(+27.*x.^2+18.*x-1).*(+9.*y.^3+9.*y.^2-y-1).*(1/256);


% P(m,k) is the value of derivative of shape functions in eta (or y) direction for  each
% quadrature point m=33..48 respond to points 1..16 indicate it is the derivative of shape
% and k indicate the quadrature points

P(33,:)=(-9.*x.^3+9.*x.^2+x-1).*(-27.*y.^2+18.*y+1).*(1/256);
P(34,:)=(+3.*x.^3-x.^2-3.*x+1).*(-27.*y.^2+18.*y+1).*(9/256);
P(35,:)=(-3.*x.^3-x.^2+3.*x+1).*(-27.*y.^2+18.*y+1).*(9/256);
P(36,:)=(+9.*x.^3+9.*x.^2-x-1).*(-27.*y.^2+18.*y+1).*(1/256);

P(37,:)=(-9.*x.^3+9.*x.^2+x-1).*(+9.*y.^2-2.*y-3).*(9/256);
P(38,:)=(+3.*x.^3-x.^2-3.*x+1).*(+9.*y.^2-2.*y-3).*(81/256);
P(39,:)=(-3.*x.^3-x.^2+3.*x+1).*(+9.*y.^2-2.*y-3).*(81/256);
P(40,:)=(+9.*x.^3+9.*x.^2-x-1).*(+9.*y.^2-2.*y-3).*(9/256);

P(41,:)=(-9.*x.^3+9.*x.^2+x-1).*(-9.*y.^2-2.*y+3).*(9/256);
P(42,:)=(+3.*x.^3-x.^2-3.*x+1).*(-9.*y.^2-2.*y+3).*(81/256);
P(43,:)=(-3.*x.^3-x.^2+3.*x+1).*(-9.*y.^2-2.*y+3).*(81/256);
P(44,:)=(+9.*x.^3+9.*x.^2-x-1).*(-9.*y.^2-2.*y+3).*(9/256);
```

```
P(45,:)=(-9.*x.^3+9.*x.^2+x-1).*(+27.*y.^2+18.*y-1).*(1/256);
P(46,:)=(+3.*x.^3-x.^2-3.*x+1).*(+27.*y.^2+18.*y-1).*(9/256);
P(47,:)=(-3.*x.^3-x.^2+3.*x+1).*(+27.*y.^2+18.*y-1).*(9/256);
P(48,:)=(+9.*x.^3+9.*x.^2-x-1).*(+27.*y.^2+18.*y-1).*(1/256);


% J11, J12, J21 and J22 are each member of Jacobian.

J11=Gx*P(17:32,:);
J12=Gy*P(17:32,:);
J21=Gx*P(33:48,:);
J22=Gy*P(33:48,:);

for i=1:NP                                  % NP is the number of quadrature points
 Jaco(i)=det([J11(i),J12(i);J21(i),J22(i)]); % Jaco(i) is the value of Jacobian at each
end                                         % quadrature point

for i=1:5
 for j=1:5
  D(i,j)=0;                                 % D is the constant value in stiffness matri$
 end
end

if(ac==0)                                   % if there is no actuator on the element all$
 Ea=0;                                      % PZT constants will be zero
 ta=0;
 nua=0;
 rhoa=0;
end

D(1,1)=(ts^3)/12*(Es/(1-nus^2)-Ea/(1-nua^2))+2*Ea/(3*(1-nua^2))*(ts/2+ta)^3;
D(2,2)=D(1,1);
D(1,2)=(ts^3)/12*(nus*Es/(1-nus^2)-nua*Ea/(1-nua^2))+2*nua*Ea/(3*(1-nua^2))*(ts/2+ta)^3;
D(2,1)=D(1,2);
D(3,3)=ts^3/24*(Es/(1+nus)-Ea/(1+nua))+Ea/(3*(1+nua))*(ts/2+ta)^3;
D(4,4)=Es/(1+nus)*ts/2+Ea*ta/(1+nua);
D(5,5)=D(4,4);

for i=1:48
```

```
 for j=1:48
  K(i,j)=0;              % stifness matrix
  M(i,j)=0;              % mass matrix
  Q(i,j)=0;              % actuator forcing matrix
 end
end

for m=1:NP               % NP is the number of quadrature points
 for i=1:5               % Loop over the strains
  for j=1:48             % loop over the element d.o.f.
   B(i,j)=0;             % initialize the strain-displacement relation
  end
 end
 L=1;                     % begin 4th row of B
 for k=1:16               % loop over the nodes
  B(4,L)=-(P(16+k,m).*J21(m)./(-Jaco(m))+P(32+k,m).*J11(m)./Jaco(m));
  L=L+3;                  % step to the next node
 end
 L=1;                     % start row 5 of B
 for k=1:16
  B(5,L)=-(P(16+k,m).*J22(m)./Jaco(m)+P(32+k,m).*J12(m)./(-Jaco(m)));
  L=L+3;                  % step to the next node
 end
 L=2;                     % start row 1 of B column 2
 for k=1:16
  B(1,L)=(P(16+k,m).*J22(m)./Jaco(m)+P(32+k,m).*J12(m)./(-Jaco(m)));
  L=L+3;
 end
 L=2;                     % start row 3 of B column 2
 for k=1:16
  B(3,L)=(P(16+k,m).*J21(m)./(-Jaco(m))+P(32+k,m).*J11(m)./Jaco(m));
  L=L+3;
 end
 L=2;                     %start row 5 of B column 2
 for k=1:16
   B(5,L)=P(k,m);
  L=L+3;
 end
 L=3;                     % start row 2 of B column 3
 for k=1:16
```

```
  B(2,L)=(P(16+k,m).*J21(m)./(-Jacc(m))+P(32+k,m).*J11(m)./Jacc(m));
  L=L+3;
 end
 L=3;                    % start row 3 of B column 3
 for k=1:16
  B(3,L)=(P(16+k,m).*J22(m)./Jacc(m)+P(32+k,m).*J12(m)./(-Jacc(m)));
  L=L+3;
 end
  L=3;                    % start row 4 of B column 3
 for k=1:16;
  B(4,L)=P(k,m);
  L=L+3;
 end
 K=K+B'*D*B*Jacc(m)*W(m); % form K by adding over the quadrature points
end


for i=1:3                % initialize the basis functions
  for j=1:48
   phi(i,j)=0.0;
  end
end

% rho effective should calculated here

T(1,1)=2*rhos*(ts/2)+2*ac*rhoa*ta;
T(2,2)=2/3*(rhos*(ts/2)^3+ac*rhoa*((ts/2+ta)^3-(ts/2)^3));
T(3,3)=2/3*(rhos*(ts/2)^3+ac*rhoa*((ts/2+ta)^3-(ts/2)^3));

for i=1:48
 for j=1:48
   M(i,j)=0;
 end
end


for m=1:NP                       % This loop calculate the mass matrix
 for i=1:16
  phi(1,(i-1)*3+1)=P(i,m);  % row 1
  phi(2,(i-1)*3+2)=P(i,m);  % row 2
```

```
  phi(3,(i-1)*3+3)=P(i,m);  % row 3
 end
 H=H+phi'*T*phi*Jacc(m)*W(m);
end
```

A.9 EIGV.m

```
function [deltai,LogLhi,delta2,LogLh2]=eigvsim1(GK,GM)
% This program find the eigen values and eigen vectors

global NEx NEy LX LY Nnode ts ta Es Ea d31 rhos rhoa nus nua ac delta LogLh Bond Tnn Bc Co nod;
k=1;
SI=size(Bond);
for i=1:Tnn
  if(i~=Bond)
    NBc(k)=i;
    k=k+1;
  end
end
l=1;
q=1;
sii=size(Bond);
si2=size(NBc);
for i=1:Tnn
  for j=1:sii(2)
    if(any(i==Bond(j)))
     if(any(Bond(j)==nod(1,1:sqrt(Tnn)-1)) | any(Bond(j)==nod(1:sqrt(Tnn)-1,1)))
       Bc(l)=(i-1)*3+2;
       Bc(l+1)=(i-1)*3+3;          % Bc is the C & R in global coord. without any constrains
       l=l+2;
      end
      if(any(Bond(j)==nod(sqrt(Tnn),2:sqrt(Tnn)-1)) )
        Bc(l)=(i-1)*3+1;
        co(q)=l;
        q=q+1;
        Bc(l+1)=(i-1)*3+2;
        l=l+2;
      end
```

```
      if(any(Bond(j)==nod(2:sqrt(Tnn)-1,sqrt(Tnn))))
        Bc(l)=(i-1)*3+1;
        co(q)=l;
        q=q+1;
        Bc(l+1)=(i-1)*3+3;
        l=l+2;
      end
      if(Bond(j)==nod(sqrt(Tnn),sqrt(Tnn)))
        Bc(l)=(i-1)*3+1;
        co(q)=l;
        q=q+1;
        l=l+1;
      end
      if(Bond(j)==nod(sqrt(Tnn),1))
        Bc(l)=(i-1)*3+2;
        l=l+1;
      end
      if(Bond(j)==nod(1,sqrt(Tnn)))
        Bc(l)=(i-1)*3+3;
        l=l+1;
      end
    end
  end
  if(all(i'=Bond))
    Bc(l)=(i-1)*3+1;
    co(q)=l;
    q=q+1;
    Bc(l+1)=(i-1)*3+2;
    Bc(l+2)=(i-1)*3+3;
    l=l+3;
  end
end

DGK=GK(Bc,Bc);
DGM=GM(Bc,Bc);
DGK=(DGK+DGK')/2;
DGM=(DGM+DGM')/2;
% This prepare the point load force;

Si=size(Bc);
```

```
for i=1:Si(2)
  Force1(i,1)=0;
  if(i==(Si(2)))
    Force1(i,1)=25;
  end
end


% This prepare the distributed load force;

for i=1:Si(2)
  Force2(i,1)=0;
end
Sico=size(co);
st=sqrt(Sico(2));
for i=1:Sico(2)-st
  Force2(co(i),1)=100*(LX/(3*NEx))*(LY/(3*NEy));
end
for i=st:st:Sico(2)-1
  Force2(co(i),1)=100*(LX/(3*NEx))*(LY/(3*NEy))/2;
end
Force2(co(Sico(2)),1)=100*(LX/(3*NEx))*(LY/(3*NEy))/4;
for i=Sico(2)-st+1:Sico(2)-1
  Force2(co(i),1)=100*(LX/(3*NEx))*(LY/(3*NEy))/2;
end

Z1=DGK\Force1;
Z2=DGK\Force2;
Z1=Z1(co,1);
Z2=Z2(co,1);
Wimax=0.0;
for m=1:10
  for n=1:10
    Wimax=Wimax+((sin(m*pi/2))^2*(sin(n*pi/2))^2)/(((m/(2*LX))^2+(n/(2*LY))^2)^2);
  end
end

def=size(co);
DD=(Es*ts^3)/(12*(1-nus^2));
Wimax=Wimax*4*100/(pi^4*2*LX*2*LY*DD);
```

```
deltai=(Zi(def(2))-Wimax)/Wimax*100;
LogLhi=log10(2*LX/ts);
W2max=0.0;
for m=1:10
  for n=1:10
    W2max=W2max+(sin(m*pi*2*LX/(2*2*LY)))^3*(sin(n*pi*2*LY/(2*2*LX)))^3/...
(m*n*((m/(2*LY))^2+(n/(2*LX))^2)^2);
  end
end
W2max=W2max*16*100/(DD*pi^6);
delta2=(Z2(def(2))-W2max)/W2max*100;
LogLh2=log10(2*LX/ts);
```

A.10 EIGV1.m

```
function [u,v,co,w11,w12,w21,w22]=eigvsimi(GK,GM)
% This program find the eigen values and eigen vectors

global NEx NEy LX LY Nnode ts ta Es Ea d31 rhos rhoa nus nua ac delta LogLh Bond Tnn Bc Co nod;
k=1;
SI=size(Bond);
for i=1:Tnn
  if(i~=Bond)
    NBc(k)=i;
    k=k+1;
  end
end
l=1;
q=1;
si1=size(Bond);
si2=size(NBc);
for i=1:Tnn
  for j=1:si1(2)
    if(any(i==Bond(j)))
     if(any(Bond(j)==nod(1,1:sqrt(Tnn))) | any(Bond(j)==nod(2:sqrt(Tnn)-1,1))...
| any(Bond(j)==nod(sqrt(Tnn),1:sqrt(Tnn))) | any(Bond(j)==nod(2:sqrt(Tnn)-1,sqrt(Tnn))));
        Bc(l)=(i-1)*3+2;
        Bc(l+1)=(i-1)*3+3;          % Bc is the C & R in global coord. without any constrains
```

```
        l=l+2;
      end
    end
  end
  if(all(i~=Bcnd))
    Bc(l)=(i-1)*3+1;
    co(q)=l;
    q=q+1;
    Bc(l+1)=(i-1)*3+2;
    Bc(l+2)=(i-1)*3+3;
    l=l+3;
  end
end

DGK=GK(Bc,Bc);
DGM=GM(Bc,Bc);
DGK=(DGK+DGK')/2;
DGM=(DGM+DGM')/2;

[u,v]=eig(DGK,DGM);
u=real(u);
v=real(v);
v=diag(v);
v=sqrt(v)/(2*pi);

DD=(Es*ts^3)/(12*(1-nus^2));
w11=pi^2*((1/LX)^2+(1/LY)^2)*sqrt(DD/(rhos*ts))/(2*pi);
w12=pi^2*((1/LX)^2+(2/LY)^2)*sqrt(DD/(rhos*ts))/(2*pi);
w21=pi^2*((2/LX)^2+(1/LY)^2)*sqrt(DD/(rhos*ts))/(2*pi);
w22=pi^2*((2/LX)^2+(2/LY)^2)*sqrt(DD/(rhos*ts))/(2*pi);
```

A.11 PERDIS.m

```
load RESUL2ecal1
clapi=A1;
cladi=A2;
clear A1;
clear A2;
```

```
load RESUL2ecale4
clap4=A1;
clad4=A2;
clear A1;
clear A2;
load RESUL2esimi
simp1=A1;
simd1=A2;
clear A1;
clear A2;
load RESUL2esime4
simp4=A1;
simd4=A2;
clear A1;
clear A2;
subplot(211),plot(simp1(:,1),simp1(:,2),'--',clap1(:,1),clap1(:,2),'-',...
simp4(:,1),simp4(:,2),'--',clap4(:,1),clap4(:,2),'-');
subplot(211),xlabel('Log(L/t)');
subplot(211),ylabel('Percentage of Error')
subplot(211),title('Percentage of disagreement between computed and exact solution');
subplot(211),grid;
subplot(212),plot(simd1(:,1),simd1(:,2),'--',cladi(:,1),cladi(:,2),'-',...
simd4(:,1),simd4(:,2),'--',clad4(:,1),clad4(:,2),'-');
subplot(212),xlabel('Log(L/t)');
subplot(212),ylabel('Percentage of Error')
subplot(212),title('Percentage of disagreement between computed and exact solution');
subplot(212),grid;
subplot(211),hold;
subplot(211),plot(1,30,1,-30);
subplot(211),text(1,-22.0,'  ---- Simply supported boundary condition')
subplot(211),text(1,-25.0,'  ---- Clamped boundary condition')
subplot(211),text(2.5,3.5,'4 elements');
subplot(211),text(4.2,7.5,'1 elements');
subplot(212),text(1,-22.0,'  ---- Simply supported boundary condition')
subplot(212),text(1,-25.0,'  ---- Clamped boundary condition')
subplot(212),text(2.5,3.5,'4 elements');
subplot(212),text(4.2,7.5,'1 elements');
subplot(212),hold;
subplot(212),plot(1,30,1,-30);
```

A.12 ZDRAW.m

```
Tan=190;
NEx=6;
NEy=3;
load RESUL4eclamp36.mat
mod1=180;
mod2=179;
mod3=178;
mod4=177;

for i=1:NEy*3+1
 for j=1:NEx*3+1
   Z1(i,j)=0.0;
   Z2(i,j)=0.0;
   Z3(i,j)=0.0;
   Z4(i,j)=0.0;
 end
end
zz1=u(co,mod1);
zz2=u(co,mod2);
zz3=u(co,mod3);
zz4=u(co,mod4);

p=1;
for i=1:NEy*3+1
  for j=2:NEx*3+1
    Z1(i,j)=zz1(p);
    Z2(i,j)=zz2(p);
    Z3(i,j)=zz3(p);
    Z4(i,j)=zz4(p);
    p=p+1;
  end
end
subplot(221),surf(Z1);
subplot(221),title('a');
subplot(221),hold;
subplot(221),plot3(0,0,0.02);
subplot(222),surf(Z2);
subplot(222),title('b');
```

```
subplot(223),surf(Z3);
subplot(223),title('c');
subplot(224),surf(Z4);
subplot(224),title('d');
```

A.13 FRF.m

```
load RESUL4esime4;
load DATA4esime4;
vs=v;
us=u;
clear v u
load RESUL4eclame4;
vc=v;
uc=u;


smod1=112;
smod2=113;
smod3=114;
smod4=115;
smod5=116;

cmod1=117;
cmod2=118;
cmod3=121;
cmod4=120;
cmod5=119;

n=1;

% for i=vs(smod1)-1:0.313:vs(smod1)+1
%  frs(n)=us(smod1,(Tnn+1)/2)*us(smod1,(Tnn+1)/2)/(vs(smod1)^2-i^2);
%  frs(n)=abs(frs(n))*1e-6;
for i=0:0.313:30
  frs(n)=1/(vs(smod1)^2-i^2);
  frs(n)=abs(frs(n));
  fs(n)=i;
```

```
  n=n+1;
end

% for i=vs(smod2)-1:0.05:vs(smod2)+1
%  frs(n)=us(smod2,(Tnn+1)/2)*us(smod2,(Tnn+1)/2)/(vs(smod2)^2-i^2);
for i=30:0.3:50
  frs(n)=1/(vs(smod2)^2-i^2);
  frs(n)=abs(frs(n));
  fs(n)=i;
  n=n+1;
end

for i=vs(smod3)-1:0.05:vs(smod3)+1
%  frs(n)=us(smod3,(Tnn+1)/2)*us(smod3,(Tnn+1)/2)/(vs(smod3)^2-i^2);
  frs(n)=1/(vs(smod3)^2-i^2);
  frs(n)=abs(frs(n))*.75;
  fs(n)=i;
  n=n+1;
end
for i=vs(smod4)-1:0.05:vs(smod4)+1
%  frs(n)=us(smod4,(Tnn+1)/2)*us(smod4,(Tnn+1)/2)/(vs(smod4)^2-i^2);
  frs(n)=1/(vs(smod4)^2-i^2);
  frs(n)=abs(frs(n))*0.6;
  fs(n)=i;
  n=n+1;
end

% for i=vs(smod5)-1:0.05:vs(smod5)+1
%  frs(n)=us(smod5,(Tnn+1)/2)*us(smod5,(Tnn+1)/2)/(vs(smod5)^2-i^2);
for i=vs(smod5)-1:0.05:100
  frs(n)=1/(vs(smod5)^2-i^2);
  frs(n)=abs(frs(n))*0.5;
  fs(n)=i;
  n=n+1;
end


subplot(211),plot(fs,frs);
subplot(211),grid;
subplot(211),xlabel('Frequency (Hz)');
```

```
subplot(211),ylabel('Inertance (ms^-2/N)');
subplot(211),title('a')

n=1;
% for i=10:0.2:vc(cmod1)+1
%  frc(n)=uc(cmod1,(Tnn+1)/2)*uc(cmod1,(Tnn+1)/2)/(vc(cmod1)^2-i^2);
for i=0:0.2:45
  frc(n)=1/(vc(cmod1)^2-i^2);
  frc(n)=abs(frc(n));
  fc(n)=i;
  n=n+1;
end

%for i=45:0.05:vc(cmod2)+1
%  frc(n)=uc(cmod2,(Tnn+1)/2)*uc(cmod2,(Tnn+1)/2)/(vc(cmod2)^2-i^2);
for i=50:0.21:75
  frc(n)=1/(vc(cmod2)^2-i^2);
  frc(n)=abs(frc(n))*0.9;
  fc(n)=i;
  n=n+1;
end

% for i=vc(cmod3)-1:0.05:vc(cmod3)+1
%  frc(n)=uc(cmod3,(Tnn+1)/2)*uc(cmod3,(Tnn+1)/2)/(vc(cmod3)^2-i^2);
for i=75:0.17:84
  frc(n)=1/(vc(cmod3)^2-i^2);
  frc(n)=abs(frc(n))*0.75;
  fc(n)=i;
  n=n+1;
end

% for i=vc(cmod4)-1:0.05:vc(cmod4)+1
%  frc(n)=uc(cmod4,(Tnn+1)/2)*uc(cmod4,(Tnn+1)/2)/(vc(cmod4)^2-i^2);
for i=84:0.19:100
  frc(n)=1/(vc(cmod4)^2-i^2);
  frc(n)=abs(frc(n))*.6;
  fc(n)=i;
  n=n+1;
end
```

```
subplot(212),plot(fc,frc);
subplot(212),grid;
subplot(212),xlabel('Frequency (Hz)');
subplot(212),ylabel('Inertance (ms^-2/N)');
subplot(212),title('b')
```

Appendix B

SYSTEM DYNAMIC RESPONSE MATRICES

$$
\begin{aligned}
a_{11} &= \begin{bmatrix} e^{-\xi_{11}\omega_{11}t}[\cos(\omega_{11}t) + \xi_{11}\sin(\omega_{11}t)] \\ e^{-\xi_{12}\omega_{12}t}[\cos(\omega_{12}t) + \xi_{12}\sin(\omega_{12}t)] \\ e^{-\xi_{21}\omega_{21}t}[\cos(\omega_{21}t) + \xi_{21}\sin(\omega_{21}t)] \\ e^{-\xi_{22}\omega_{22}t}[\cos(\omega_{22}t) + \xi_{22}\sin(\omega_{22}t)] \end{bmatrix} = \begin{bmatrix} e^{-2.38t}[\cos(47.62t) + .05\sin(47.62t)] \\ e^{-5.51t}[\cos(110.22t) + .05\sin(110.22t)] \\ e^{-6.39t}[\cos(127.89t) + .05\sin(127.89t)] \\ e^{-9.52t}[\cos(190.48t) + .05\sin(190.48t)] \end{bmatrix} \\
a_{12} &= \begin{bmatrix} \frac{e^{-\xi_{11}\omega_{11}t}}{\omega_{11}}\sin(\omega_{11}t) \\ \frac{e^{-\xi_{12}\omega_{12}t}}{\omega_{12}}\sin(\omega_{12}t) \\ \frac{e^{-\xi_{21}\omega_{21}t}}{\omega_{21}}\sin(\omega_{21}t) \\ \frac{e^{-\xi_{22}\omega_{22}t}}{\omega_{22}}\sin(\omega_{22}t) \end{bmatrix} = \begin{bmatrix} \frac{e^{-2.38t}}{47.62}\sin(47.62t) \\ \frac{e^{-5.51t}}{110.22}\sin(110.22t) \\ \frac{e^{-6.39t}}{127.89}\sin(127.89t) \\ \frac{e^{-9.52t}}{190.48}\sin(190.48t) \end{bmatrix} \\
a_{21} &= \begin{bmatrix} \omega_{11}e^{-\xi_{11}\omega_{11}t}\sin(\omega_{11}t) \\ \omega_{12}e^{-\xi_{12}\omega_{12}t}\sin(\omega_{12}t) \\ \omega_{21}e^{-\xi_{21}\omega_{21}t}\sin(\omega_{21}t) \\ \omega_{22}e^{-\xi_{22}\omega_{22}t}\sin(\omega_{22}t) \end{bmatrix} = \begin{bmatrix} 47.62e^{-2.38t}\sin(47.62t) \\ 110.22e^{-5.51t}\sin(110.22t) \\ 127.89e^{-6.39t}\sin(127.89t) \\ 190.48e^{-9.52t}\sin(190.48t) \end{bmatrix} \\
a_{22} &= \begin{bmatrix} e^{-\xi_{11}\omega_{11}t}[\cos(\omega_{11}t) - \xi_{11}\sin(\omega_{11}t)] \\ e^{-\xi_{12}\omega_{12}t}[\cos(\omega_{12}t) - \xi_{12}\sin(\omega_{12}t)] \\ e^{-\xi_{21}\omega_{21}t}[\cos(\omega_{21}t) - \xi_{21}\sin(\omega_{21}t)] \\ e^{-\xi_{22}\omega_{22}t}[\cos(\omega_{22}t) - \xi_{22}\sin(\omega_{22}t)] \end{bmatrix} \begin{bmatrix} e^{-2.38t}[\cos(47.62t) - .05\sin(47.62t)] \\ e^{-5.51t}[\cos(110.22t) - .05\sin(110.22t)] \\ e^{-6.39t}[\cos(127.89t) - .05\sin(127.89t)] \\ e^{-9.52t}[\cos(190.48t) - .05\sin(190.48t)] \end{bmatrix}
\end{aligned}
\tag{B.1}
$$

$$[\gamma_{su}] = \overline{\gamma}_{su}\begin{bmatrix} \sin(\frac{\pi\xi_1}{L_x})\sin(\frac{\pi L_p}{2L_x})\sin(\frac{\pi\eta_1}{L_y}) & \sin(\frac{\pi\xi_2}{L_x})\sin(\frac{\pi L_p}{2L_x})\sin(\frac{\pi\eta_2}{L_y}) & \sin(\frac{\pi\xi_3}{L_x})\sin(\frac{\pi L_p}{2L_x})\sin(\frac{\pi\eta_3}{L_y}) \\ \sin(\frac{\pi\xi_1}{L_x})\sin(\frac{\pi L_p}{2L_x})\sin(\frac{2\pi\eta_1}{L_y}) & \sin(\frac{\pi\xi_2}{L_x})\sin(\frac{\pi L_p}{2L_x})\sin(\frac{2\pi\eta_2}{L_y}) & \sin(\frac{\pi\xi_3}{L_x})\sin(\frac{\pi L_p}{2L_x})\sin(\frac{2\pi\eta_3}{L_y}) \\ 2\sin(\frac{2\pi\xi_1}{L_x})\sin(\frac{\pi L_p}{L_x})\sin(\frac{\pi\eta_1}{L_y}) & 2\sin(\frac{2\pi\xi_2}{L_x})\sin(\frac{\pi L_p}{L_x})\sin(\frac{\pi\eta_2}{L_y}) & 2\sin(\frac{2\pi\xi_3}{L_x})\sin(\frac{\pi L_p}{L_x})\sin(\frac{\pi\eta_3}{L_y}) \\ 2\sin(\frac{2\pi\xi_1}{L_x})\sin(\frac{\pi L_p}{L_x})\sin(\frac{2\pi\eta_1}{L_y}) & 2\sin(\frac{2\pi\xi_2}{L_x})\sin(\frac{\pi L_p}{L_x})\sin(\frac{2\pi\eta_2}{L_y}) & 2\sin(\frac{2\pi\xi_3}{L_x})\sin(\frac{\pi L_p}{L_x})\sin(\frac{2\pi\eta_3}{L_y}) \end{bmatrix} \tag{B.2}$$

$$[\gamma_{yu}] = \overline{\gamma}_{yu}\begin{bmatrix} \sin(\frac{\pi\xi_4}{L_x})\sin(\frac{\pi L_p}{2L_y})\sin(\frac{\pi\eta_4}{L_y}) & \sin(\frac{\pi\xi_5}{L_x})\sin(\frac{\pi L_p}{2L_y})\sin(\frac{\pi\eta_5}{L_y}) & \sin(\frac{\pi\xi_6}{L_x})\sin(\frac{\pi L_p}{2L_y})\sin(\frac{\pi\eta_6}{L_y}) \\ 2\sin(\frac{\pi\xi_4}{L_x})\sin(\frac{\pi L_p}{L_y})\sin(\frac{2\pi\eta_4}{L_y}) & 2\sin(\frac{\pi\xi_5}{L_x})\sin(\frac{\pi L_p}{L_y})\sin(\frac{2\pi\eta_5}{L_y}) & 2\sin(\frac{\pi\xi_6}{L_x})\sin(\frac{\pi L_p}{L_y})\sin(\frac{2\pi\eta_6}{L_y}) \\ \sin(\frac{2\pi\xi_4}{L_x})\sin(\frac{\pi L_p}{2L_y})\sin(\frac{\pi\eta_4}{L_y}) & \sin(\frac{2\pi\xi_5}{L_x})\sin(\frac{\pi L_p}{2L_y})\sin(\frac{\pi\eta_5}{L_y}) & \sin(\frac{2\pi\xi_6}{L_x})\sin(\frac{\pi L_p}{2L_y})\sin(\frac{\pi\eta_6}{L_y}) \\ 2\sin(\frac{2\pi\xi_4}{L_x})\sin(\frac{\pi L_p}{L_y})\sin(\frac{2\pi\eta_4}{L_y}) & 2\sin(\frac{2\pi\xi_5}{L_x})\sin(\frac{\pi L_p}{L_y})\sin(\frac{2\pi\eta_5}{L_y}) & 2\sin(\frac{2\pi\xi_6}{L_x})\sin(\frac{\pi L_p}{L_y})\sin(\frac{2\pi\eta_6}{L_y}) \end{bmatrix} \tag{B.3}$$

where $\overline{\gamma}_{su} = \sqrt{\frac{16\pi^2}{\rho h L_x^3 L_y}}$ and $\overline{\gamma}_{yu} = \sqrt{\frac{16\pi^2}{\rho h L_x L_y^3}}$.

$$[P] = [R] = \begin{bmatrix} \sin(\frac{\pi\zeta_1}{L_x})\sin(\frac{\pi\eta_1}{L_y}) & \sin(\frac{\pi\zeta_1}{L_x})\sin(\frac{2\pi\eta_1}{L_y}) & \sin(\frac{2\pi\zeta_1}{L_x})\sin(\frac{\pi\eta_1}{L_y}) & \sin(\frac{2\pi\zeta_1}{L_x})\sin(\frac{2\pi\eta_1}{L_y}) \\ \sin(\frac{\pi\zeta_2}{L_x})\sin(\frac{\pi\eta_2}{L_y}) & \sin(\frac{\pi\zeta_2}{L_x})\sin(\frac{2\pi\eta_2}{L_y}) & \sin(\frac{2\pi\zeta_2}{L_x})\sin(\frac{\pi\eta_2}{L_y}) & \sin(\frac{2\pi\zeta_2}{L_x})\sin(\frac{2\pi\eta_2}{L_y}) \\ \sin(\frac{\pi\zeta_3}{L_x})\sin(\frac{\pi\eta_3}{L_y}) & \sin(\frac{\pi\zeta_3}{L_x})\sin(\frac{2\pi\eta_3}{L_y}) & \sin(\frac{2\pi\zeta_3}{L_x})\sin(\frac{\pi\eta_3}{L_y}) & \sin(\frac{2\pi\zeta_3}{L_x})\sin(\frac{2\pi\eta_3}{L_y}) \\ \sin(\frac{\pi\zeta_4}{L_x})\sin(\frac{\pi\eta_4}{L_y}) & \sin(\frac{\pi\zeta_4}{L_x})\sin(\frac{2\pi\eta_4}{L_y}) & \sin(\frac{2\pi\zeta_4}{L_x})\sin(\frac{\pi\eta_4}{L_y}) & \sin(\frac{2\pi\zeta_4}{L_x})\sin(\frac{2\pi\eta_4}{L_y}) \\ \sin(\frac{\pi\zeta_5}{L_x})\sin(\frac{\pi\eta_5}{L_y}) & \sin(\frac{\pi\zeta_5}{L_x})\sin(\frac{2\pi\eta_5}{L_y}) & \sin(\frac{2\pi\zeta_5}{L_x})\sin(\frac{\pi\eta_5}{L_y}) & \sin(\frac{2\pi\zeta_5}{L_x})\sin(\frac{2\pi\eta_5}{L_y}) \\ \sin(\frac{\pi\zeta_6}{L_x})\sin(\frac{\pi\eta_6}{L_y}) & \sin(\frac{\pi\zeta_6}{L_x})\sin(\frac{2\pi\eta_6}{L_y}) & \sin(\frac{2\pi\zeta_6}{L_x})\sin(\frac{\pi\eta_6}{L_y}) & \sin(\frac{2\pi\zeta_6}{L_x})\sin(\frac{2\pi\eta_6}{L_y}) \end{bmatrix} \tag{B.4}$$

$$[w] = \begin{bmatrix} 1.86 & 0.00 & 0.00 & 0.00 & 0.00 & 0.00 & 0.00 & 0.00 \\ 1.32 & 0.00 & 1.86 & 0.00 & 0.00 & 0.00 & 0.00 & 0.00 \\ 1.32 & 0.00 & -1.86 & 0.00 & 0.00 & 0.00 & 0.00 & 0.00 \\ 1.86 & 0.00 & 0.00 & 0.00 & 0.00 & 0.00 & 0.00 & 0.00 \\ 1.32 & 1.86 & 0.00 & 0.00 & 0.00 & 0.00 & 0.00 & 0.00 \\ 1.32 & -1.86 & 0.00 & 0.00 & 0.00 & 0.00 & 0.00 & 0.00 \end{bmatrix}$$

$$\int_0^t e^{\mathcal{A}(t-\tau)} \begin{bmatrix} 0.00 & 0.00 & 0.00 & 0.00 & 0.00 & 0.00 & 0.00 \\ 0.00 & 0.00 & 0.00 & 0.00 & 0.00 & 0.00 & 0.00 \\ 0.00 & 0.00 & 0.00 & 0.00 & 0.00 & 0.00 & 0.00 \\ 0.00 & 0.00 & 0.00 & 0.00 & 0.00 & 0.00 & 0.00 \\ 0.47 & 1.98 & 1.40 & 1.40 & 1.55 & 1.09 & 1.09 \\ 0.85 & 0.00 & 0.00 & 0.00 & 0.00 & 6.15 & -6.15 \\ 0.77 & 0.00 & 7.87 & -7.87 & 0.00 & 0.00 & 0.00 \\ 1.38 & 0.00 & 0.00 & 0.00 & 0.00 & 0.00 & 0.00 \end{bmatrix} \begin{bmatrix} \mathcal{F}(\tau) \\ \mathcal{T}_1(\tau) \\ \mathcal{T}_2(\tau) \\ \mathcal{T}_3(\tau) \\ \mathcal{T}_4(\tau) \\ \mathcal{T}_5(\tau) \\ \mathcal{T}_6(\tau) \end{bmatrix} d\tau \tag{B.5}$$

References

[1] Mason W. P. *Piezoelectric Crystals and Their Application to Ultrasonics.* Van Nostrand Company, Inc., New York, 3rd edition, 1950.

[2] Rakesh K. Kapania and Stefano Raciti. Recent advances in analysis of laminated beam and plates. *AIAA Journal*, 27(7):923–946, 1989.

[3] Yang P. C., Norris C. H. and Stavsky Y. Elastic wave propagation in heterrogeneous plates. *Int. J. Solids. Struc.*, 2:665–684, 1966.

[4] Basset A. B. On the extension and flexture of cylindrical and spherical thin elastic shells. *Phil. Trans. Royal Soc.*, 6(181):433–480, 1890.

[5] Mindlin R. D. Influence of rotatory inertia and shear on flextural motions of isotropic, elastic plates. *J. Appl. Mech.*, 18:A31, 1951.

[6] Hencky A. Uber die berucksichtigung der schbverzerrung in ebenen platten. *Ing. Arch*, 16, 1947.

[7] Hildebrand F. B., Reissner E. and Thomas G. B. Theory of small displacements of isotropic shells. *NACA Tech. Note No.1833*, 3, 1949.

[8] Reissner E. Twelfth order theory of transverse bending of transversely isotropic plates. *Zeitschrift fur angewandlte Mathematic und Mechanik*, 63:285–291, 1983.

[9] Reddy J. N. and Chao W. C. A comparison of closed form and finite element solutions of thick laminated anisotropic rectangular plates. *Nuclear Engineerin Designs*, 64(4):153–167, 1981.

[10] Lajczok M. R. New approach in the determination of interlaminar shear stresses from results of msc/nastran. *Computer and Structures*, 23(2):139–146, 1986.

[11] Phan N. D. and Reddy J. N. Analysis of laminated composite plates using a higher order shear deformation theory. *International Journal for Numerical Methods in Engineering*, 21:2201–2219, 1985.

[12] Bhimaraddi A. and Stephens L. K. A higher order theory for free vibrations of orthotropic, homogeneous, and laminated rectangular plates. *Journal of Applied Mechanics*, 51:195–198, 1984.

[13] Krishna Murty A. V. and Vellaichamy S. On high order shear deformatiion theory of laminated composite panels. *Composite Structures*, 8(4):247–270, 1987.

[14] Reddy J. N. A review of the literature on finite element modeling of laminated composite plates. *Shock and Vibration digest*, 4(17):3–8, 1985.

[15] Green A. E. and Naghdi P. M. A theory of laminated composite plates. *IMA Journal of Applied Mathematics*, 29(1):1–23, 1982.

[16] Rehfield L. W. and Valisetty. A comprehensive theory of planar bending of composite laminates. *Jounal of Composite Structures*, 2:441–449, 1983.

[17] Liaw B. D. and Little R. W. Theory of bending multilayer sandwich plates. *AIAA J.*, 5:301–304, 1967.

[18] Azar J. J. Bending theory of multilayer orthotropic sandwich plates. *AIAA J.*, 6:2166–2169, 1968.

[19] Chen C. T. *Introduction to Linear System Theory.* Holt, Rinehart and Winston, New York, 1970.

[20] Tzou H. S. Integrated distributed sensing and active vibration suppression of flexible manipulators using distributed piezoelectrics. *Journal of Robotic System*, 6(6):745–767, 1989.

[21] Lammering R. The application of a finite shell element for composites containing piezo-electric polymers in vibration control. *Computers & Structures*, 41(5):1101–1109, 1991.

[22] Lee L. J. and Fan Y. J. Bending and vibration analysis of composite sandwich plates. *Journal of Computer and Structures*, 60(1):103–112, 1996.

[23] Wang X. Chen C. and Shen Y. Finite element approach of vibration control using self-sensing piezoelectric actuators. *Computers & Structures*, 60(3):505–512, 1996.

[24] Lee C. K. Theory of laminated piezoelectric plates for the design of distributed sensors/actuators. *J. Acoust. Soc. Am.*, 87(3):1144–1158, 1990.

[25] Patnaik B. R. Control of a tip-impacted flexible arm and piezoelectric vibration suppression. Master's thesis, University of Waterloo, 1994.

[26] Shames I. H. and Clive L. D. *Energy and Finite Element Methods in Structural Mechanics.* Hemisphere Publishing Corporation, 1985.

[27] Cook Robert D. Malkus David S. Plesha Michael E. *Concepts and Applications of Finite Element Analysis.* John Wiley & Sons, New York Brisbane Chichester Toronto Singapore, 1989.

[28] Hughes T. J. R. The heterosis finite element for plate bending. *Computers & Structures*, 9:445–450, 1978.

[29] McNeill N. J. *An improved mindlin plate bending element and compatible quarter point carack tip derivative.* Master's thesis, University of Toronto, 1982.

[30] Heppler G. R. and Hansen J. S. A mindlin element for thick and deep shells. *Computer Methods in Applied Mechanics and Engineering*, 54:21–47, 1986.

[31] Szilard Rudolph. *Theory and Analysis of Plates.* Prentice-Hall, Inc., Englewood Cliffs, New Jersey, 1974.

[32] Timoshenko S. Woinowsky-Krieger S. *Theory of Plates and Shells.* McGraw-Hill Inc., New York and London, 2rd edition, 1959.

[33] Soedel Werner. *Vibration of Shells and Plates.* Marcel Dekker, Inc., New York and Basel, 1993.

[34] Ewins D. J. *Modal Testing (Theory and Practice).* John Wiley & Sons Inc., New York Brisbane Chichester Toronto Singapore, 1984.

[35] Chung W. H., Hagood N. W. and Flotow A. Modelling of piezoelectric actuator dynamics for active structural control. In *AIAA paper 31th Structures, Structural Dynamics and Materials Conferenc*, April 2-4 1990.

[36] Young D. Vibration of rectangular plates by the Ritz method. *Journal of Applied Mechanics*, 12(1):448–453, 1950.

[37] G. B Warburton. The vibration of rectangular plates. *Journal of Applied Mechanics*, 12(1):371–381, 1950.

[38] Rajalingham C. Bhat R. B. and Xistris G. D. Vibration of rectangular plates using plate characteristic functions. *Journal of sound and vibration*, 193(2):497–509, 1996.

[39] Baz A. and Poh S. Performance of an active control system with piezoelectric actuators. *Journal of Sound and Vibration*, 126:327–343, 1988.

[40] Friswell M. I. Candidate reduced order models for structural parameter estimation. *Journal of Vibration and Acoustics*, 112:93–97, 1990.

[41] Hung Y. S. and Muzlifah. Hankel-norm model reduction with fixed modes. *IEEE Transaction on Automatic Control*, 35(3):373–377, 1990.

[42] Hughes P. C. and Skelton R. E. Modal truncation for flexible spacecraft. *Journal of Guidance and Control*, 4(3):4291–297, 1981.

[43] Yousuff A., Wagie D. A. and Skelton R. E. Linear system approximation via covariance equivalent realization. *Journal of Mathematical Analysis and Applications*, 106:91–115, 1985.

[44] Fariborzi F., Golnaraghi M. F. and Heppler G. R. Experimental control of free and forced structural vibration using linear coupling strategy. *Journal of Smart Materials and Structures*, 6:1–9, 1997.

[45] Hughes P. C. and Skelton R. E. Controllability and observability of linear matrix-second-order systems. *Journal of Applied Mechanics*, 47(2):415–420, 1980.

[46] Skelton R. E. and Hughes P. C. Modal cost analysis for linear matrix-second-order systems. *Journal of Dynamic Systems, Measurement, and Control*, 102:151–158, 1980.

[47] Fariborzi F., Golnarghi M. F. and Heppler G. R. Active vibration control of free and forced oscillation of flexible beam. In *AIAA/ASME/ASCE/AHS Symposium on Nonlinear Dynamics and Stochastic Mechanics*, Dallas,Texas, USA, 1997.

[48] Crawley E. F., Luis N. W. Hagood and Anderson E. H. Development of piezoelectric technology for applications in control of intelligent structures. *a*, a(a):a, a.

[49] Tzou H. S. Tseng C. I. and Wan G. C. Distributed structural dynamics control of flexible manipulators. *Computers & Structures*, 35(6):679–687, 1990.

[50] Bailey T. and Hubbard J. E. Distributed piezoelectric-polymer active vibration control of a cantilever beam. *J. Guidance*, 8(5):605–611, 1985.

[51] Crawley E. F. and Lazarus K. B. Induced strain actuation of isotropic and anisotropic plates. *AIAA J.*, 29(6):944–951, 1991.

[52] Edberg D. L. Control of flexible structures by applied thermal gradients. *AIAA J.*, 25(6):877–883, 1987.

[53] Uchino K. Electrostrictive actuators: Materials and applications. *Am. Ceram. Soc. Bull.*, 65:647–652, 1986.

[54] Cross L. E. Electrostrictive behavior of lead magnesium niobate based dielectrics. *Ferroelectrics*, 27(1-4):31–34, 1980.

[55] Butler J. L. Application manual for the design of etrema tefenol-d magnetrostrictive transducers. In *Edge Technologies, Inc*, 1988.

[56] Roger1 C. A. and Robertshow H. H. Shape memory aloy reinforced composites. *Soc. of Engineering Sciences, Inc*, (6):20–22, 1988.

[57] Shimizu K. and Otsuka K. Pseudoelasticity and shape memory effect in alloys. *Int. Metals*, 31(3):93–114, 1986.

[58] Stevens J. C. and Ahuja K. K. Recent advances in active noise control. *AIAA J.*, 29(7):1058–1067, 1991.

[59] Inman Daniel J. *Engineering Vibration.* Prentice Hall, Englewood Clifffs, New Jersey 07632, 1994.

[60] Thomson William T. *Theory of Vibration with Applications.* Prentice Hall, Englewood Clifffs, New Jersey 07632, 3rd edition, 1988.

[61] Burke S. and Hubbard J. E. Distributed transducer control dsign for thin plates. *Electrco-Optical Materials for Switches, Coatings, Sensor Optics, and Detectors*, 1307:222–231, 1990.

[62] Tzou H. S. A new distributed sensor and actuator theory for intelegent shells. *Journal of Sound and Vibration*, 153(2):335–349, 1992.

[63] Tzou H. S. Modal sensors/actuators. *Journal of Applied Mechanics*, 57(6):434–441, 1990.

[64] Falangas E. T. Dworak J. A. and S. Koshigoe. Controlling plate vibrations using piezoelectric actuators. *IEEE Control Systems*, 14(8):34–41, 1994.

[65] Fariborzi F., Golnaraghi M. F. and Heppler G. R. Development of mathematical model of a laminated plate for active vibration suppression. *Journal of vibration and control*, Accepted, 1997.

[66] Golnaraghi M. F. Regulation of flexible structures via nonlinear coupling. *Journal of Dynamics and Control*, 1:405–428, 1991.

[67] Tuer K.L., Duquette A.P. and Golnaraghi M.F. Vibration control of a flexible beam using a rotational internal resonance controller, part i:theoretical development and analysis. *Journal of Sound and Vibration*, 167(1):41–62, 1993.

[68] Skelton Robert E. *Dynamic Systems Control.* John Wiley & Sons Inc., New York, 1st edition, 1988.

[69] Young H. L. *Beating vibrations to death.* Master's thesis, University of Waterloo, 1996.

[70] Ogata Katsuhiko. *Modern Control Engineering.* Prentice Hall, Prentice Hall, Inc. Englewood Cliffs, New Jersey 07632, 2nd edition, 1990.

[71] Fuller C. R. Active control of sound transmission/radiation from elastic plate by vibration inputs. *J. Sound Vib.*, 136(1):1–15, 1990.

[72] Clark R. L. and Fuller C. R. Control of sound radiation with adaptive structures. *Intelligent Mater. Syst. Struct.*, 2(3):431–452, 1991.

[73] Clark R. L. and Fuller C. R. Experiments on active control of structurally radiated sound using multiple piezoceramic actuators. *J. Acoust. Soc. Am.*, 91(6):3313–3318, 1992.

[74] Gu Y., Clark R. L., Fuller C. R. and Zander A. C. Experiments on active control of plate vibration using piezoelectric actuators and polyvinylidene fluoride modal sensors. *Journal of Vibration and Acoustics*, 116(7):303–308, 1994.

[75] Tuer K. L. *Towards the Formulation of Generalized Vibration Suppression Law Using Linear and Nonlinear Coupling Paradigms.* PhD thesis, University of Waterloo, 1994.

[76] Ahmadian Hamid. *Finite Element Model Updating Using Modal Testing Data.* PhD thesis, University of Waterloo, 1994.

[77] Lang G. F. Understanding vibration measurements. *Journal of Sound and Vibration*, 10(3):26–37, 1976.

[78] Khajepour A. *Application of Centre Manifold and Normal Form to Nonlinear Controller Design.* PhD thesis, University of Waterloo, 1995.

IMAGE EVALUATION
TEST TARGET (QA-3)

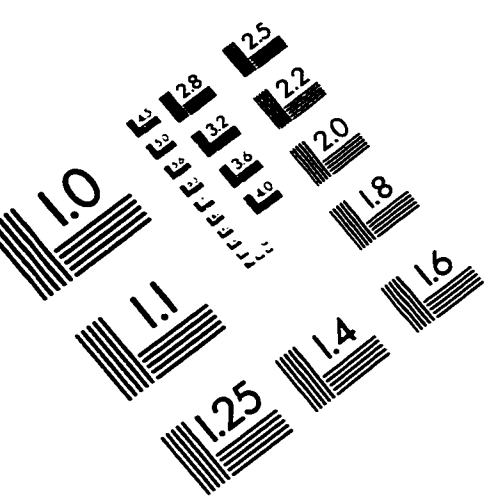

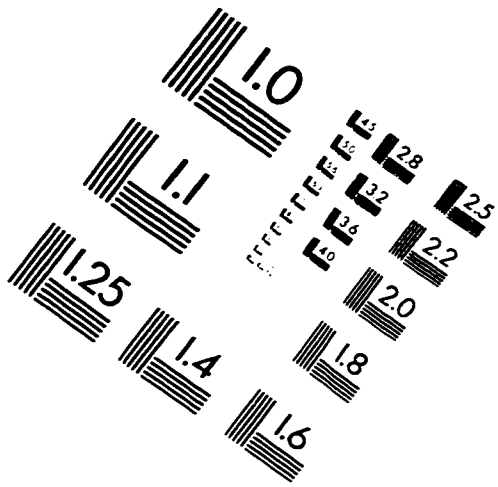

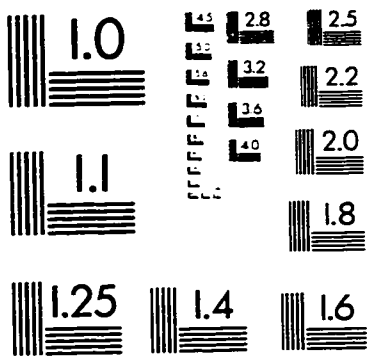

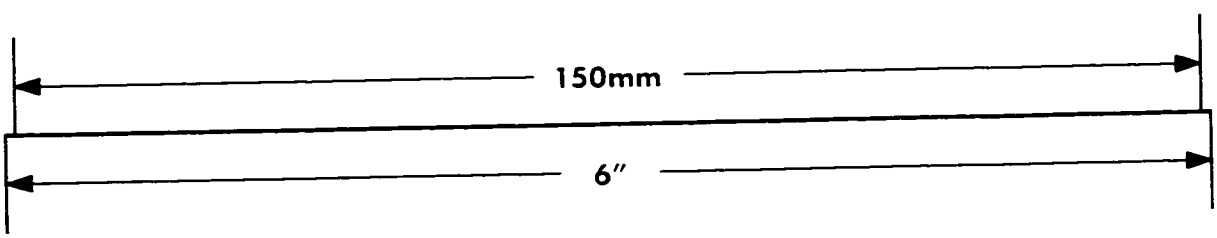

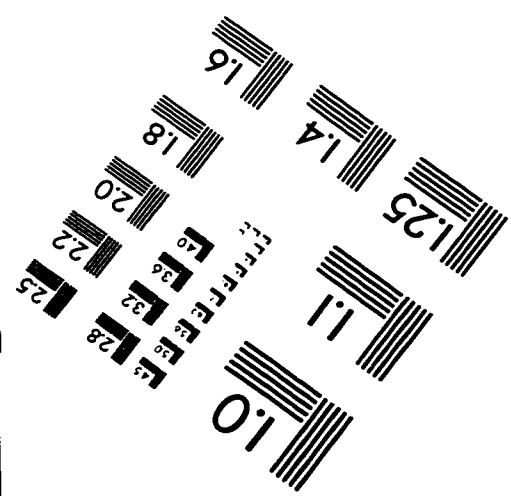

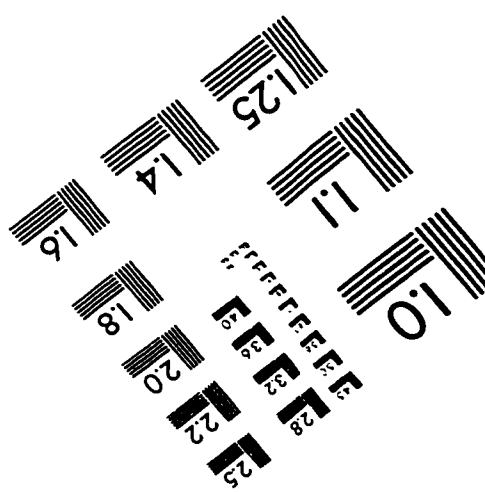

APPLIED IMAGE, Inc
1653 East Main Street
Rochester, NY 14609 USA
Phone: 716/482-0300
Fax: 716/288-5989